R. & M. No. 3293

MINISTRY OF AVIATION

AERONAUTICAL RESEARCH COUNCIL
REPORTS AND MEMORANDA

Charts of Peak Amplitudes in Incidence and Sideslip in Rolling Manoeuvres Due to Inertia Cross Coupling

By W. J. G. PINSKER

LONDON: HER MAJESTY'S STATIONERY OFFICE
1962
PRICE £1 12s. 6d. NET

Charts of Peak Amplitudes in Incidence and Sideslip in Rolling Manoeuvres Due to Inertia Cross Coupling

By W. J. G. PINSKER

COMMUNICATED BY THE DIRECTOR-GENERAL OF SCIENTIFIC RESEARCH (AIR), MINISTRY OF SUPPLY

*Reports and Memoranda No. 3293**
April, 1958

Summary. Based on a series of systematic analogue computations, charts are given for the determination of peak amplitudes in incidence and sideslip for a general family of rolling and rolling pull-out manoeuvres of aircraft subject to inertia cross coupling. The principal parameters governing the stability and response characteristics of aircraft in rolling manoeuvres are discussed and formulae and data are given for their determination.

1. *Introduction.* In order to increase performance the aircraft designer is forced to build more and more structural weight and equipment into airframes, which have hardly increased in volume during the last decade or so. As a consequence aircraft mass and inertias have increased without corresponding increases of the aerodynamic surfaces to stabilize the aircraft. Moreover, the supersonic aircraft being essentially a compromise between requirements at subsonic and supersonic speeds is likely to show aerodynamic deficiencies at some speeds. This may further accentuate the discord between inertias and aerodynamic forces.

One of the more dramatic consequences of these trends is the emergence of gyroscopically induced instabilities in rolling manoeuvres. These phenomena were first observed in the U.S.A. in several flight incidents and have recently been confirmed by flight tests in this country[1]. These divergent flight conditions were theoretically predicted earlier by W. Phillips[2].

Phillips' theory, which together with some later refinements of the basic analysis will be outlined in the first part of this report, can be briefly summarized to state:

(i) The gyroscopic moments on modern highly inertia-loaded aircraft reach such a magnitude during rolling manoeuvres that they can no longer be neglected in their analysis. These terms couple the lateral and longitudinal motions of the aircraft which must now be considered simultaneously, contrary to conventional stability theory.

(ii) The aircraft will become divergent in pitch and yaw if rate of roll exceeds either

$$|p| > \sqrt{\left(\frac{N_\beta}{B-A}\right)} \text{ or } |p| > \sqrt{\left(\frac{M_\alpha}{B}\right)} = \omega_\theta$$

whichever value is reached first by progressively increasing rate of roll from zero.

* Previously issued as R.A.E. Report No. Aero. 2604—A.R.C. 20,196.

(iii) Aerodynamic (or artificial) aircraft damping in pitch and yaw raise these limits, but for practical values the benefit is limited.

In Ref. 3 it has been shown that the effect of the angular momentum of rotating engines will modify these stability boundaries so as to make them asymmetric with respect to the sign of the rolling velocity, e.g., with an engine rotating anticlockwise slightly higher rates of roll are permissible to port than to starboard and *vice versa*. For present configurations the effect is, however, not very significant.

In Ref. 4 the existence of an autorotational instability of the rolling motion itself was predicted, which is also caused by aircraft inertia effects. This phenomenon will occur predominantly at negative incidences of the principal inertia axis.

This is briefly the picture presented to date by stability theory. It was, however, soon realized that the knowledge of these unstable flight conditions by itself is an inadequate guide for the designer and the operator of aircraft to assess the actual structural and piloting hazards in practical flight.

In Ref. 4 it has been shown that excessive peak values of sideslip or incidence may occur in manoeuvres with rolling velocities well within the stable range and that in other cases these critical roll rates may be safely exceeded for a limited period. It is now generally accepted that structural stressing and the determination of manoeuvring limitations must be based on full response calculations. Manual computation of the relevant equations of motion is quite impracticable. Only electronic computors either of the digital or preferably of the analogue type are capable of handling this task and even then, due to the great number of flight conditions to be considered, considerable effort may be required.

In order to obtain more readily-available design data, a systematic series of analogue computations was carried out on GEPUS, a general-purpose simulator in the Royal Aircraft Establishment. Approximately 8800 individual responses were computed and evaluated for peak loads in sideslip and incidence. The results cover a very wide range of the most relevant aircraft parameters and a comprehensive range of rolling manoeuvres.

In the first section of the report the theory of the stability of the aircraft as affected by inertia cross coupling will be briefly discussed. The main part of the report will then give the results of the response calculations in the form of charts and a discussion of all the relevant parameters which have to be considered in their application.

2. *The Stability of the Rolling Aircraft with Inertia Cross Coupling.* The fundamental physical phenomena which affect the stability of the lateral and longitudinal motion of the aircraft in steady rolling are discussed.

2.1. *The Equations of Motion.* In order to simplify the analysis, principal inertia axes are used throughout, as illustrated in Fig. 1. The derivatives are consequently defined in these axes and have to be computed with respect to principal inertia axes, whenever this would make a significant difference. In the equilibrium flight condition the principal x-axis is at an incidence α_0 with respect to the flight path. From Fig. 2 it can be seen that the instantaneous incidence:

$$\alpha = \alpha_0 + \Delta\alpha \tag{1}$$

where $\Delta\alpha$ is the incremental incidence.

It is generally accepted (e.g., Refs. 2 and 4) that speed can be considered as constant. Using the full Euler equations otherwise, the aircraft motion is now described by the differential equations:

$$\frac{1}{mV}\{Y_\beta\beta + Y_r r + Y_p p\} + \frac{g}{V}\sin\phi - r + p\alpha = \dot{\beta} \tag{2}$$

$$\frac{1}{mV}\{Z_\alpha\Delta\alpha + Z_q q + Z_{\dot{\alpha}}\dot{\alpha}\} - \frac{g}{V}(1-\cos\phi) + q - p\beta = \dot{\alpha} \tag{3}$$

$$L_\xi\xi + L_\beta\beta + L_p p + L_r r + (B-C)qr = A\dot{p} \tag{4}$$

$$M_\alpha\Delta\alpha + M_{\dot{\alpha}}\dot{\alpha} + M_q q + (C-A)rp = B\dot{q} \tag{5}$$

$$N_\xi\xi + N_\beta\beta + N_p p + N_r r + (A-B)pq = C\dot{r}. \tag{6}$$

Rudder and elevator are assumed fixed, pitch and yaw angles small, to simplify the kinematic relations, and it is assumed that there is no pitching moment due to aileron deflection, $M_\xi = 0$.

The gyroscopic product terms in the three moment equations are explained in Figs. 3 and 4 and in Appendix I as centrifugal moments. The terms $p\alpha$ and $p\beta$ are illustrated in Figs. 5 and 6 as expressing purely kinematic relations.

It has been shown in some examples in Refs. 2 and 4, that gravity can generally be neglected at least for the relatively-fast rolling motions in which inertia cross coupling is significant. The minor derivatives Y_r, Y_p, Z_q and $Z_{\dot{\alpha}}$ can also be neglected. As the product terms couple the lateral and longitudinal equations and moreover make the equations non-linear, conventional methods of calculus are impracticable.

If one assumes that the pilot can and will control the rolling motion itself within reasonable limits, rate of roll can be treated as an independent variable

$$p(t) = F(t)p_0 \tag{7}$$

where $F(t) = p(t)/p_0$ is a given function of time and p_0 a nominal constant value of rate of roll. This assumption renders the rolling-moment equation (4) redundant, which could now be used to compute the aileron manoeuvre required to perform the given rolling manoeuvre $p(t)$. Equations (2 to 6) are now reduced to

$$\frac{1}{mV}\{Y_\beta\beta\} - r + p_0 F\Delta\alpha - \dot{\beta} = -p_0 F\alpha_0 \tag{8}$$

$$\frac{1}{mV}Z_\alpha\Delta\alpha + q - p_0 F\beta - \dot{\alpha} = 0 \tag{9}$$

$$M_\alpha\Delta\alpha + M_{\dot{\alpha}}\dot{\alpha} + M_q q + (C-A)p_0 Fr - B\dot{q} = 0 \tag{10}$$

$$N_\beta\beta + N_r r + (A-B)p_0 Fq - C\dot{r} = -N_p p_0 F - N_\xi\xi(t). \tag{11}$$

Using only the four equations (8 to 11), $\xi(t)$ is now indeterminate apart from the particular case where it is justifiable to assume

$$\xi(t) = \text{const}\, p(t) \tag{12}$$

otherwise the last term in the yawing-moment equation has to be omitted, though this may constitute a noticeable error.

In order to reduce the number of parameters for systematic analysis, the damping terms are replaced by a single equivalent effective derivative in pitch and in yaw respectively:

Z_α, M_q and $M_{\dot\alpha}$ replaced by $M_{\dot\theta}$

Y_β, N_r and possibly the effect of the suppressed rolling mode of the lateral oscillation are replaced by $N_{\dot\psi}$.

It should be noted that the derivatives $M_{\dot\theta}$ and $N_{\dot\psi}$ as used here and defined by equations (15) and (16) are not those derived from oscillatory wind-tunnel tests.

Introducing the parameters:

$$\omega_\theta = \sqrt{-\frac{M_\alpha}{B}} = \text{undamped frequency of pitching oscillation} \tag{13}$$

$$\omega_\psi = \sqrt{\frac{N_\beta}{C}} = \text{undamped frequency of lateral oscillation} \tag{14}$$

$$\delta_\theta = -\frac{\pi}{\left(\frac{\omega_\theta}{p_0}\right)}\frac{M_{\dot\theta}}{p_0 B} = \text{log decrement of pitching oscillation} \tag{15}$$

$$\delta_\psi = -\frac{\pi}{\left(\frac{\omega_\psi}{p_0}\right)}\frac{N_{\dot\psi}}{p_0 C} = \text{log decrement of lateral oscillation} \tag{16}$$

to express the aerodynamic characteristics of the aircraft and introducing non-dimensional time (tp_0) and the differential operator

$$D = \frac{d}{d(tp_0)} \tag{17}$$

and the variables

$$\bar r = \frac{r}{p_0},\ \bar q = \frac{q}{p_0} \tag{18}$$

equations (8 to 11) can be now written:

$$-\bar r + F(t)\Delta\alpha - D\beta = -F(t)\alpha_0 \tag{19}$$

$$\bar q - F(t)\beta - D\Delta\alpha = 0 \tag{20}$$

$$-\left(\frac{\omega_\theta}{p_0}\right)^2\Delta\alpha - \frac{\delta_\theta}{\pi}\left(\frac{\omega_\theta}{p_0}\right)\bar q + \frac{C-A}{B}F(t)\bar r - D\bar q = 0 \tag{21}$$

$$\left(\frac{\omega_\psi}{p_0}\right)^2\beta - \frac{\delta_\psi}{\pi}\left(\frac{\omega_\psi}{p_0}\right)\bar r - \frac{B-A}{C}F(t)\bar q - D\bar r = -\frac{N_p}{Cp_0}F(t) - \frac{N_\xi}{Cp_0}\frac{\xi(t)}{p_0}. \tag{22}$$

2.2. *Stability for Constant Rate of Roll* p_0. Phillips[1] has analysed these equations for constant rate of roll, i.e., for $F(t) = 1$. As for conventional designs the structure of an aircraft is distributed predominantly within the wing plane, the inertias are approximately related as:

$$C = A + B \tag{23}$$

and equations (19 to 22) are now reduced to the system of linear differential equations:

$$-\bar{r} + \Delta\alpha - D\beta = \alpha_0 \tag{24}$$

$$\bar{q} - \beta - D\Delta\alpha = 0 \tag{25}$$

$$-\left(\frac{\omega_\theta}{p_0}\right)^2 \Delta\alpha - \frac{\delta_\theta}{\pi}\left(\frac{\omega_\theta}{p_0}\right)\bar{q} + \bar{r} - D\bar{q} = 0 \tag{26}$$

$$\left(\frac{\omega_\psi}{p_0}\right)^2 \beta - \frac{\delta_\psi}{\pi}\left(\frac{\omega_\psi}{p_0}\right)\bar{r} - \frac{B-A}{B+A}\bar{q} - D\bar{r} = -\frac{N_p}{Cp_0} \tag{27}$$

Neglecting aircraft damping these equations will give the roots

$$D^2 = -\tfrac{1}{2}\left\{\left(\frac{\omega_\psi}{p_0}\right)^2 + \left(\frac{\omega_\theta}{p_0}\right)^2 + 1 + \frac{B-A}{B+A}\right\} \pm$$

$$\pm\sqrt{\left[\tfrac{1}{4}\left\{\left(\frac{\omega_\theta}{p_0}\right)^2 + \left(\frac{\omega_\psi}{p_0}\right)^2 + 1 + \frac{B-A}{B+A}\right\}^2 - \left(\frac{\omega_\psi}{p_0}\right)^2\left(\frac{\omega_\theta}{p_0}\right)^2 + \left(\frac{\omega_\psi}{p_0}\right)^2 - \frac{B-A}{B+A}\left\{1 - \left(\frac{\omega_\theta}{p_0}\right)^2\right\}\right]}. \tag{28}$$

The stability boundaries determined by this equation are plotted against the parameters $(\omega_\theta/p_0)^2$ and $(\omega_\psi/p_0)^2$ in Fig. 7. For low rates of roll, i.e., in the upper right-hand quadrant the aircraft will display two stable oscillatory modes, each of which is a combined lateral-longitudinal oscillation. As rate of roll is increased one of the two stability boundaries is eventually reached and for

$$|p| \geqslant \omega_\theta$$

or

$$|p| \geqslant \omega_\psi\sqrt{\frac{B+A}{B-A}}.$$

(whichever of the two is reached first) one mode becomes divergent. With further increasing rate of roll, the second stability boundary is crossed and the motion will be again oscillatory and stable in the quadrant near the origin of the stability graph.

This is illustrated in Fig. 8 for three examples:

(i) Aircraft 'A', poor directional stability. Increasing p_0 progressively from nought, the vertical boundary is reached first and the aircraft will be divergent (predominantly in yaw) for

$$\omega_\theta > |p_0| > \omega_\psi\sqrt{\frac{B+A}{B-A}}.$$

(ii) Aircraft 'B', directional and longitudinal stabilities are 'Tuned' so that $\omega_\theta = \omega_\psi(B+A)/(B-A)$. No instability over the full range of p_0. It should be noted, however, that stability will be very marginal near the intersection of the stability boundaries, i.e., for $p \approx \omega_\theta$.

(iii) Aircraft 'C', poor static longitudinal stability. The motion will be divergent (now predominantly in pitch) if

$$\omega_\theta < |p_0| < \omega_\psi\sqrt{\frac{B+A}{B-A}}.$$

If inertia in roll, A, is increased in relation to inertia in pitch, B, the vertical (yaw) divergence region contracts towards the origin. For $A = B$ this unstable region vanishes as illustrated in Fig. 9. (Fig. 8 applied to $A/B = 1/5$, i.e. $(A-B)/(A+B) = 0{\cdot}666$.) Taking again the three aircraft previously quoted as examples:

Aircraft 'A' is now stable to higher rates of roll, but the divergent condition remains there up to infinite rates.

Aircraft 'B' does now become unstable after exceeding $p_0 = \omega_\theta$.

Aircraft 'C' will become unstable at the same rate of roll as before, but the instability remains up to infinite rolling velocities.

All three aircraft have now the same critical condition, i.e., they will become divergent if

$$\infty > |p_0| > \omega_\theta .$$

A physical explanation of the occurrence of these divergent conditions is given in Appendix I. The aircraft motion in the stable condition at very high rates of roll (or vanishing aerodynamic restoring moments) is illustrated in Fig. 10. The motion during a pitch divergence is illustrated in Fig. 11 and the corresponding yaw divergence in Fig. 12. The stabilizing effect of inertia in roll on this mode is illustrated in Fig. 13.

2.3. *Effect of Aircraft Damping.* Retaining δ_θ and δ_ψ in equations (25 to 27), the characteristic equation will be a quartic

$$D^4 + a_1 D^3 + a_2 D^2 + a_3 D + a_4 = 0 \tag{29}$$

with the coefficients

$$\begin{aligned}
a_1 &= \frac{\delta_\theta}{\pi}\left(\frac{\omega_\theta}{p_0}\right) + \frac{\delta_\psi}{\pi}\left(\frac{\omega_\psi}{p_0}\right) \\
a_2 &= \frac{B-A}{B+A} + 1 + \left(\frac{\omega_\theta}{p_0}\right)^2 + \left(\frac{\omega_\psi}{p_0}\right)^2 + \frac{\delta_\theta}{\pi}\left(\frac{\omega_\theta}{p_0}\right)\frac{\delta_\psi}{\pi}\left(\frac{\omega_\psi}{p_0}\right) \\
a_3 &= \left(\frac{\omega_\theta}{p_0}\right)^2 \frac{\delta_\psi}{\pi}\left(\frac{\omega_\psi}{p_0}\right) + \left(\frac{\omega_\psi}{p_0}\right)^2 \frac{\delta_\theta}{\pi}\left(\frac{\omega_\theta}{p_0}\right) - \frac{\delta_\psi}{\pi}\left(\frac{\omega_\psi}{p_0}\right) - \frac{\delta_\theta}{\pi}\left(\frac{\omega_\theta}{p_0}\right) \\
a_4 &= \frac{\delta_\theta}{\pi}\left(\frac{\omega_\theta}{p_0}\right)\frac{\delta_\psi}{\pi}\left(\frac{\omega_\psi}{p_0}\right) + \left\{\frac{B-A}{B+A} - \left(\frac{\omega_\psi}{p_0}\right)^2\right\}\left\{1 - \left(\frac{\omega_\theta}{p_0}\right)^2\right\}.
\end{aligned} \tag{30}$$

Setting $a_4 = 0$ gives the stability boundaries as:

$$\left(\frac{\omega_\psi}{p_0}\right) = \tfrac{1}{2}\frac{\delta_\psi}{\pi}\frac{\delta_\theta}{\pi}\frac{\left(\frac{\omega_\theta}{p_0}\right)}{1 - \left(\frac{\omega_\theta}{p_0}\right)^2} \pm \sqrt{\left\{\frac{B-A}{B+A} + \left(\tfrac{1}{2}\frac{\delta_\psi}{\pi}\frac{\delta_\theta}{\pi}\frac{\left(\frac{\omega_\theta}{p_0}\right)}{1 - \left(\frac{\omega_\theta}{p_0}\right)^2}\right)^2\right\}} \tag{31}$$

These boundaries are shown for three values of $(\delta_\theta \delta_\psi)$ as compared with those for the undamped aircraft in Fig. 14. The three ratios A/B considered are those used later in the computation of the peak-amplitude charts. Damping has relatively little effect on the stability of the motion except in the region where the two boundaries intersect each other for $\delta = 0$. There damping separates the two unstable regions, allowing a margin in 'Tuning' the stabilities of the aircraft i.e., the ratio $\omega_\theta/\omega_\psi$ for stability through the full range of rolling velocities. This is illustrated in Fig. 15 for the case $A/B = 0$.

2.4. *Effect of Engine Momentum.* In Ref. 5 engine momentum is shown to couple the lateral and longitudinal motion of an aircraft and to destabilize one of the two oscillatory modes of motion

in the absence of rolling. This effect is symmetric, i.e., independent of the sense of the engine rotation. The effect of the engine on the rolling divergence as analysed in Refs. 3 and 6 is however dependent on the sense of the engine rotation and of the rolling velocity.

Introducing engine momentum $K = \omega_e I_e$ equations (20) and (21) are now

$$-\left(\frac{\omega_\theta}{p_0}\right)^2 \Delta\alpha - \frac{\delta_\theta}{\pi}\left(\frac{\omega_\theta}{p_0}\right)\bar{q} + \frac{C-A}{B}F(t)\bar{r} + \frac{K}{Bp_0}\bar{r} - D\bar{q} = 0 \tag{32}$$

$$\left(\frac{\omega_\psi}{p_0}\right)^2 \beta - \frac{\delta_\psi}{\pi}\left(\frac{\omega_\psi}{p_0}\right)\bar{r}\frac{B-A}{C}F(t)\bar{q} + \frac{K}{Cp_0}\bar{q} - D\bar{r} = -\frac{N_p}{Cp_0}F(t) - \frac{N_\xi}{Cp_0}\frac{\xi(t)}{p_0}. \tag{33}$$

The asymptotic values of the stability boundaries are then modified by the engine effect to:

$$\left[\left(\frac{\omega_\theta}{p_0}\right)^2\right]_{(\omega_\theta/p_0)=\infty} = \frac{C-A}{B} - \frac{K}{Bp_0} \tag{34}$$

$$\left[\left(\frac{\omega_\theta}{p_0}\right)^2\right]_{(\omega_\theta/p_0)=0} = \frac{C-A}{B} - \frac{K}{Bp_0} + \frac{\left(\frac{\delta_\theta}{\pi}\right)\left(\frac{\omega_\theta}{p_0}\right)\frac{\delta_\psi}{\pi}\left(\frac{\omega_\psi}{p_0}\right)}{\frac{B-A}{C} - \frac{K}{Cp_0}} \tag{35}$$

$$\left[\left(\frac{\omega_\psi}{p_0}\right)^2\right]_{(\omega_\theta/p_0)=\infty} = \frac{B-A}{C} - \frac{K}{Cp_0} \tag{36}$$

$$\left[\left(\frac{\omega_\psi}{p_0}\right)^2\right]_{(\omega_\theta/p_0)=0} = \frac{B-A}{C} - \frac{K}{Cp_0} + \frac{\frac{\delta_\theta}{\pi}\left(\frac{\omega_\theta}{p_0}\right)\frac{\delta_\psi}{\pi}\left(\frac{\omega_\psi}{p_0}\right)}{\frac{C-A}{B} - \frac{K}{Bp_0}}. \tag{37}$$

The term $K/p_0 = \omega_e I_e/p_0$ is dependent on the sign of both engine rotation ω_e and rate of roll p_0. Thus for a given aircraft there will be two stability boundaries for rolling to port and to starboard respectively. This is illustrated in Fig. 16. Stability is maintained to higher rates of roll if both engine and aircraft rotate in the same sense and *vice versa*. In Ref. 6 it has been shown that the effect of engine momentum on inertia cross coupling can be satisfactorily represented by data computed without considering the engine. Such data as e.g., the charts given in this report, will apply to the condition with engines rotating, if the two Phillips' parameters ω_θ/p_0 and ω_ψ/p_0 are reinterpreted as being 'effective' frequencies, i.e.,

$$\left(\frac{\omega_\theta}{p_0}\right)_M^2 = \left(\frac{\omega_\theta}{p_0}\right)^2 + \frac{I_e\omega_e}{Bp_0} \text{ and } \left(\frac{\omega_\psi}{p_0}\right)_M^2 = \left(\frac{\omega_\psi}{p_0}\right)^2 + \frac{I_e\omega_e}{Cp_0} \tag{38}$$

as illustrated in Fig. 17. For present designs the effect of the engine can be shown to be relatively unimportant.

2.5. *Autorotational Rolling.* For the present investigation, rate of roll is generally considered as an independent variable, i.e., the pilot is assumed to control the rolling velocity positively. In Ref. 4, it has, however, been shown, that aircraft may become unstable in roll once a certain critical rolling velocity is exceeded, and to diverge towards an autorotationally stable rate of roll. The critical

rolling velocity and the autorotational rate of roll are given as the lower and upper value respectively of the solution of

$$\left(\frac{p}{\omega_{\psi 0}}\right) = \tfrac{1}{2}\left\{1 + \left(\frac{\omega_\theta}{\omega_\psi}\right)^2 + \alpha_0\nu\right\} \pm \sqrt{\left[\tfrac{1}{4}\left\{1 + \left(\frac{\omega_\theta}{\omega_\psi}\right)^2 + \alpha_0\nu\right\}^2 - \left(\frac{\omega_\theta}{\omega_{\psi 0}}\right)^2 - \kappa\right]} \tag{39}$$

where

$$\omega_{\psi 0}{}^2 = \omega_\psi{}^2 \frac{B + A}{B - A}$$

$$\nu = Z_w \frac{l_v}{l_p} \frac{i_B(4l^2/b^2) - i_A}{n_v}$$

$$\kappa = Z_w \frac{m_q}{n_v}\left(1 - \frac{A}{B}\right)\frac{(2l/b)^2}{\mu_2}.$$

This instability is largely confined to flight conditions at negative incidence α_0 of the principal inertia axis. The critical values of $(\alpha_0\nu)$ below which autorotational rolling can occur can be deduced from equation (39) and are plotted in Fig. 18 against the relevant parameters. For a more thorough treatment of this effect reference is made to Ref. 4.

3. *Response Computations.* The study of stability at constant values of p is of great value for the understanding of the phenomena induced by the gyroscopic aircraft moment. For an assessment of the severity of these phenomena during actual flight manoeuvres, however, the peak excursion in incidence and sideslip must be obtained from fully-computed aircraft responses. A large number of such computations covering a large range of aircraft parameters and rolling manoeuvres was carried out on GEPUS, an analogue computor in the R.A.E. with the aim of obtaining generalized design data.

3.1. *The Equations of Motion.* Retaining only major terms the simulator was set up to represent equations (19 to 22) in the form

$$-\bar{r} + F(t)\Delta\alpha - D\beta = -F(t)\alpha_0 \tag{40}$$

$$\bar{q} - F(t)\beta - D\Delta\alpha = 0 \tag{41}$$

$$-\left(\frac{\omega_\theta}{p_0}\right)^2 \Delta\alpha - \frac{\delta_\theta}{\pi}\left(\frac{\omega_\theta}{p_0}\right)\bar{q} + F(t)\bar{r} - D\bar{q} = 0 \tag{42}$$

$$\left(\frac{\omega_\psi}{p_0}\right)^2 \beta - \frac{\delta_\psi}{\pi}\left(\frac{\omega_\psi}{p_0}\right)\bar{r} - \frac{B - A}{B + A}F(t)\bar{q} - D\bar{r} = -\frac{N_p}{Cp_0}F(t). \tag{43}$$

This is a system of linear differential equations with variable coefficients according to the assumed time history in roll as defined by the function $F(t) = p_0(t)/p_0$. The terms on the right-hand side of equations (40) and (43) represent the forcing functions, both being proportional to the roll-manoeuvre function $F(t)$. The response of the aircraft to these two inputs can be linearly superimposed from two separately-computed solutions to the forcing functions $\alpha_0 F(t)$ and $(N_p/Cp_0)F(t)$, e.g.,

$$\Delta\alpha(t) = \Delta\alpha_1(t) + \Delta\alpha_2(t) \tag{44}$$

It is, however, not possible to add peak values of α_1 and α_2 as they will generally not occur at the same instant.

It was originally intended to compute aircraft responses to both inputs. However, after computation of the much more important contribution due to the term $F(t)\alpha_0$, the simulator was no longer available for this work and the contributions of the secondary effect of N_p had to be neglected. Should there

be evidence of a need for considering an N_p contribution, the computations may be resumed at some later date and compiled into a series of charts complementary to those given in the present report.

3.2. *The Scope of the Computations on GEPUS.* Neglecting N_p, equations (41 to 43) are determined by the parameters:

$$\left(\frac{\omega_\theta}{p_0}\right), \left(\frac{\omega_\psi}{p_0}\right), \delta_\theta, \delta_\psi, \frac{A}{B} \text{ and } F(t) \tag{45}$$

and by the constant α_0 to which the solution will be proportional.

The problem of obtaining design data from a systematic series of computations is now resolved into

(i) the choice of a readily-computed and fully-representative type of rolling manoeuvre, i.e., of a family of functions $F(t)$, which can be expressed by not more than two parameters

(ii) the computation of the aircraft response to these rolling manoeuvres $F(t)$ for a representation range of the aircraft parameters, equation (45)

(iii) extracting peak values of $\Delta\alpha$ and β as the structurally most significant data from these responses and finally compiling these into a manageable number of charts.

3.3. *Choice of a Standard Rolling Manoeuvre $F(t)$.* Flight experience and theoretical work in Ref. 4 has shown that the peak loads experienced by an aircraft during rolling manoeuvres vary substantially with both the duration of the manoeuvre and with the manner in which rolling is initiated and terminated. A realistic estimate of the manoeuvring loads on an aircraft subject to inertia cross coupling must therefore take into consideration not only the potential steady-rolling performance but also representative—and of course—critical time histories of control application, or as this has been shown to be an adequate substitute, of rate of roll. The steady rate of roll p_0, which in a dynamic manoeuvre may be a fictitious value never actually reached before the roll is terminated, is contained in our non-dimensionalized treatment {equations (40 to 43)} in the parameters (ω_ψ/p_0) and (ω_θ/p_0). The dynamic characteristics of the manoeuvre is then defined by the function $p(t)/p_0 = F(t)$. $F(t)$ is a non-dimensional function, defining the way in which a roll is executed but not the actual level of rate of roll. Fixing both frequency parameters ω/p_0 and $F(t)$ will then completely define the manoeuvre. The problem of presenting generally-applicable design data resolves now into two tasks.

(i) a manoeuvre function $F(t)$ must be found which is representative of all practical rolling manoeuvres, and which at the same time is defined by not more than 2 independent parameters, so as to keep the volume of computing to a reasonable level.

(ii) the parameters defining this idealized manoeuvre function $F(t)$ must be related to the aerodynamic and dynamic characteristics of a given aircraft, so as to enable the designer to select the manoeuvre function $F(t)$ appropriate to his design.

3.3.1. *The roll-manoeuvre function $F(t)$.* Inspection of a large number of flight records of $p(t)$ has shown that practically all rolling manoeuvres involving no actual roll reversal—as distinct from bank reversal, which is represented—can be closely fitted to the family of functions illustrated in Fig. 19. This manoeuvre function $F(t)$ is generated by two exponentials, an asymptotic rise towards a steady value (i.e., towards steady rate of roll p_0) followed at a specified instant t_1 by an exponential decay towards zero rate of roll. Both the rise and the decay are governed by the same time constant t_p.

Introducing non-dimensionalized time (tp_0) it is now apparent that this manoeuvre function $F(tp_0)$ which shall henceforth be referred to as the 'standard manoeuvre' is fully defined by two independent parameters

($t_p p_0$), the non-dimensionalized response time constant

($t_1 p_0$), the non-dimensionalized duration.

Integrating the response function

$$\int_0^\infty F(tp_0)d(tp_0) = \int_0^\infty \frac{p}{p_0}(t)p_0\,dt = \int_0^\infty p(t)dt = \Delta\phi \tag{46}$$

gives the 'manoeuvre bank angle' $\Delta\phi$, i.e., the total bank-angle change during the manoeuvre.

When applied to the 'standard manoeuvre' (*see* Fig. 20).

$$F(tp_0) = 1 - \exp\left\{-\left(\frac{tp_0}{t_p p_0}\right)\right\} \text{ for } 0 < t < t_1 \tag{47}$$

$$F(tp_0) = \left[1 - \exp\left\{-\left(\frac{t_1}{t_p}\right)\right\}\right] \exp\left\{-\left(\frac{tp_0 - t_1 p_0}{t_p p_0}\right)\right\} \text{ for } t > t_1 \tag{48}$$

we get

$$\int_0^\infty F(tp_0)d(tp_0) = t_1 p_0 = \Delta\phi, \tag{49}$$

i.e., the non-dimensionalized duration parameter ($t_1 p_0$) is identical to the manoeuvre bank angle $\Delta\phi$ and thus a most useful parameter describing a roll manoeuvre. Having established a standard manoeuvre upon which the computation of aircraft responses can be based, it is now necessary to correlate the parameters describing this response function to the appropriate response characteristics of the aircraft.

3.3.2. *Aircraft response in roll.* It is apparent that the rolling manoeuvre adopted as the 'standard manoeuvre' in this report is the response of an aircraft with freedom in roll only to a square-top function application of aileron as illustrated in Fig. 21. In this case the time constant of the aircraft response is of course given by the roll subsidence root, which is obtained from Ref. 7 as

$$t_\xi p_0 = \left| 13{\cdot}05\xi_0 \frac{W/S}{\sigma} \frac{l_\xi}{l_p^2} \frac{i_A}{b/2} \right| \tag{50}$$

where ξ_0 is the aileron angle applied. $t\xi$ is the 'natural aircraft time constant'. This need not necessarily be representative of the actual roll response achieved by a pilot controlling the aircraft. There are two effects which may cause a pilot to depart from the execution of a pure step-function type of control application. Firstly the reaction forces in the aileron circuit (aerodynamic—or spring feel, inertia, friction etc.) will slow his stick movement down and as a consequence the resulting response of the aircraft in roll. This effect will be particularly noticeable, if the 'natural' aircraft response is very fast, say if $t\xi < 0{\cdot}5$ sec. On the other hand it is known that pilots will speed up an unsatisfactory slow rolling response by initially applying aileron in excess of the intended steady value ξ_0, provided, of course, the desired amount of excess aileron is physically available, i.e., $\xi_0 < \xi_{MAX}$. Similar arguments will apply at the end of the manoeuvre. For simplicity it has been assumed here that in fact the pilot will control the aircraft so that its response when building up rate of roll and when terminating the roll is governed by the same time constant.

This 'pilot modified time constant' t_p is now taken as the basis of our computed standard manoeuvre. In Fig. 22 an attempt has been made to give a realistic relation between the natural

aircraft time constant t_ξ as determined by equation (50) and the actual roll-response time t_p a pilot can be assumed to achieve with this aircraft. The two basic assumptions used in the construction of this graph are:

(i) The pilot will need approximately 0·2 sec to move the stick to the final position corresponding to ξ_0. This will give a minimum for the response time t_p of approximately 0·15 sec if the aircraft response were instantaneous, i.e., $t_\xi = 0$.

(ii) The pilot will try to control the aircraft so as to keep the effective response time below 1·8 sec.

The full line in the graph Fig. 22 is simply obtained by fairing between these two conditions. The amount of excess aileron required to achieve the assumed improved aircraft response when $t_\xi > 0{\cdot}5$ has been calculated and plotted against t_ξ in Fig. 23. For conditions where only a fraction or none of this excess control is available the corresponding achievable values of t_p are given as dotted lines in Fig. 22.

Finally it should be noted that the shortest possible response time t_p should always be selected as this will inevitably produce the most violent aircraft reaction to inertia cross coupling. This is well illustrated by the example of computed values of peak sideslip angles to a rolling manoeuvre with various response time constants t_p in Fig. 24.

3.4. *Rolling Pull-Out.* The most severe manoeuvre when considering inertia cross coupling will frequently be the rolling pull-out. It is obviously very desirable to cover this case in an assessment of the extreme loading conditions. For high-speed aircraft the rates of pitch achieved in even a sharp pull-out are quite negligible when compared with the pitching velocities occurring during inertia cross-coupled rolling. Consequently it seems justifiable to neglect this rate of pitch in a computation and the only remaining parameter which is significantly affected by the pull-out will be the increased incidence α_0 corresponding to the 'g' applied. If this incidence α_0 is put on in the rolling pull-out manoeuvre before the pilot applies aileron, the 'standard manoeuvre' considered in this Report is fully representative, provided the value of α_0 chosen represents the incidence under 'g'.

3.5. *Bank Reversal.* As the 'standard manoeuvre' does not contain a reversal of the rate of roll, any manoeuvre demanding such a motion is not covered by the results given in this Report.

Rolling from a given steady bank angle to a steady bank in the opposite direction can, however, be considered as equivalent to a rolling pull-out, if one assumes that the pilot maintains initial 'g' throughout the manoeuvre. This manoeuvre is thus covered by the computations based on the standard manoeuvre.

3.6. *Computation of Aircraft Response to Standard Rolling Manoeuvre.* Neglecting N_p and N_ξ the response of this aircraft to a given roll manoeuvre $F(t)$ is described by equations (40 to 43) which can be divided through by α_0 and are thus reduced to

$$-\frac{\bar{r}}{\alpha_0} + F(tp_0)\frac{\Delta\alpha}{\alpha_0} - D\frac{\beta}{\alpha_0} = -F(tp_0) \tag{51}$$

$$\frac{\bar{q}}{\alpha_0} - F(tp_0)\frac{\beta}{\alpha_0} - D\frac{\Delta\alpha}{\alpha_0} = 0 \tag{52}$$

$$-\left(\frac{\omega_\theta}{p_0}\right)^2\frac{\Delta\alpha}{\alpha_0} - \frac{\delta_\theta}{\pi}\left(\frac{\omega_\theta}{p_0}\right)\frac{\bar{q}}{\alpha_0} + F(tp_0)\frac{\bar{r}}{\alpha_0} - D\frac{\bar{q}}{\alpha_0} = 0 \tag{53}$$

$$\left(\frac{\omega_\psi}{p_0}\right)^2\frac{\beta}{\alpha_0} - \frac{\delta_\psi}{\pi}\left(\frac{\omega_\psi}{p_0}\right)\frac{\bar{r}}{\alpha_0} - \frac{B-A}{B+A}F(tp_0)\frac{\bar{q}}{\alpha_0} - D\frac{\bar{r}}{\alpha_0} = 0. \tag{54}$$

As the only significant results, $\Delta\alpha/\alpha_0$ and β/α_0, have been recorded for the full range of the aircraft parameters, i.e., for all combinations of

$$\left(\frac{\omega_\theta}{p_0}\right)^2 = 0{\cdot}25,\ 0{\cdot}5,\ 1{\cdot}0,\ 1{\cdot}5,\ 2,\ 4,\ 8,\ 16$$

$$\left(\frac{\omega_\psi}{p_0}\right) = 0{\cdot}25,\ 0{\cdot}5,\ 1{\cdot}0,\ 1{\cdot}5,\ 2,\ 4,\ 8,\ 16$$

$$\left.\begin{matrix}\delta_\theta = 0{\cdot}2\\ \delta_\psi = 0{\cdot}1\end{matrix}\right\} \text{representing poor damping} \qquad \left.\begin{matrix}\delta_\theta = 2{\cdot}0\\ \delta_\psi = 0{\cdot}5\end{matrix}\right\} \text{representing good damping}$$

$$\frac{A}{B} = 0,\ \tfrac{1}{3},\ 1{\cdot}0$$

and for the roll manoeuvres defined by

$$(t_\rho p_0) = 0{\cdot}1,\ 0{\cdot}5,\ 2{\cdot}0$$

over the range of $\Delta\phi$ from 0 to 10 radians, i.e., to approximately 570°. It should be emphasized again that $\Delta\phi$ is the total change of bank angle for the manoeuvre considered.

From each of these records of $(\Delta\alpha/\alpha_0)(t)$ and $(\beta/\alpha_0)(t)$, of which a typical example is given in Fig. 25, the maxima of both variables, $(\Delta\alpha/\alpha_0)_{\text{MAX}}$ and $(\beta/\alpha_0)_{\text{MAX}}$ have been computed and have then been plotted against the manoeuvre bank angle $\Delta\phi$ {equation (49)} for each of the recorded conditions. It was found that these graphs of $(\Delta\alpha/\alpha_0)_{\text{MAX}} = f(\Delta\phi)$ and $(\beta/\alpha_0)_{\text{MAX}} = f(\Delta\phi)$ can be separated into four distinct types, which are associated systematically with the four stability quadrants in the applicable stability diagrams Figs. 7 to 9. These types are illustrated in Fig. 26 and their association with the quadrants in the $(\omega_\theta/p_0)^2 - (\omega_\psi/p_0)^2$ plane is shown in Fig. 27. As there were 2204 such diagrams computed, the data contained in them had again to be concentrated into a more presentable form.

3.7. *Relationships between Peak Values of* $\Delta\alpha$ *and* β *and Manoeuvre Bank Angle* $\Delta\phi$. Examination of the four types of curves $(\Delta\alpha/\alpha_0)_{\text{MAX}}$ and $(\beta/\alpha_0)_{\text{MAX}}$ as functions of $\Delta\phi$ as shown in Fig. 26 reveals some prominent features which lead to further simplification.

Type [A] occurs in the stable quadrants. Prolonged rolling does not lead to progressively increasing peak loads, as the motion is inherently stable. This does not mean, however, that the peak loads occurring in this condition might not be excessive, as indeed they very often are.

For the purpose of presenting the essential information from these graphs it is sufficient to give the ceiling values of $(\Delta\alpha/\alpha_0)_{\text{MAX}}$ or $(\beta/\alpha_0)_{\text{MAX}}$, to indicate the absolute maximum that can occur for any rolling manoeuvre in this flight condition. For banking manoeuvres through smaller bank angles $\Delta\phi$ it is further necessary to give the initial slope of the peak values $(\Delta\alpha/\alpha_0)_{\text{MAX}}$ or $(\beta/\alpha_0)_{\text{MAX}}$ with $\Delta\phi$, i.e.,

$$\frac{d\left(\frac{\Delta\alpha}{\alpha_0}\right)}{d\phi} \text{ or } \frac{d\left(\frac{\beta}{\alpha_0}\right)}{d\phi}.$$

In the actual presentation of the data the suffix $_{\text{MAX}}$ has been dropped as only maximum values will be discussed. From those data, i.e., ceiling value and initial slope, the essential features of the original graph $(\Delta\alpha/\alpha_0) = f(\Delta\phi)$ can be reconstructed, i.e., the peak values of incidence and sideslip

for any of the banking manoeuvres considered can be approximately computed. The same procedure has been applied to the other three types of peak-amplitude graphs.

Type [B] always occurs in that unstable quadrant in which the divergence is predominantly in the freedom (incidence or sideslip) which is associated with a corresponding lack in static stability (m_w or n_v respectively), *see* Fig. 27. This type of diagram is defined, as shown in Fig. 29, by three quantities, the initial slope, the final slope and the intersection of the final slope with the abscissa, i.e., by the 'critical bank angle' ϕ_T. There is a further feature which allows further simplification of the presentation of the final slope values. When the final slopes for the peak-load diagrams for the three computed values of $(t_p p_0)$ are compared they are practically identical, so that one common value of $\{d(\Delta\alpha/\alpha_0)/d\phi\}_{\text{FINAL}}$ and $\{d(\beta/\alpha_0)/d\phi\}_{\text{FINAL}}$ need only be given for all the complete range of roll-response constants $(t_p p_0)$.

Type [C] occurs at all points along the stability boundaries and is indicative of the neutrally stable state of the aircraft motion in this configuration. This diagram is fully represented by a slope only.

Finally type [D] occurs throughout in that unstable quadrant in which the divergence is due to insufficient static stability in the freedom not associated with the variable in question, i.e., low n_v or ω_ψ for $\Delta\alpha$ and low m_w or ω_θ for β, *see* Fig. 27. The peak loads contained in this type of diagram are essentially small when compared with the corresponding values in the other freedom, i.e., $\Delta\alpha \ll \beta$ or *vice versa*. Thus it was considered sufficient to give only an approximate mean slope through the curve, as they are not likely to constitute a severe design case.

The technique outlined above whereby peak-amplitude data are related to the quadrants of the stability diagram is summarized in Fig. 30 for both $\Delta\alpha$ and β.

3.8. *Presentation of Peak-Amplitude Charts.* For presentation of these data in design charts they were finally entered numerically into a grid of points in the $(\omega_\theta/p_0)^2 - (\omega_\psi/p_0)^2$ plane of a stability diagram for the given values of the inertia ratio A/B, the aircraft damping parameters δ_θ and δ_ψ and the roll-response time constant $(t_p p_0)$. By graphically interpolating between the points obtained, curves were drawn for constant values of all the relevant data, ceiling values, initial slopes, final slopes and critical bank angles. $\Delta\alpha$ and β data are given in separate charts which are arranged in pairs on opposite pages. Each group of charts, representing a given inertia ratio A/B and a given combination of damping parameters δ_θ and δ_ψ is preceded by a single chart for the final slopes for both $\Delta\alpha$ and β as applicable to this group in one common diagram. The charts are plotted against logarithmic co-ordinates of $(\omega_\theta/p_0)^2$ and $(\omega_\psi/p_0)^2$. An index to the charts and an illustration of their arrangement is given in Fig. 31.

4. *The Use and Interpretation of the Peak-Amplitude Charts.* This section will summarize the previous text into the form of instructions for the determination of design peak values of $\Delta\alpha$ and β in cross-coupled rolling manoeuvres.

(i) The frequencies of the basic aircraft oscillations in pitch and in yaw, ω_θ and ω_ψ, must be first obtained either from theoretical or tunnel data, of m_w and n_v and expressed in the form

$$\omega_\theta^2 = -\frac{m_w}{i_B^*}\frac{[V_i/(b/2)]^2}{\mu_{10}} = -\frac{m_w}{i_B}\frac{(V_i/l)^2}{\mu_{10}} \tag{55}$$

and

$$\omega_\psi^2 = \frac{n_v}{i_c}\frac{[V_i/(b/2)]^2}{\mu_{20}} \tag{56}$$

where μ_{20} and μ_{10} are sea-level values of μ_2 and μ_1.

The conditions found not infrequently when either or both of the static stabilities are non-linear is of course not covered in the present investigations. If the non-linearities are only slight, the use of suitably chosen mean values might suffice, in more severe cases, such as with pronounced pitch up, only detailed computations will give satisfactory results.

(ii) The damping of the two aircraft oscillations, δ_θ and δ_ψ must then be determined. δ_ψ being essentially small is of relatively little importance to the present problem, so that an approximate value is usually adequate, as given by the simple expression:

$$\delta_\psi = -0{\cdot}2406 \frac{\frac{n_r}{i_c} + y_v}{\omega_\psi} \frac{\sigma V}{W/S} \tag{57}$$

Similarly:

$$\delta_\theta = -0{\cdot}2406 \frac{\frac{m_q}{i_B} + Z_W}{\omega_\theta} \frac{\sigma V}{W/S}. \tag{58}$$

In the charts two levels of aircraft damping have been considered:

poor damping with $\delta_\psi = 0{\cdot}1$ and $\delta_\theta = 0{\cdot}2$

good damping with $\delta_\psi = 0{\cdot}5$ and $\delta_\theta = 2{\cdot}0$.

(iii) The simplified stability diagram without considering damping and engine momentum can now be established for the given inertia ratio A/B with the two boundaries at $(\omega_\theta/p_0) = 1$ and $(\omega_\psi/p_0)^2 = (B-A)/(B+A)$.

(iv) Obtain the maximum steady rolling velocities for each of the flight conditions considered and compute the corresponding minimum values of the parameters $(\omega_\theta/p_0)^2_{\text{MIN}}$ and $(\omega_\psi/p_0)^2_{\text{MIN}}$. The range of rates of roll can now be represented in the stability diagrams by radial lines as in Fig. 8 starting from the point $(\omega_\theta/p_0)^2 = (\omega_\theta/p_0)^2_{\text{MIN}}$ and $(\omega_\psi/p_0)^2 = (\omega_\psi/p_0)^2_{\text{MIN}}$. Now a rough assessment of the most critical rolling velocity p_0 can be made by taking a point nearest to the centre of the unstable region crossed by this line. More reliable answers will, of course, be obtained by inspecting the appropriate peak-amplitude chart. Due to the logarithmic scales used for these charts the radial lines representing variable rate of roll in the linear diagram, will now always be lines at 45° to the axes. In order to facilitate the location of a given condition or of a range of rolling velocities for a given flight condition, the nomogram given in Chart 43 can be cut out and used in conjunction with the peak-amplitude charts.

(v) The effect of engine momentum should now be checked by applying the corresponding corrections to the two frequency parameters:

$$\left\{\left(\frac{\omega_\theta}{p_0}\right)^2 + \frac{I_e\omega_e}{Bp_0}\right\} \text{ and } \left\{\left(\frac{\omega_\psi}{p_0}\right)^2 + \frac{I_e\omega_e}{Cp_0}\right\}$$

taking whichever sign of p will give the more severe response.

(vi) Now the roll-response time constant must be established for each flight condition by calculating first the 'natural' aircraft response time

$$t_\xi = -13{\cdot}05 \frac{W/S}{V_i\sqrt{\sigma}} \frac{i_A}{l_p}$$

and correcting this value then for the effect of pilot's control using Figs. 22 and 23 to obtain the response time constant t_p describing the actual roll manoeuvre. It is realized that in some extreme cases the range of $(t_p p_0)$ covered in the present results does not completely cover all possible control manoeuvres, it will, however, be usually possible to extrapolate beyond the largest value of $(t_p p_0) = 2{\cdot}0$ presented.

(vii) The incidence of the principal inertia axis must now be determined for each of the flight conditions, using the incidence under 'g' when rolling pull-outs or bank reversal are considered.

(viii) The peak-amplitude charts for the appropriate values of A/B, δ_θ and δ_ψ, and $(t_p p_0)$ can now be selected by referring to the index in Fig. 31. From these charts estimates of the peak values in incidence and sideslip and their variations with the duration of the manoeuvre, i.e., the manoeuvre bank angle $\Delta\phi$ can be read. This may be facilitated by using the nomograms given on Chart 43. Thus by reference to the explanatory illustrations in Fig. 30 graphs of

$$\Delta\alpha_{\mathrm{MAX}} = f(\Delta\phi) \text{ and } \beta_{\mathrm{MAX}} = f(\Delta\phi)$$

can be drawn. The incidence $\Delta\alpha$ is an incremental value and the actual peak aerodynamic incidence must be computed as

$$\alpha_{\mathrm{MAX}} = \Delta\alpha_{\mathrm{MAX}} + \alpha_0 + \alpha_w$$

where α_w is the wing incidence with respect to the principal inertia axis. If required the data may be interpolated.

(ix) The graphs of α_{MAX} $(\Delta\phi)$ and $\beta(\Delta\phi)$ will now permit the evaluation of peak amplitudes for a given change of angle of bank manoeuvre through $\Delta\phi$ or alternatively determine manoeuvring restrictions by limiting bank angle or rate of roll for structural integrity.

(x) Finally it is advisable to check for the possibility of autorotational rolling states using Fig. 18 and equation (39). This phenomenon is usually associated with a negative inclination of the principal inertia axis.

(xi) The data presented in this report cover most of the practical rolling manoeuvres and also the more important aircraft parameters. The results may therefore be taken as a guide for the assessment of the severity of the cross-coupling phenomena for a given aircraft.

However there are two important omissions:

(i) Roll reversal is not considered. This manoeuvre should be expected to give loads in excess of those obtained when rolling through a comparable bank angle in one direction only.

(ii) The aerodynamic cross-derivatives n_p (yawing due to roll) and n_ξ (yawing due to aileron) have been neglected. If any or both of these are large in relation to n_v, they may noticeably affect the aircraft response in rolls. If the results obtained from the charts in this report give critical loads it may be necessary to check these by more detailed calculations, i.e., by computing the complete equations (1 to 6) or the simplified form in equations (8 to 11).

5. *Conclusions.* Based on a large number of analogue computations, charts are presented for the evaluation of peak amplitudes in incidence and sideslip for most practical rolling manoeuvres including rolling pull-outs and bank reversals, but excluding roll-reversal.

The charts cover a comprehensive range of the principal parameters governing the effects of inertia cross coupling on the aircraft response. The derivatives n_p and n_ξ are neglected, this may in

some cases cause inaccuracies demanding more detailed calculations. The effect of the more important parameters is analysed in the text and their influence may be summarized:

(i) An aircraft will develop large amplitudes in incidence and/or sideslip or it will actually become divergent in these variables, if it is rolled with rates of roll at or near critical values. These critical rates of roll are determined by the frequencies of the familiar lateral and longitudinal oscillations of the aircraft.

(ii) Deficiencies in n_v will produce divergence predominantly in sideslip, marginal m_w will result in a divergence predominantly in pitch.

(iii) Aircraft damping will reduce the severity of the aircraft response.

(iv) Engine momentum will worsen the aircraft response slightly for rolling in a sense opposite to the rotation of the engine and *vice versa*.

(v) Increasing inertia in roll in relation to inertia in pitch will reduce the possibility of a yawing divergence, the pitch divergence for marginal m_w will, however, be unchanged.

(vi) The aircraft amplitudes and thus the loads will be proportional to the initial incidence of the principal inertia axis. Considering rolling pull-outs and bank reversal manoeuvres the incidence appropriate to the steady normal acceleration of the given manoeuvre must be taken and the response will be correspondingly more severe.

(vii) The time lag of the aircraft rolling in response to aileron application has a considerable influence on the magnitude of the peak amplitudes in sideslip and incidence, resulting from cross-coupled rolling. The shorter the roll-response time lag, the more violent will be the aircraft motion and as a consequence the resulting loads.

Acknowledgements. The task of compiling the mass of data described in this report would have been impossible but for the untiring labour of many helpers. Of these the author wishes to thank in particular, Miss L. Klanfer, who carried the main burden of the computations and the reduction of the data into charts and Messrs. W. Chinn, J. E. Nethaway and J. Burnham, for their assistance during the work on the simulator. He also wishes to acknowledge the co-operation of Mr. T. R. Stretton and his staff who have made the simulator available for this programme and given their full assistance throughout the computations.

LIST OF SYMBOLS

A Inertia in roll

B Inertia in pitch

b Span

C Inertia in yaw

$D = \frac{d}{dp_0 t}$, differential operator

$F = \frac{p}{p_0}$, non-dimensional rolling rate

g Gravitational acceleration

$i_A = \frac{A}{m(b/2)^2}$, inertia coefficient in roll

$i_B{}^* = \frac{B}{m(b/2)^2}$, inertia coefficient in pitch

$i_B = \frac{B}{ml^2}$, inertia coefficient in pitch

$i_C = \frac{C}{m(b/2)^2}$, inertia coefficient in yaw

I_e Inertia of engine rotor about rotor axis

$K = \omega_e I_e$, engine momentum (position for clockwise engine rotation)

L Rolling moment

$L_\xi = \frac{dL}{d\xi}$, aileron power

$L_p = \frac{dL}{dp}$, damping in roll

$L_v = \frac{dL}{d\beta}$, rolling moment due to sideslip

$l_\xi = \frac{dC_l}{d\xi}$

$l_p = \frac{dC_l}{d\left(\frac{pb}{2V}\right)}$

$l_v = \frac{dC_l}{d\beta}$

l Tail arm; characteristic length in longitudinal stability

M Pitching moment

$M_\alpha = \frac{dM}{d\alpha}$, static stability

$M_q = \frac{dM}{dq}$, damping in pitch

$M_{\dot{\alpha}} = \frac{dM}{d\dot{\alpha}}$

$m_w = \frac{1}{2}\frac{dC_m}{d\alpha}$, static-stability derivative

$m_q = \frac{1}{2}\frac{dC_m}{d\frac{ql}{V}}$, pitch-damping derivative

N Yawing moment

$N_\beta = \frac{dN}{d\beta}$, weathercock stability

$N_r = \frac{dN}{dr}$, damping in yaw

$n_v = \frac{dC_n}{d\beta}$, weathercock-stability derivative

$n_r = \frac{dC_n}{d\frac{rb}{2V}}$, damping in yaw derivative

p Rate of roll (rad/sec)

p_0 Steady rate of roll

$\bar{p} = \frac{p}{p_0}$, non-dimensional rate of roll

q Rate of pitch

$\bar{q} = \frac{q}{q_0}$, non-dimensional rate of pitch

r Rate of yaw

$\bar{r} = \frac{r}{p_0}$, non-dimensional rate of yaw

S Wing area

T_0 Period of the short-period longitudinal oscillation

T_ψ Period of the lateral oscillation

t Time

t_1 Duration of aileron application

t_p Roll-manoeuvre time constant

t_ξ Natural roll-response time constant

Y Side force

$Y_\beta = \frac{dY}{d\beta}$

$Y_r = \frac{dY}{dr}$

$Y_p = \frac{dY}{dp}$

$y_v = \frac{1}{2}\frac{dC_y}{d\beta}$, side-force derivative

V True speed (ft/sec)

V_i Indicated speed (ft/sec)

W Aircraft weight

Z Vertical force

$Z_\alpha = \frac{dZ}{d\alpha}$

$Z_q = \frac{dZ}{dq}$

$Z_{\dot\alpha} = \frac{dZ}{d\dot\alpha}$

$z_w = \frac{dC_z}{d\alpha}$, normal-force slope

α Incidence

α_0 Trimmed incidence

$\Delta\alpha$ Incremental incidence

β Angle of sideslip

δ_θ Log decrement of the short-period longitudinal oscillation

δ_ψ Log decrement of the lateral oscillation

ψ Angle of yaw

θ Angle of pitch

ϕ Angle of bank

ϕ_T Critical angle of bank

$\Delta\phi$ Total bank-angle change in a rolling manoeuvre

ω_θ = $\frac{2\pi}{T_\theta}$, frequency of short-period pitching oscillation

ω_ψ = $\frac{2\pi}{T_\psi}$, frequency of lateral oscillation

ω_e Angular velocity of engine (positive clockwise)

ξ Aileron angle

ξ_0 Steady aileron angle

μ_{20} = $26{\cdot}2\frac{W/S}{b}$, relative lateral density at sea level

μ_{10} = $13{\cdot}10\frac{W/S}{l}$, relative longitudinal density at sea level

σ = ρ/ρ_0 Relative density

REFERENCES

No.	*Author*	*Title, etc.*
1	J. E. Nethaway and J. Clark	Inertia cross coupling effects during rolling of a delta aircraft (Boulton Paul IIIA). A.R.C. 22,113. February, 1960.
2	William H. Phillips	Effect of steady rolling on longitudinal and directional stability. N.A.C.A. Tech. Note 1627. June, 1948.
3	Ordway G. Gates and C. H. Woodling	A theoretical analysis of the effect of engine angular momentum on longitudinal and directional stability in steady rolling manoeuvres. N.A.C.A. Tech. Note 4249. April, 1958.
4	W. J. G. Pinsker	Preliminary note on the effect of inertia cross coupling on aircraft response in rolling manoeuvres. A.R.C. C.P.435. November, 1955.
5	D. E. Fry and W. J. G. Pinsker ..	Theoretical analysis of the effect of engine gyroscopic coupling on the lateral and longitudinal motion of aircraft. Unpublished M.O.A. Report.
6	Joseph Weil and Richard E. Day ..	An analogue study of the relative importance of various factors affecting roll coupling. N.A.C.A. Research Memo. H56A06. TIL 5077. April, 1956.
7	W. J. G. Pinsker	Aileron control of small aspect ratio aircraft in particular delta aircraft. A.R.C. R. & M. 3188. October, 1953.

APPENDIX I

The Product Terms in the Euler Equations as Centrifugal Moments

The gyroscopic cross-coupling terms appear in the Euler equations in the form:

$$\Delta M = pr(C-A) \tag{59}$$

$$\Delta N = pq(A-B) \tag{60}$$

$$\Delta L = qr(B-C) \tag{61}$$

Their interpretation and thus the understanding of the resulting divergent flight conditions may be assisted if they are reduced to readily-visualised physical terms.

Taking equation (61) for the pitching moment as an example, it can be seen from Fig. 3 that the two simultaneous angular velocities p and r add up vectorially to a resultant angular velocity

$$\Omega_{pr} = \sqrt{(p^2+r^2)} \tag{62}$$

the axis of which is inclined to the principal inertia axis of the aircraft at an angle ϵ defined by

$$\tan\epsilon = \frac{r}{p} \tag{63}$$

For simplicity, the inertias of the aircraft are represented by two pairs of identical masses so that inertia in yaw

$$C = 2m_1x_1^2 \tag{64}$$

and inertia in roll

$$A = 2m_2x_2^2 \tag{65}$$

It is now readily seen that rotating the aircraft about the axis of the Ω-vector will release centrifugal forces in the sense that the pair of m_1 masses produces a positive (nose up) pitching moment and the m_2-pair, i.e., the contributions to inertia in roll, a negative (nose down) pitching moment, if both the rates of roll and yaw have identical signs. The reverse applies if the two rates have opposite signs so that the angle $\epsilon = \tan^{-1} r/p$ becomes negative.

The centrifugal pitching moment is

$$M = \sum F_1x_1\cos\epsilon + \sum F_2x_2\sin\epsilon \tag{66}$$

with the centrifugal forces given as

$$F = m(x\sin\epsilon - 2\cos\epsilon)\Omega^2 \tag{67}$$

$$M = \Omega^2\{\sum m_1x_1^2 - \sum m_2x_2^2\}\sin\epsilon\cos\epsilon$$

using equations (64), (66) and (67)

$$M = p^2\left\{1+\left(\frac{r}{p}\right)^2\right\}\tan\epsilon\cos^2\epsilon\{C-A\}$$

and with equation (65)

$$M = pr\{C-A\}.$$

The gyroscopic Eulerian term equation (59) is thus explained as the action of centrifugal forces acting on the body spinning about an axis not coincident with one of its principal axes.

The same phenomenon is illustrated in Fig. 4 for the yawing-moment term according to equation (62).

The terms $p\alpha$ and $p\rho$ are simply kinematic relations as illustrated in Figs. 5 and 6. In both Figures the aircraft is assumed to perform pure rolling about its body axis. If the aircraft motion starts with an initial incidence α_0, positive sideslip will develop so that after rolling through 90° this sideslip will equal the initial incidence α_0.

Similarly if the aircraft is initially under a sideslip β_0, negative incidence will develop so that after rolling through 90° incidence will be $\alpha = -\beta_0$.

APPENDIX II

Physical Explanation of the Divergencies Due to Rolling

Based on the physical concepts of the product terms affecting the motion of a rolling aircraft as derived in Appendix I, the phenomena leading to divergencies in pitch and yaw can now readily be visualized.

(*a*) The stable region near the origin of the ω_θ-ω_ψ-graph corresponding to very high rates of roll and vanishing static stabilities, i.e., very small values of ω_θ and ω_ψ. If an aircraft rolls around its principal inertia axis with a steady rate p_0, as illustrated in Fig. 10 and this axis is initially inclined to the flight paths it will experience a periodic variation of incidence and sideslip. If the aerodynamic restoring moments m_w and n_v are vanishingly small, this motion goes on undisturbed—the condition is stable. The principal inertia axis will retain its attitude in space.

(*b*) Divergence in pitch of a rolling aircraft with low m_w and large n_v.

Assuming the aircraft again rolls with p_0 about its principal inertia axis, which is initially at an incidence α with respect to the flight paths. (Fig. 11. I.) Due to the kinematic relation

$$p\alpha = \dot{\beta}$$

sideslip tends to develop as shown by the dotted condition in Fig. 11. IIa. If however directional stability n_v is assumed to be very large, this will be suppressed and the aircraft is forced back to line up directionally with the flight path. This imposes a yawing motion into the aircraft which is equal to the $\dot{\beta}$ it is suppressing, i.e.,

$$r = p\alpha. \tag{68}$$

This rate of yaw will combine with rate of roll to a resultant angular velocity Ω, which is aligned with the flight path. As a consequence the centrifugal forces as shown in Fig. 11. IIb will produce a pitching moment

$$M_\alpha = pr(C-A) \approx prB = p^2\alpha B. \tag{69}$$

If this pitching moment is greater than the aerodynamic restoring moment

$$M_R = \alpha M_\alpha \tag{70}$$

holding the aircraft at this incidence, the incidence will increase and so on *ad infinitum*. The motion is thus unstable if

$$M_G > -M_R,$$

i.e., if

$$p^2 > -\frac{M_\alpha}{B} = \omega_\theta{}^2. \tag{71}$$

(*c*) A similar process is responsible for the divergence in yaw for aircraft with small n_v and large m_w (Fig. 12). The aircraft rolls with an initial disturbance in sideslip β which gives kinematically

$$p\beta = -\dot{\alpha}$$

and if m_w is large enough to suppress this build up in α

$$p\beta = q. \tag{72}$$

If the gyroscopic yawing moment

$$N_G = pq(A-B) = p^2\beta(A-B) \tag{73}$$

is larger than the directional restoring moment

$$N_R = \beta N_\beta$$

sideslip will increase progressively. Thus the motion is unstable if

$$N_G > -N_R$$

or

$$p^2 > -\frac{N_\beta}{A-B} = +\frac{N_\beta}{C}\frac{C}{B-A},$$

i.e., if

$$p^2 > \omega_\psi{}^2 \frac{C}{B-A}.$$

If inertia in roll $A \geqslant B$, this type of instability will not occur for even very low values of ω_ψ, as is illustrated in Fig. 13.

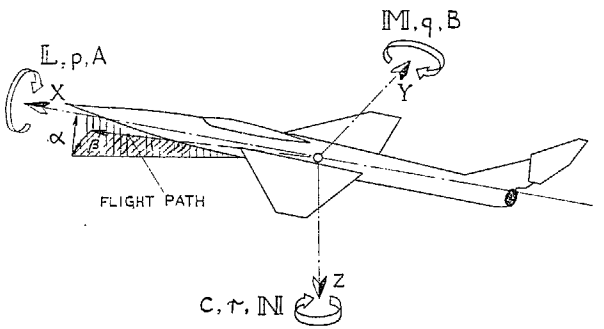

FIG. 1. System of axes used in the analysis.

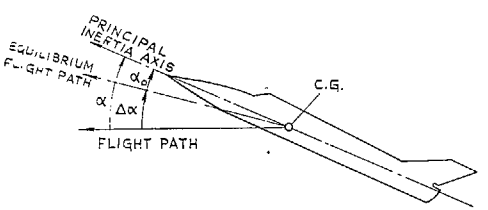

FIG. 2. Definitions of incidences.

α_0 = Initial trimmed
α = Instantaneous
$\Delta\alpha$ = Incremental

} Incidence of principal inertia axis.

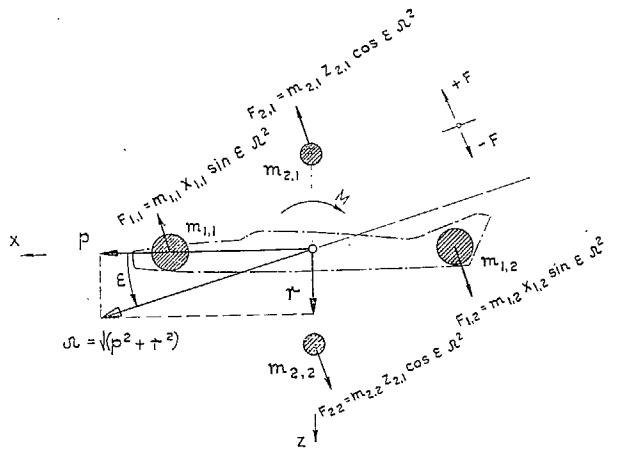

FIG. 3. The gyroscopic product terms as centrifugal moments. Pitching moment, $M = pr(C-A)$.

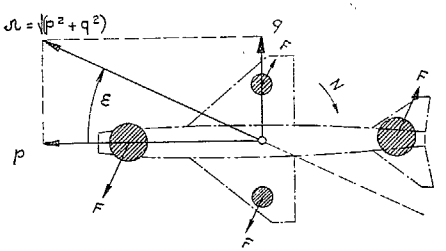

FIG. 4. The gyroscopic yawing moment, $N = pq(A-B)$.

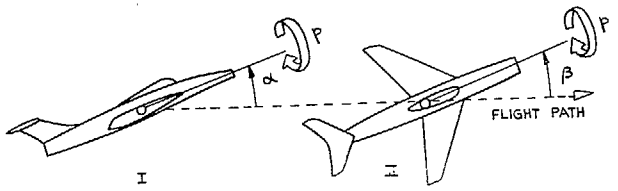

FIG. 5. The effect of the kinematic term $p\alpha = \dot{\beta}$ on the build up of sideslip when rolling about the body axis at an incidence to the flight path.

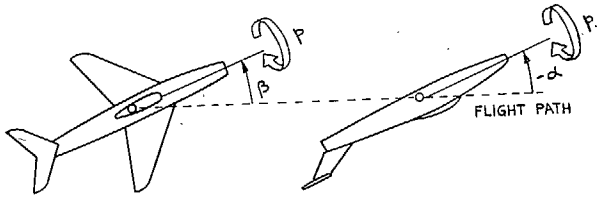

FIG. 6. The effect of the kinematic term $p\beta = -\dot{\alpha}$ on the build up of negative incidence when rolling about the body axis at an angle of sideslip β to the flight path.

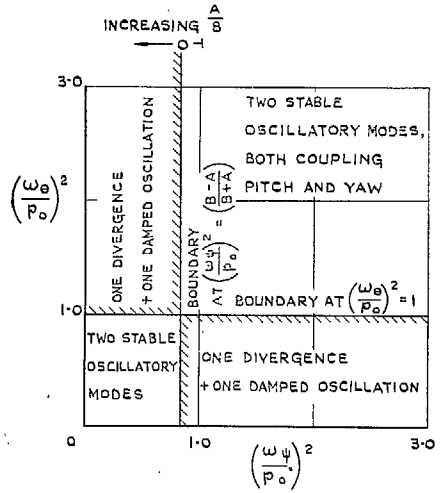

FIG. 7. Stability of the rolling aircraft (Phillip's diagram).

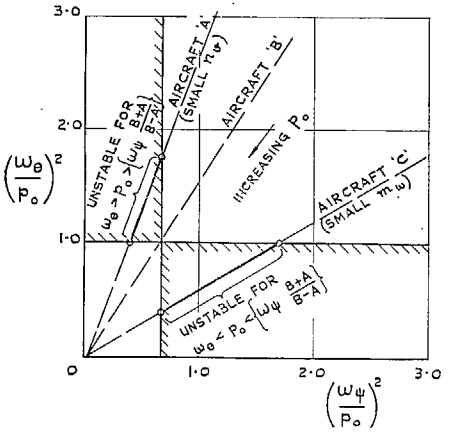

FIG. 8. Stability changes over the range of rolling velocities for three aircraft configurations.

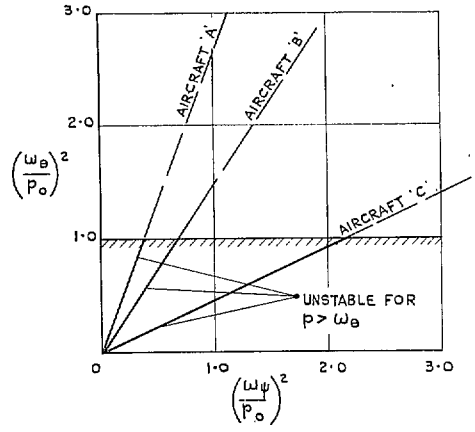

FIG. 9. Effect of increasing inertia in roll A to $A = B$.

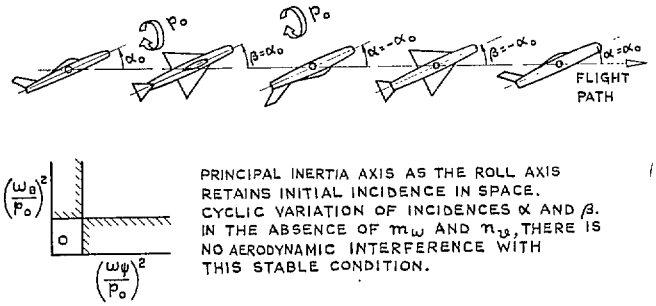

FIG. 10. Stable rolling motion with vanishingly small aerodynamic restoring moments m_w and n_ϑ or very large rates of roll p_0.

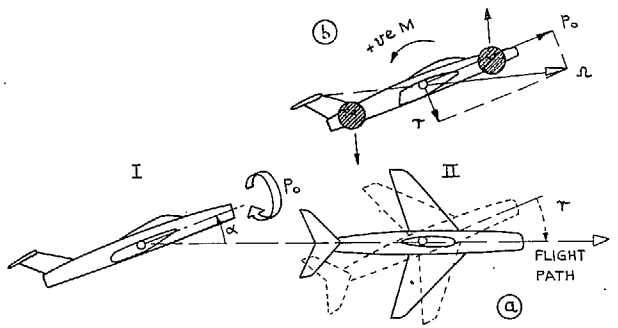

INSTANT I AIRCRAFT ROLLS WITH STEADY RATE p_o. INITIAL INCIDENCE α.

INSTANT II a) DUE TO THE KINEMATICS OF THE MOTION, SIDESLIP WANTS TO DEVELOP. THE POWERFUL DIRECTIONAL STABILITY n_v HOWEVER, FORCES THE AIRCRAFT BACK TO LINE UP DIRECTIONALLY. WITH THE FLIGHT PATH, THEREBY IMPOSING A POSITIVE RATE OF YAW Υ.

b) THIS RATE OF YAW Υ COMBINES WITH RATE OF ROLL p_o TO CAUSE THE AIRCRAFT TO ROLL ALONG AN AXIS APP. COINCIDENT WITH THE FLIGHT PATH. RESULTING CENTRIFUGAL FORCES WILL TEND TO INCREASE THE INCIDENCE. THIS WILL LEAD TO A VICIOUS CYCLE IF THE STATIC STABILITY IN PITCH IS INSUFFICIENT TO PREVENT A PROGRESSIVE BUILD UP OF α.

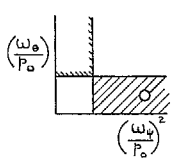

FIG. 11. Illustration of the rolling motion leading to divergence in pitch due to inadequate m_w.

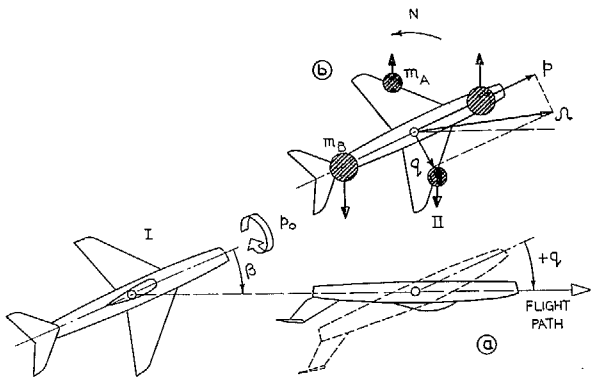

INSTANT I AIRCRAFT ROLLS WITH STEADY RATE p_o AND IS DISPLACED BY INITIAL DISTURBANCE IN SIDESLIP β_o.

INSTANT II(a) DUE TO THE KINEMATICS OF THE MOTION INCIDENCE WANTS TO DEVELOP. THE POWERFUL LONGITUDINAL STABILITY FORCES THE AIRCRAFT TO LINE UP WITH THE FLIGHT DIRECTION, THEREBY IMPOSING A POSITIVE RATE OF PITCH.

(b) THIS RATE OF PITCH WILL COMBINE WITH RATE OF ROLL SO THAT THE AIRCRAFT ROLLS ABOUT AN AXIS APP. COINCIDENT WITH THE FLIGHT PATH. THE RESULTING CENTRIFUGAL FORCES ACTING ON THE PITCH INERTIA COUPLE m_B WILL PRODUCE A YAWING MOMENT SO AS TO INCREASE THE INITIAL SIDESLIP AND LEAD TO A DIVERGENCE IF DIRECTIONAL STABILITY IS INSUFFICIENT TO PREVENT A PROGRESSIVE BUILD UP.

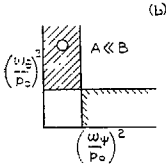

FIG. 12. Illustration of the rolling motion leading to divergence in yaw due to inadequate n_v.

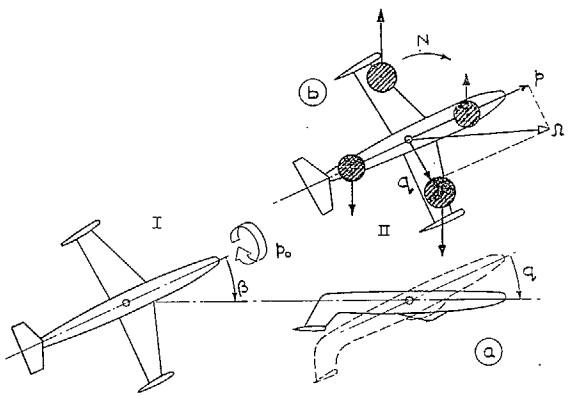

FIG. 13. Illustration of the rolling motion of an aircraft with $A \geqslant B$ being stable even for vanishing n_v.

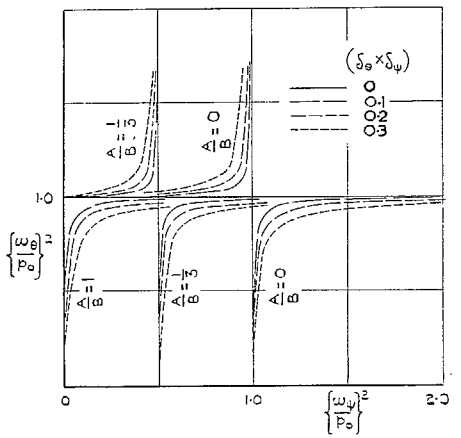

FIG. 14. Effect of aircraft damping on the stability boundaries.

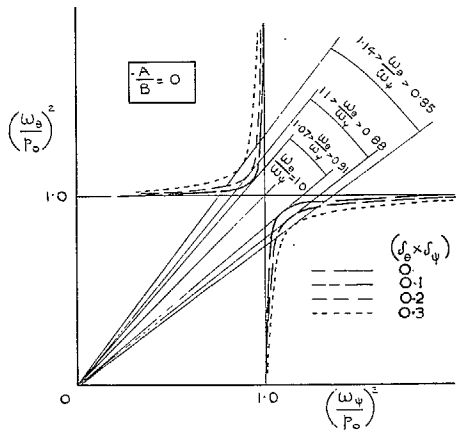

FIG. 15. Effect of aircraft damping on the range of frequency ratios $\omega_\theta/\omega_\psi$ for which no roll divergence occurs for all values of p_0.

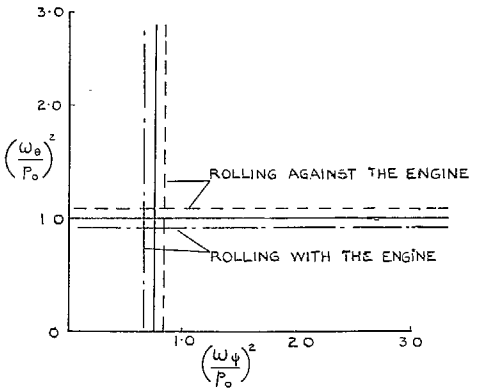

FIG. 16. Effect of engine momentum on the stability boundaries of the rolling aircraft.

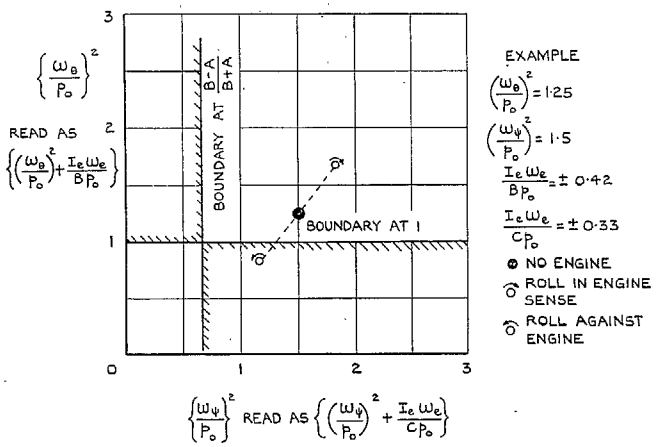

FIG. 17. Interpretation of data obtained without considering engine momentum.

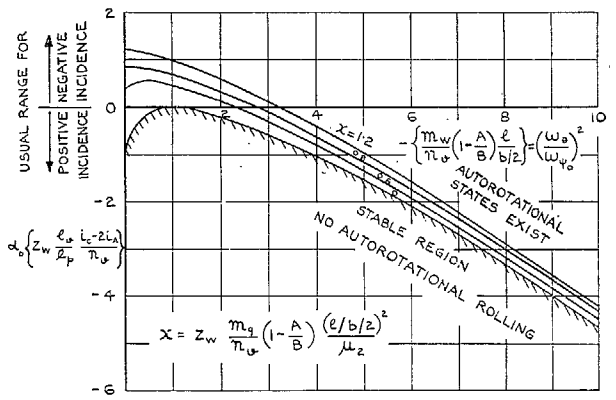

FIG. 18. Boundaries of critical values of α_0 below which autorotational instability in roll exists.

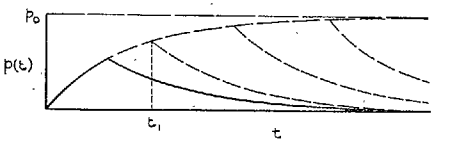

FIG. 19. Family of aircraft roll manoeuvres with varying duration.

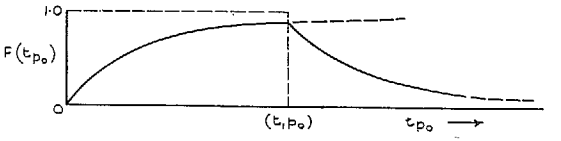

FIG. 20. Rolling manoeuvre described in non-dimensional units used in the computations.

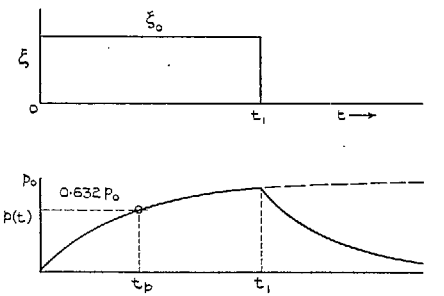

FIG. 21. Response of an aircraft with freedom in roll only to a square-top function in aileron.

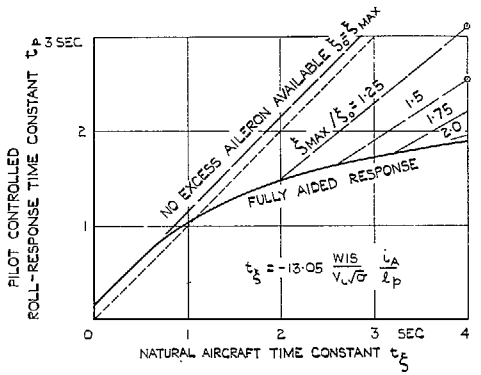

FIG. 22. Expected values of practical roll-response time constant t_p against natural time constant t_ξ of aircraft to aileron step.

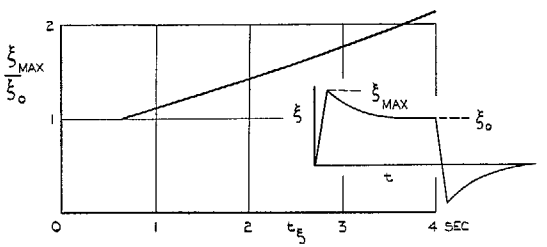

FIG. 23. Peak aileron angles ξ_{MAX} required to achieve the fully-aided response assumed in Fig. 22.

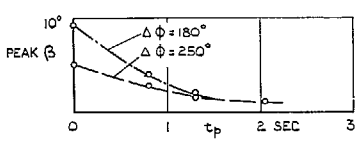

FIG. 24. Effect of roll-response time t_p on peak loads in sideslip during rolling manoeuvres.

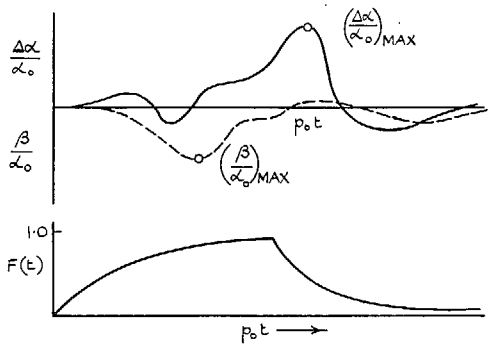

FIG. 25. Typical example of a response in $\Delta\alpha$ and β to a rolling manoeuvre and the computation of maximum values $\Delta\alpha$ and β.

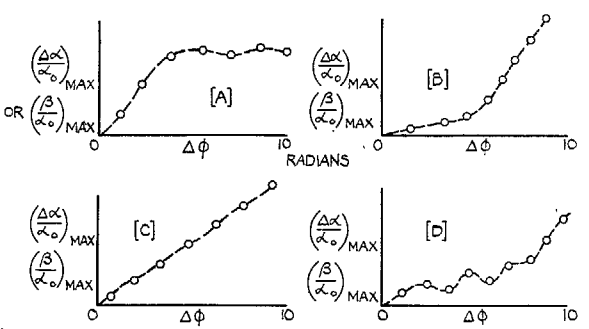

FIG. 26. The four types of plots of peak values of $\Delta\alpha$ or β against manoeuvre—bank angle $\Delta\phi$.

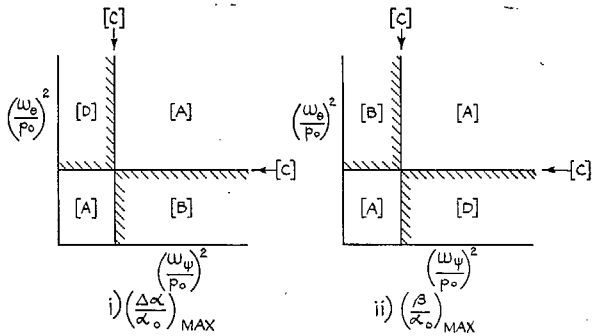

FIG. 27. Location of the four principal types of the plots $(\Delta\alpha/\alpha_0)_{MAX} = f(\Delta\phi)$ and $(\beta/\alpha_0)_{MAX} = f(\Delta\phi)$ in the stability diagram. Type [C] occurs along the stability boundaries throughout.

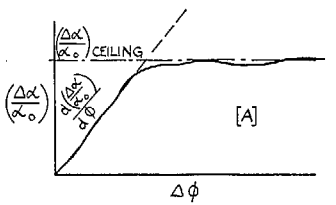

FIG. 28. Representation of peak-amplitude diagram. Type [A] by ceiling value and initial slope.

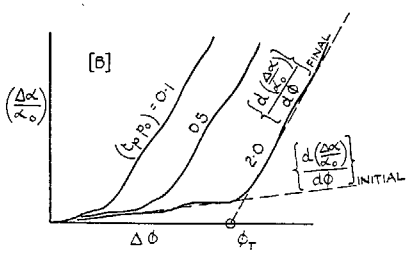

FIG. 29. Representation of peak-amplitude diagram. Type [B] by initial slope, final slope and critical bank angle ϕ_T

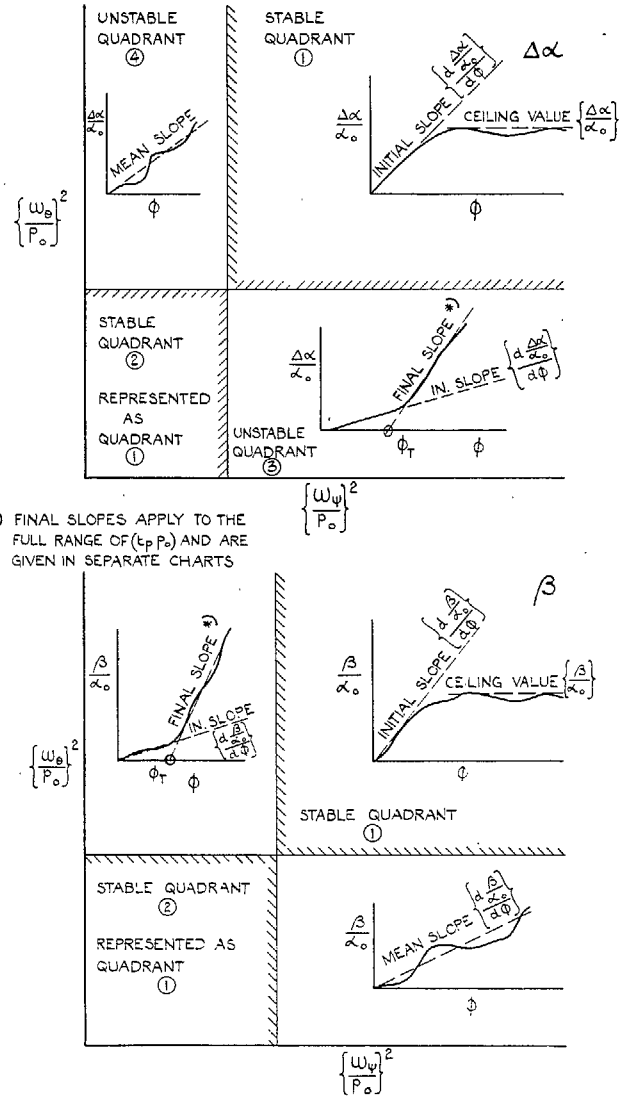

FIG. 30. Representation of peak-amplitude variation with manoeuvre bank angle ϕ in the ψ quadrants of the stability plane $(\omega_0/p_0)^2 - (\omega_\psi/p_0)^2$.

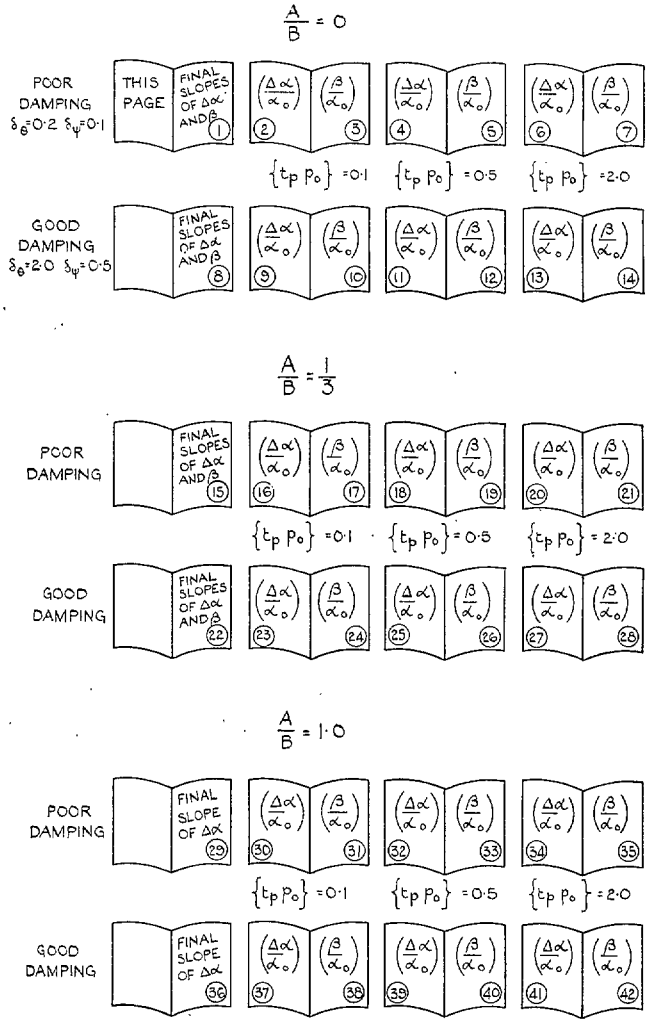

FIG. 31. Arrangement of and index to peak-amplitude charts.

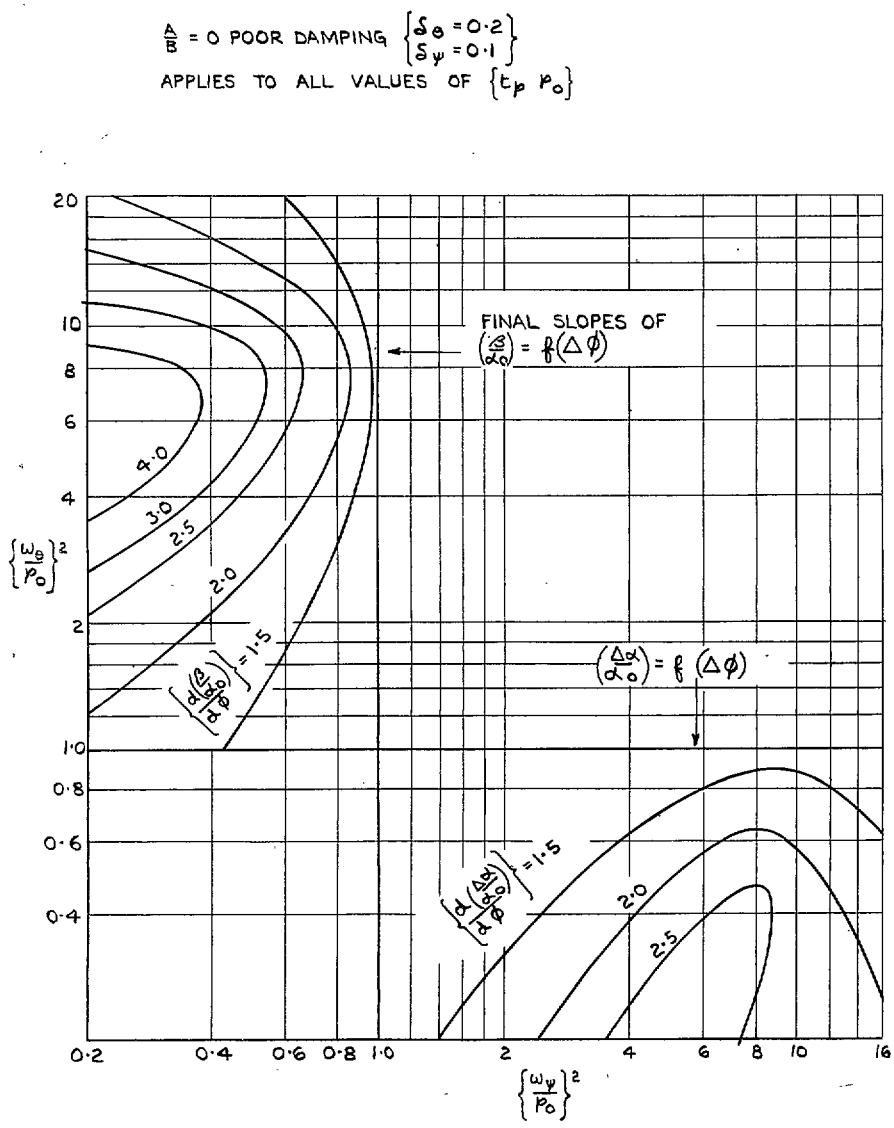

CHART 1. Final slopes of $\Delta\alpha_{MAX}$ and β_{MAX} against manoeuvre bank angle, $\Delta\phi$. $A/B = 0$, poor damping.

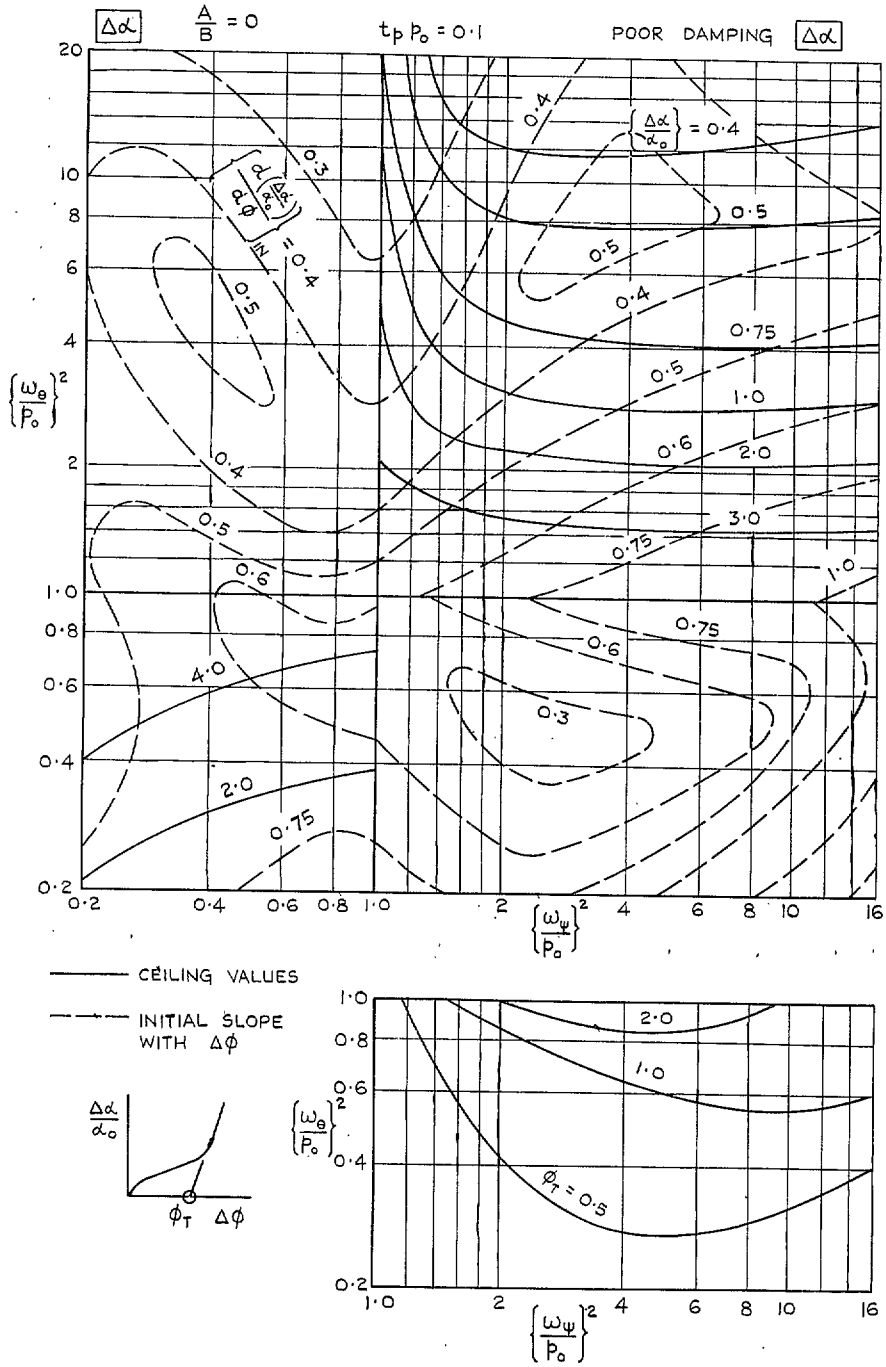

CHART 2. Ceiling values, and initial slopes with $\Delta\phi$, of incidence peak values, $\Delta\alpha_{MAX}$, and critical bank angle for pitch divergence, ϕ_T. $A/B = 0$, $(t_p p_0) = 0 \cdot 1$, poor damping.

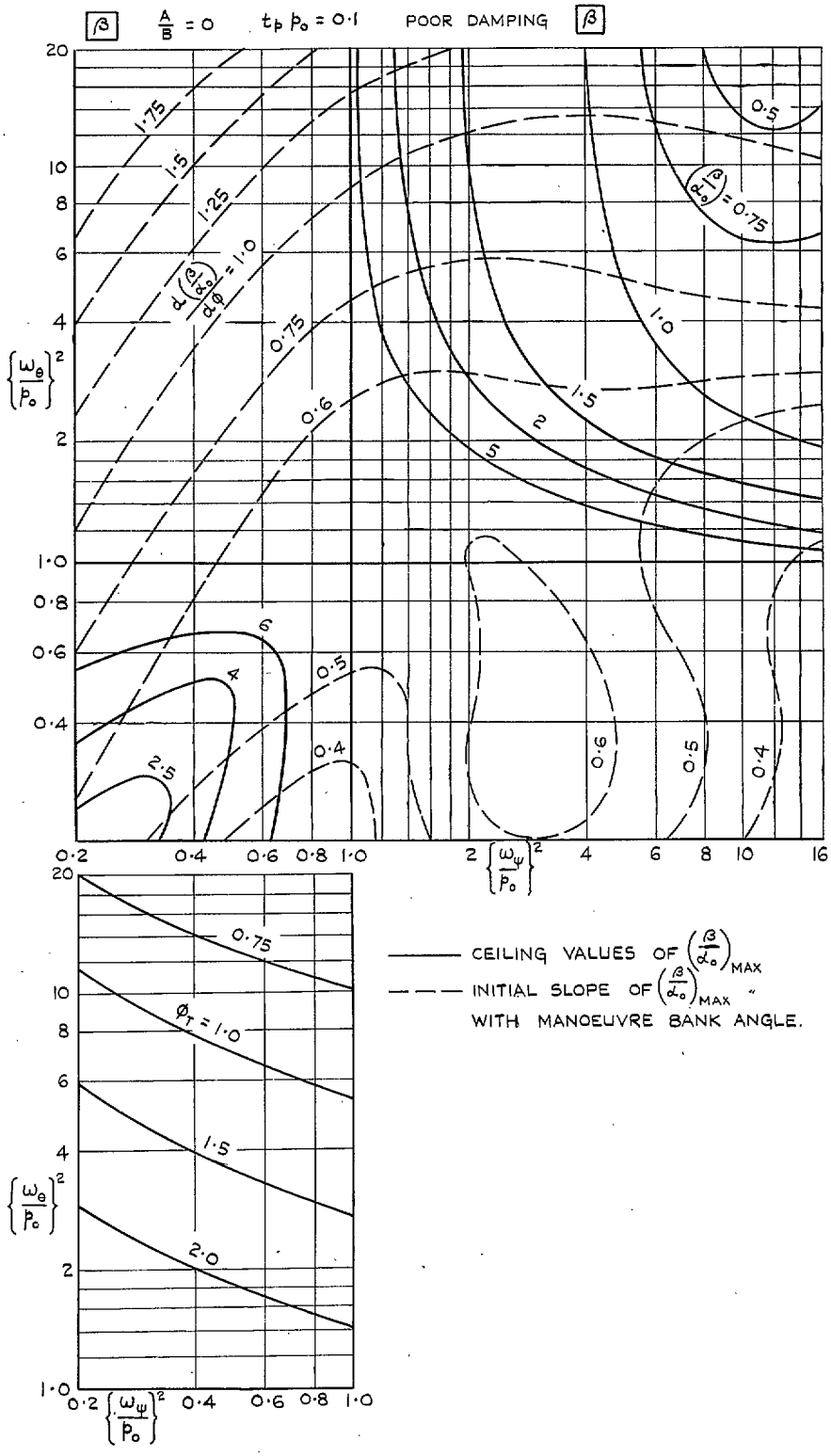

CHART 3. Ceiling values, and initial slopes with $\Delta\phi$, of sideslip peak values, β_{MAX}, and critical bank angle for yaw divergence, ϕ_T.

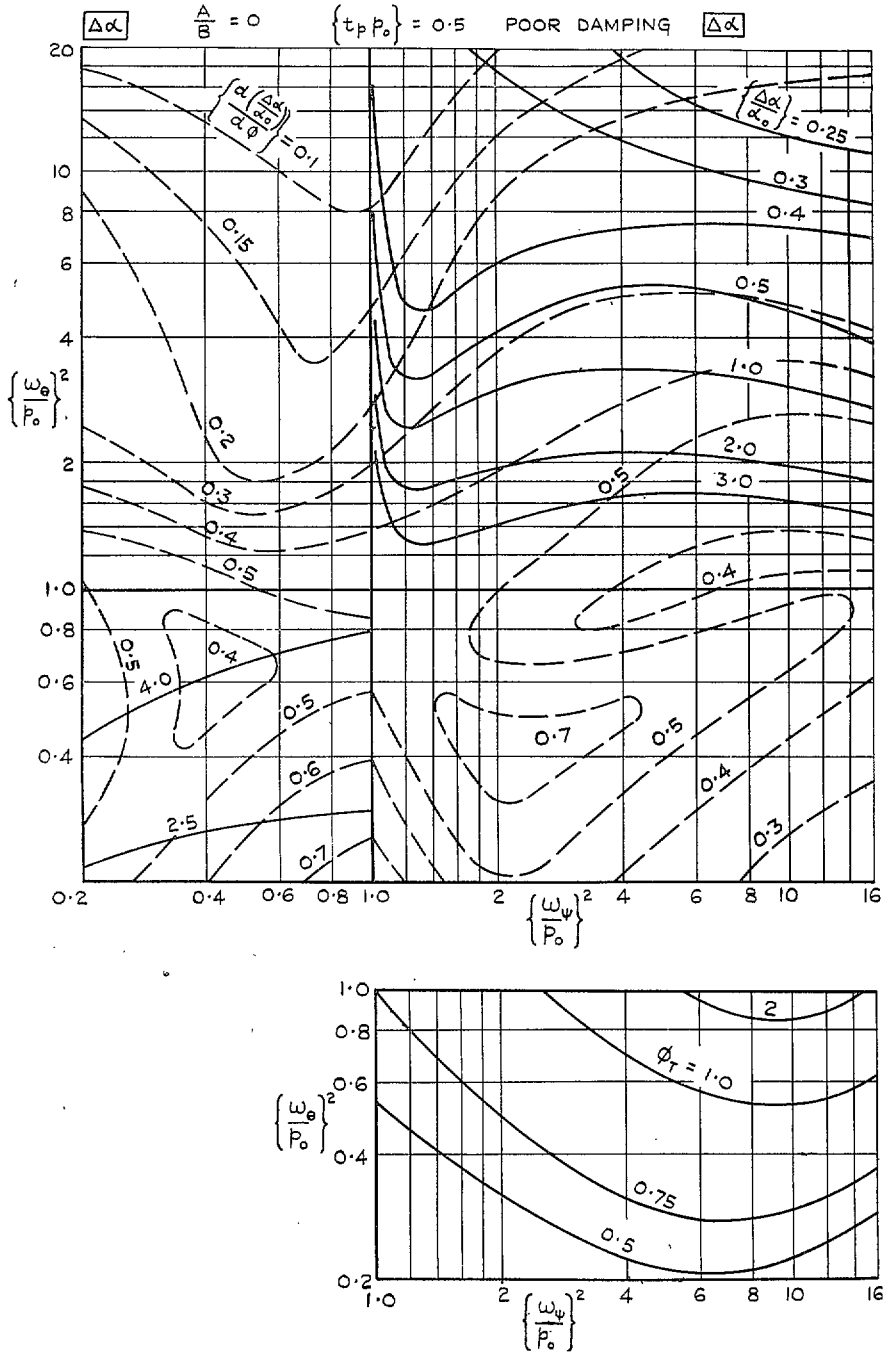

CHART 4. Ceiling values and initial slopes with $\Delta\phi$, of incidence peak values, $\Delta\alpha_{MAX}$, and critical bank angle for pitch divergence, ϕ_T. $A/B = 0$, $\{t_p p_0\} = 0{\cdot}5$, poor damping, $\delta_\theta = 0{\cdot}2$, $\delta_\psi = 0{\cdot}1$.

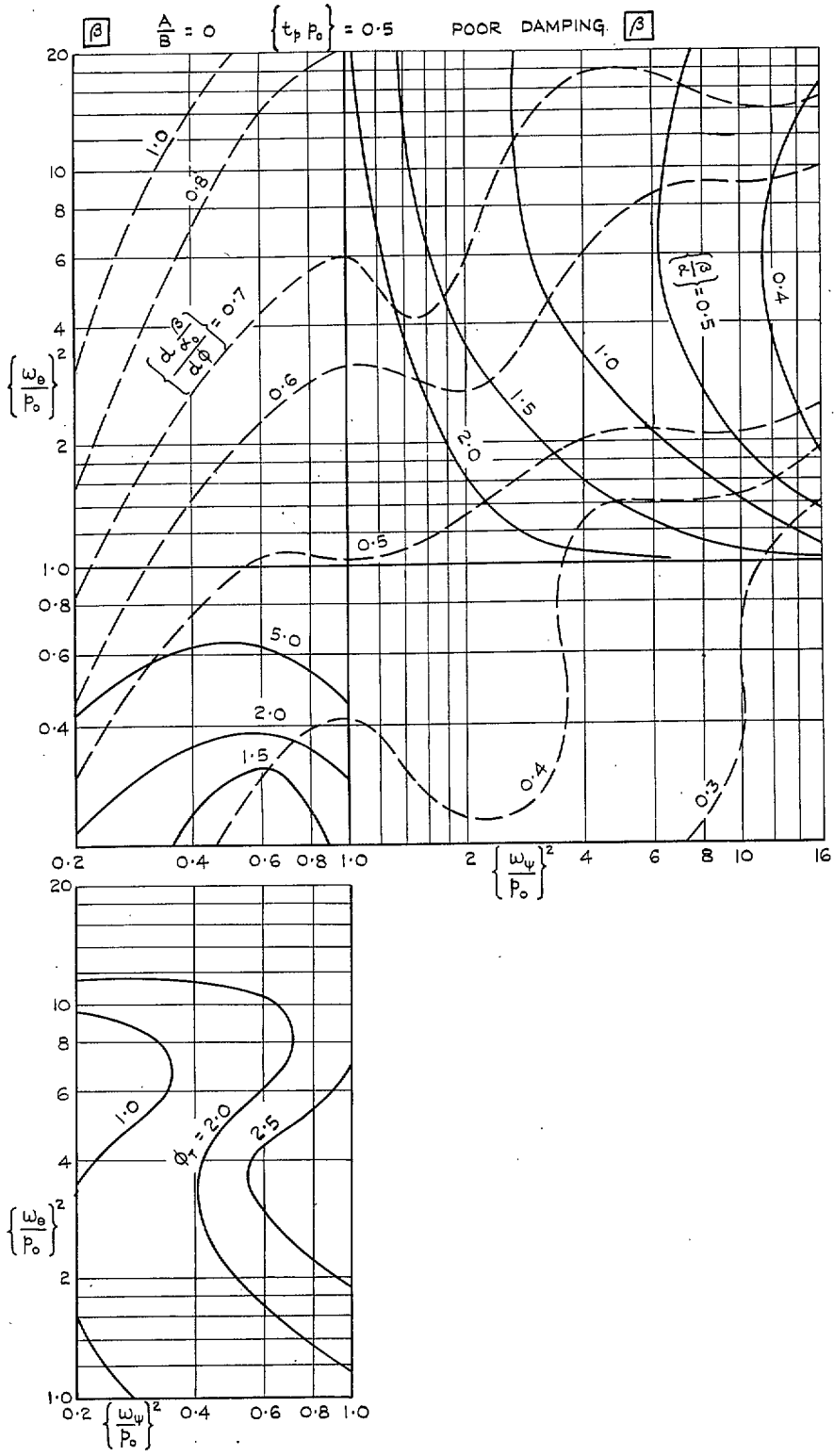

CHART 5. Ceiling values, and initial slopes with $\Delta\phi$, of sideslip peak values, β_{MAX}, and critical bank angle for yaw divergence, ϕ_T. $A/B = 0$, $\{t_p p_0\} = 0{\cdot}5$, poor damping, $\delta_\theta = 0{\cdot}2$, $\delta_\psi = 0{\cdot}1$.

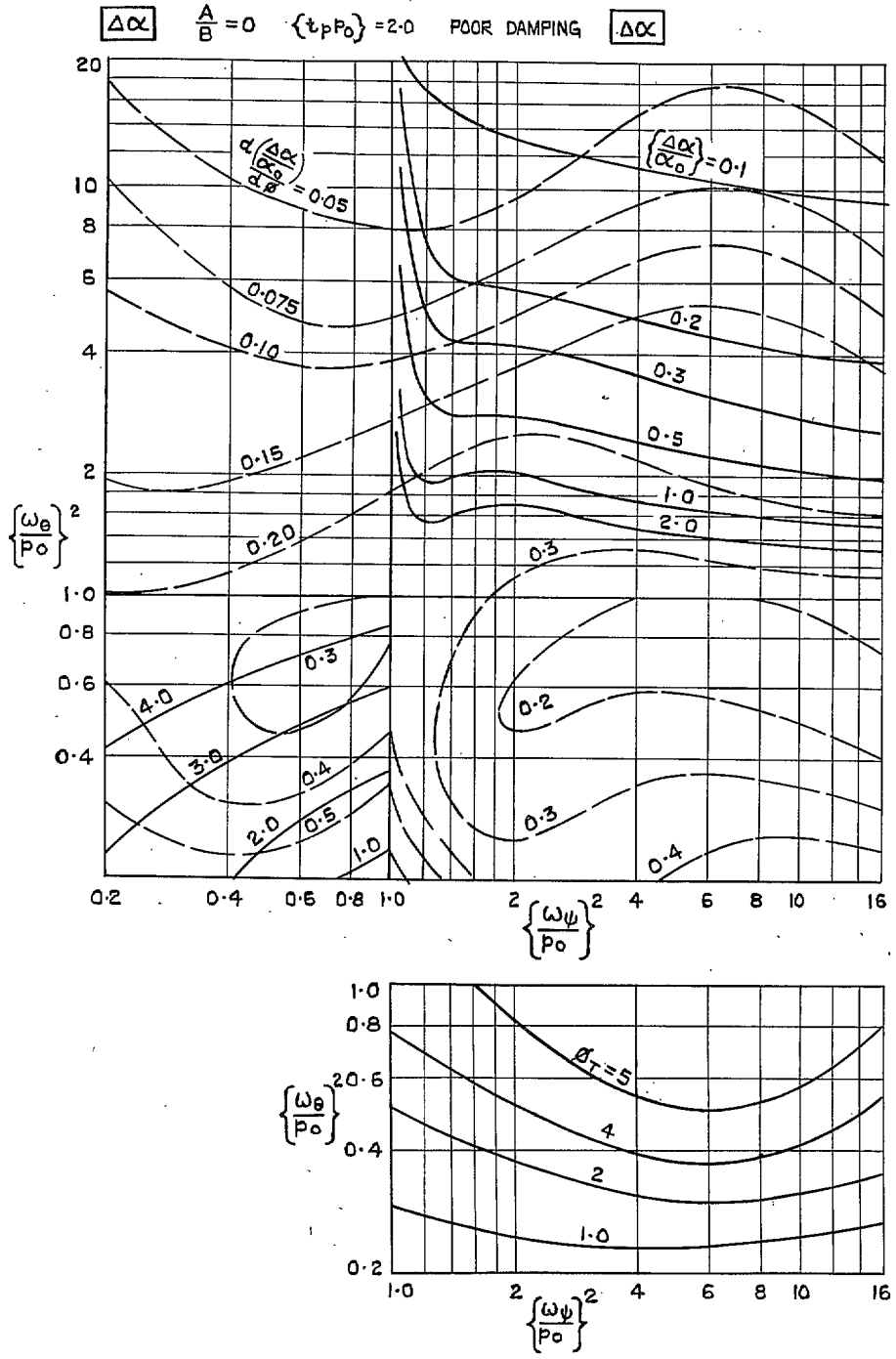

CHART 6. Ceiling values, and initial slopes with $\Delta\phi$, of incidence peak values, $\Delta\alpha_{MAX}$, and critical bank angle for pitch divergence, ϕ_T. $A/B = 0$, $\{t_p p_0\} = 2{\cdot}0$, $\delta_\theta = 0{\cdot}2$, $\delta_\psi = 0{\cdot}1$.

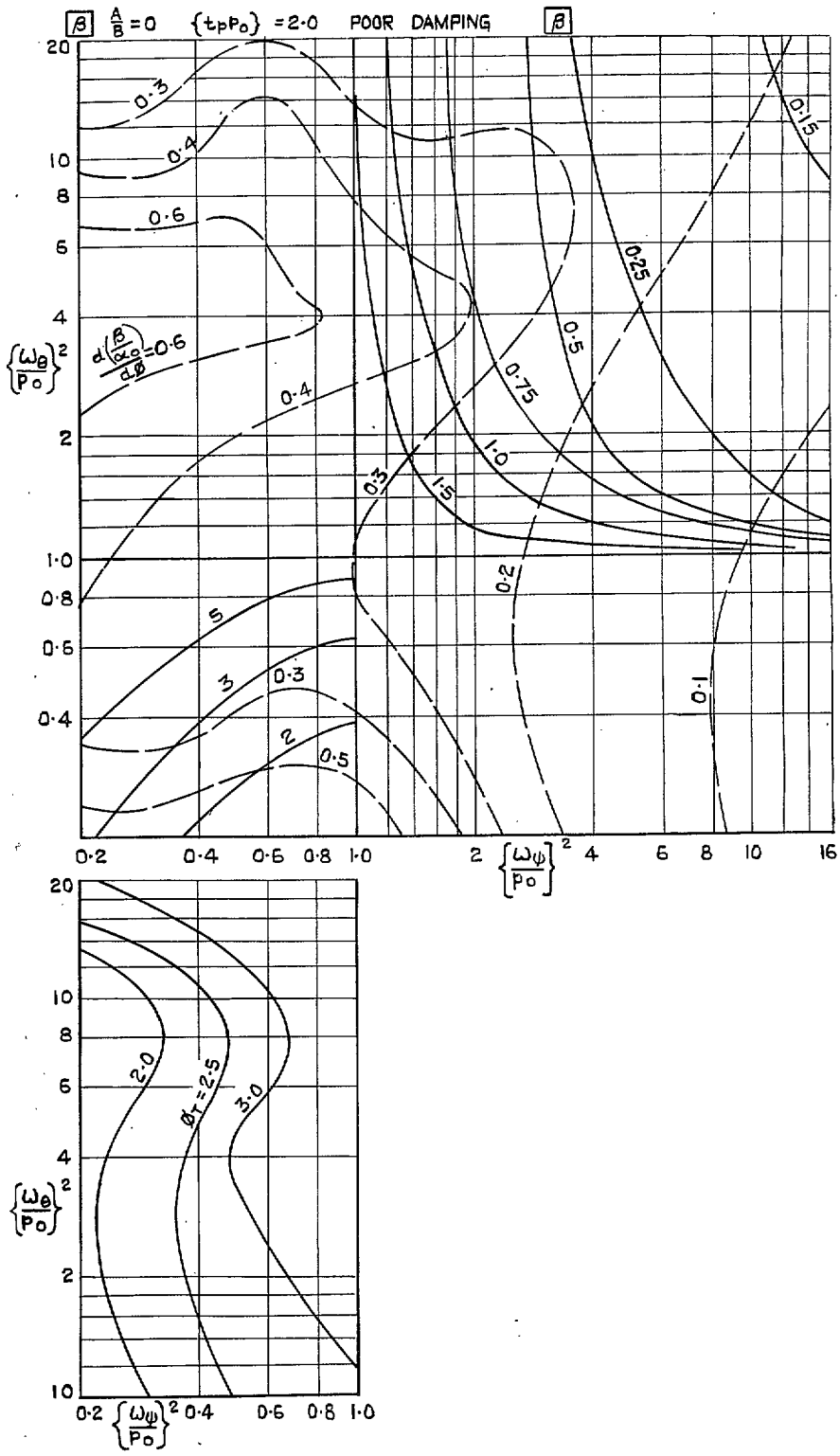

CHART 7. Ceiling values, and initial slopes with $\Delta\phi$, of sideslip peak values, β_{MAX}, and critical bank angle for yaw divergence, ϕ_T. $A/B = 0$, $\{t_p p_0\} = 2{\cdot}0$, $\delta_\theta = 0{\cdot}2$, $\delta_\psi = 0{\cdot}1$.

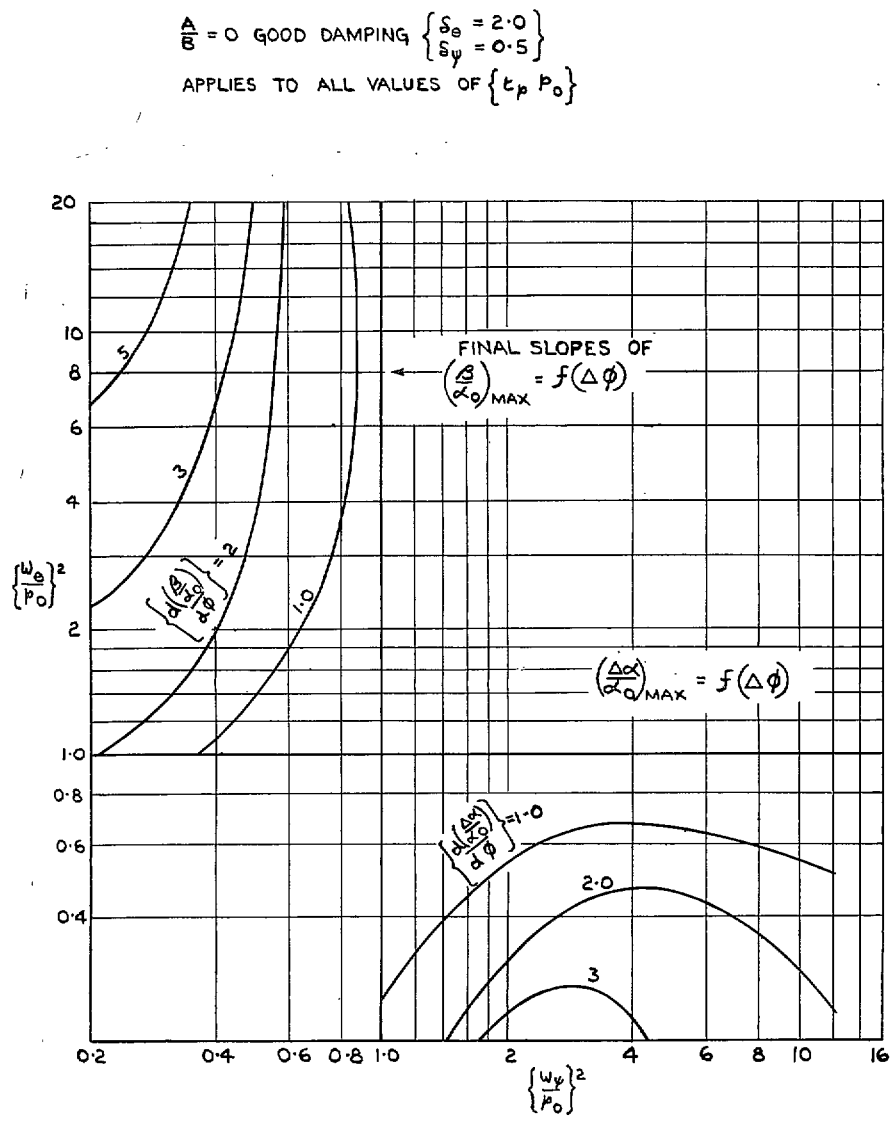

CHART 8. Final slopes of $\Delta\alpha_{MAX}$ and β_{MAX} with manoeuvre bank angle, $\Delta\phi$.

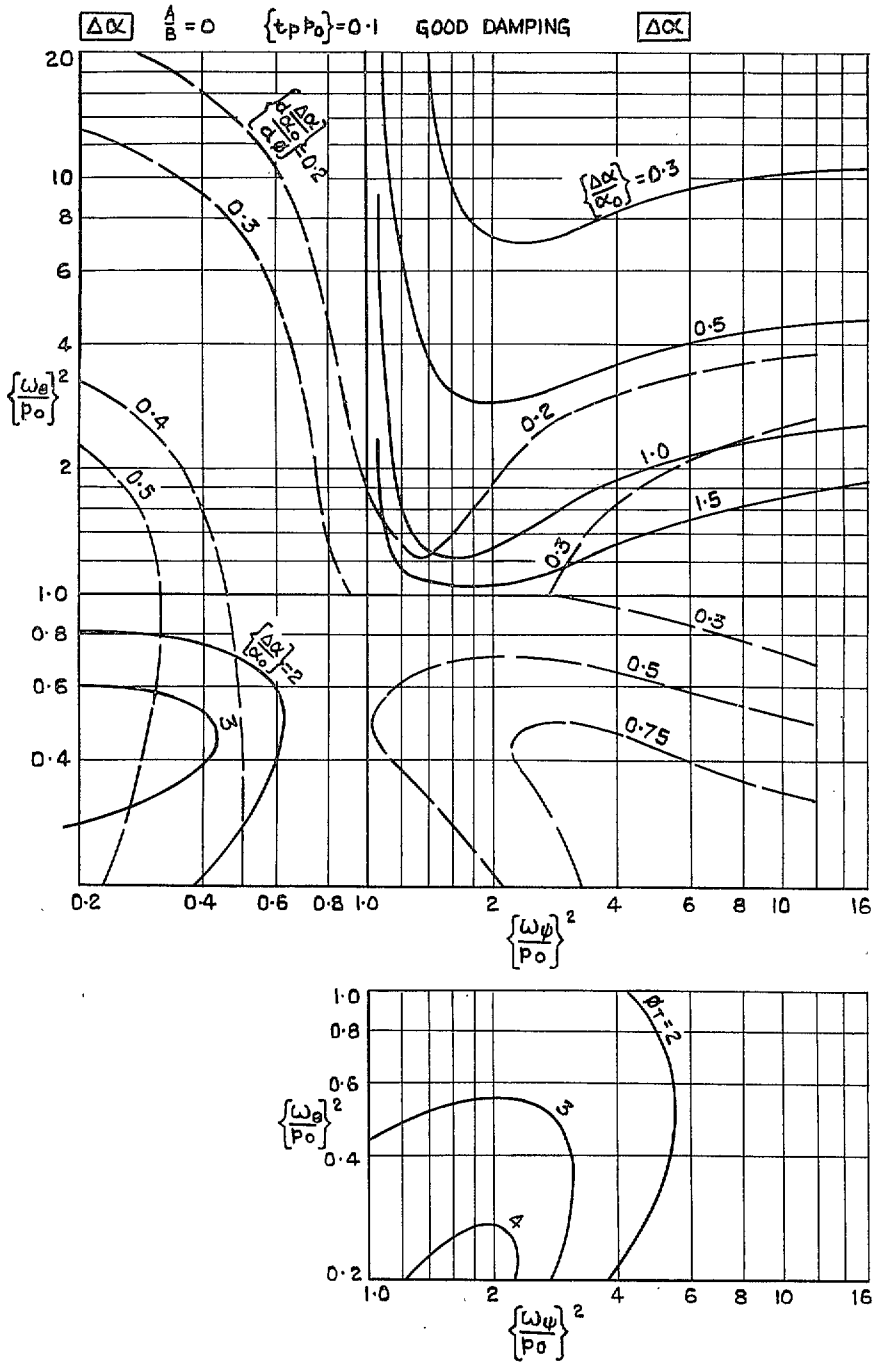

CHART 9. Ceiling values, and initial slopes with $\Delta\phi$, of incidence peak values, $\Delta\alpha_{MAX}$, and critical bank angle for pitch divergence, ϕ_T. $A/B = 0$, $\{t_p p_0\} = 0{\cdot}1$, $\delta_\theta = 2{\cdot}0$, $\delta_\psi = 0{\cdot}5$.

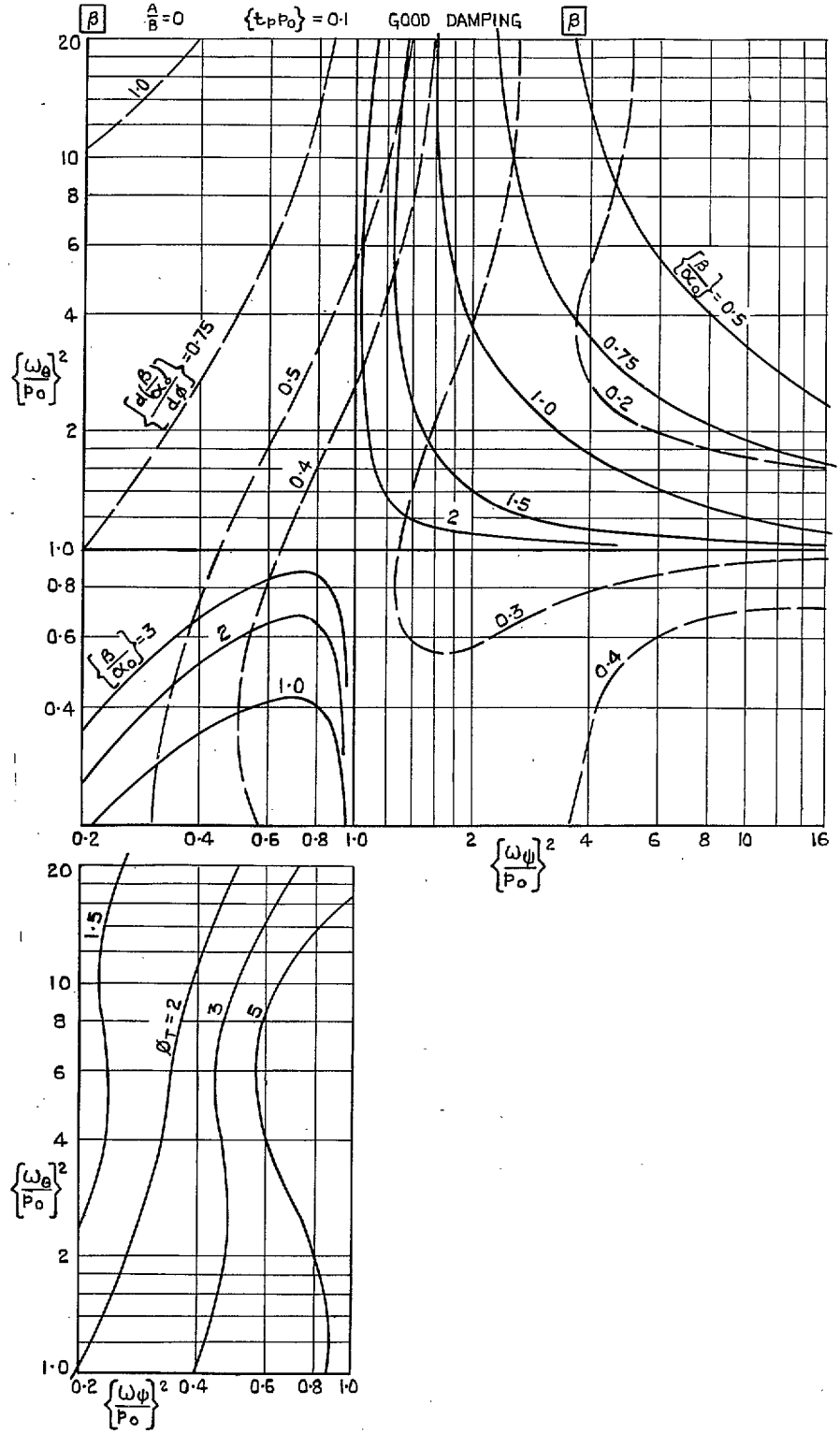

CHART 10. Ceiling values, and initial slopes with $\Delta\phi$, of sideslip peak values, β_{MAX}, and critical bank angle for yaw divergence, ϕ_T. $A/B = 0$, $\{t_p p_0\} = 0{\cdot}1$, $\delta_\theta = 2{\cdot}0$, $\delta_\psi = 0{\cdot}5$.

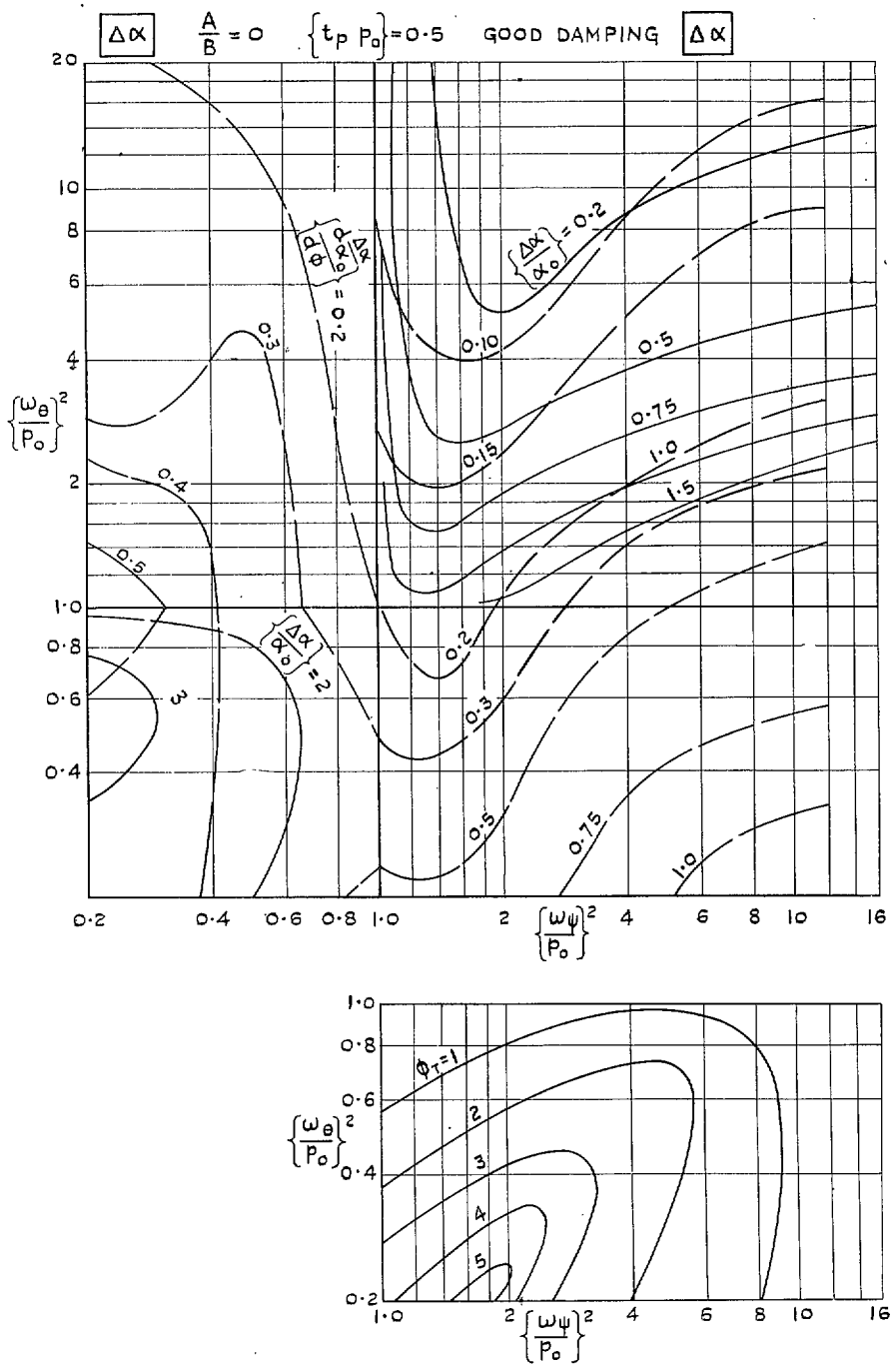

CHART 11. Ceiling values, and initial slopes with $\Delta\phi$, of incidence peak values, $\Delta\alpha_{MAX}$, and critical bank angle for pitch divergence, ϕ_T. $A/B = 0$, $\{t_p p_0\} = 0{\cdot}5$, $\delta_\theta = 2{\cdot}0$, $\delta_\psi = 0{\cdot}5$.

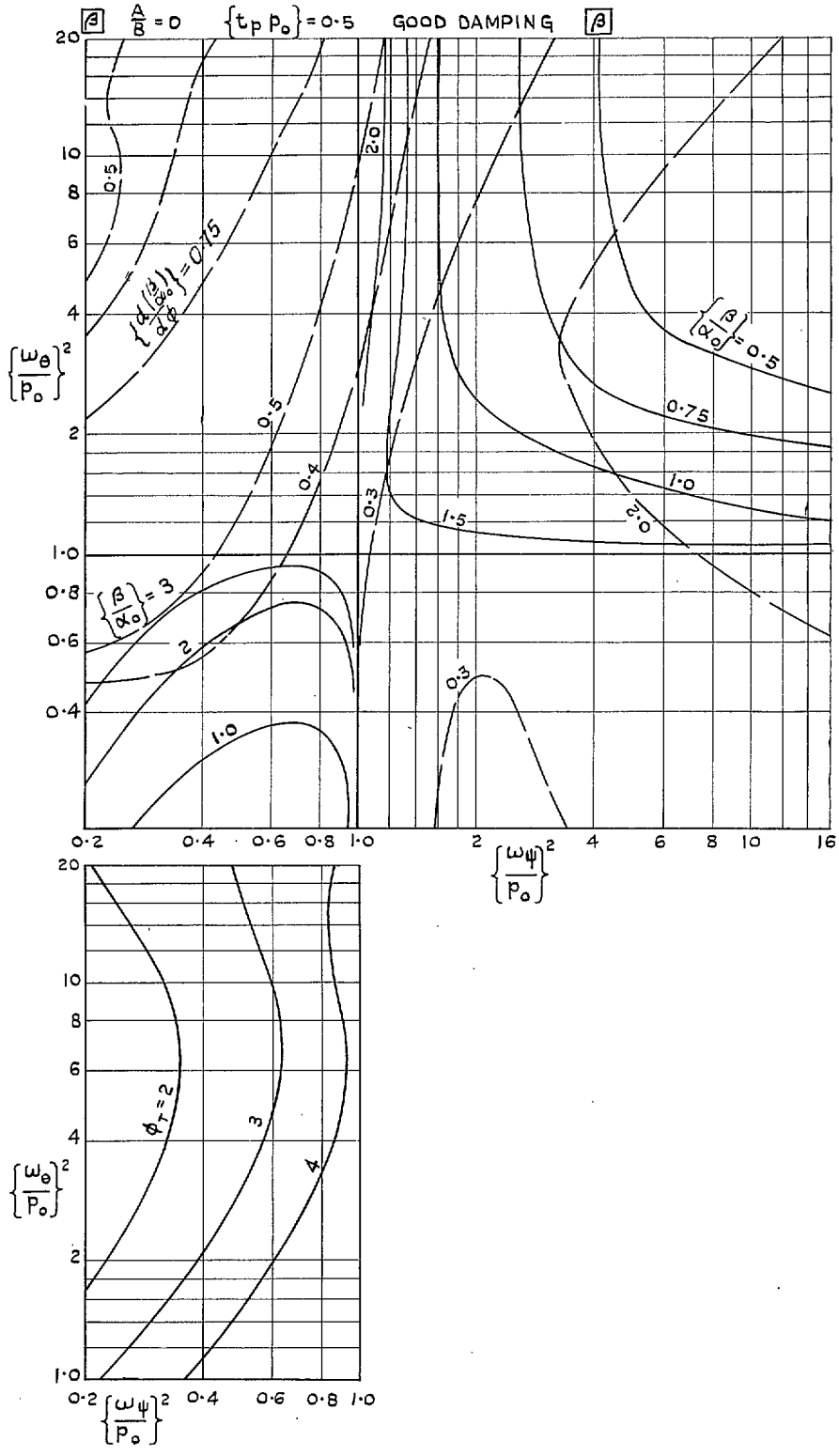

CHART 12. Ceiling values, and initial slopes with $\Delta\phi$, of sideslip peak values, β_{MAX}, and critical bank angle for yaw divergence, ϕ_T. $A/B = 0$, $\{t_p p_0\} = 0{\cdot}5$, $\delta_\theta = 2{\cdot}0$, $\delta_\psi = 0{\cdot}5$.

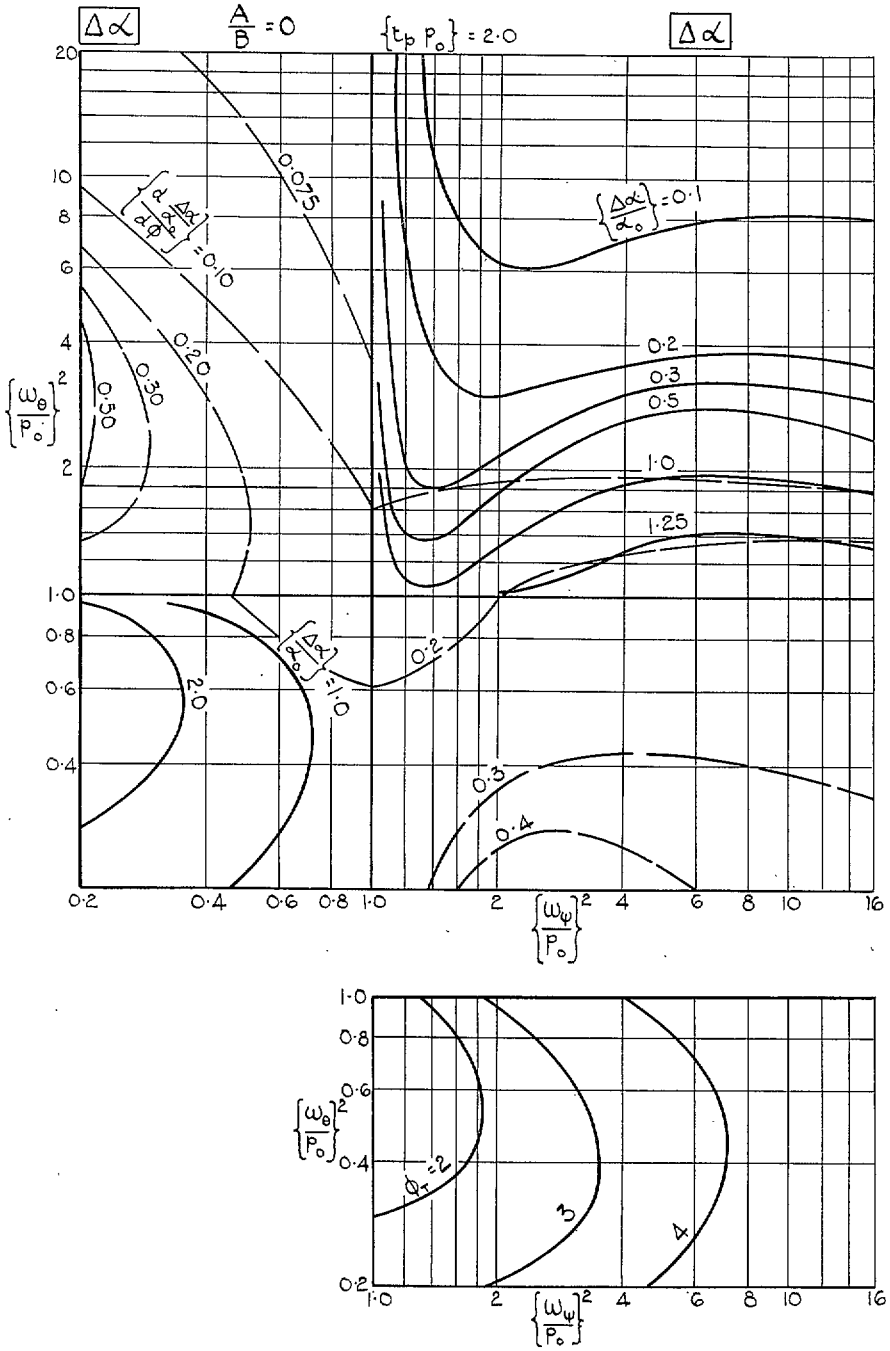

CHART 13. Ceiling values, and initial slopes with $\Delta\phi$, of incidence peak values, $\Delta\alpha_{MAX}$, and critical bank angles for pitch divergence, ϕ_T. $A/B = 0$, $\{t_p p_0\} = 2{\cdot}0$, $\delta_\theta = 2{\cdot}0$, $\delta_\psi = 0{\cdot}5$.

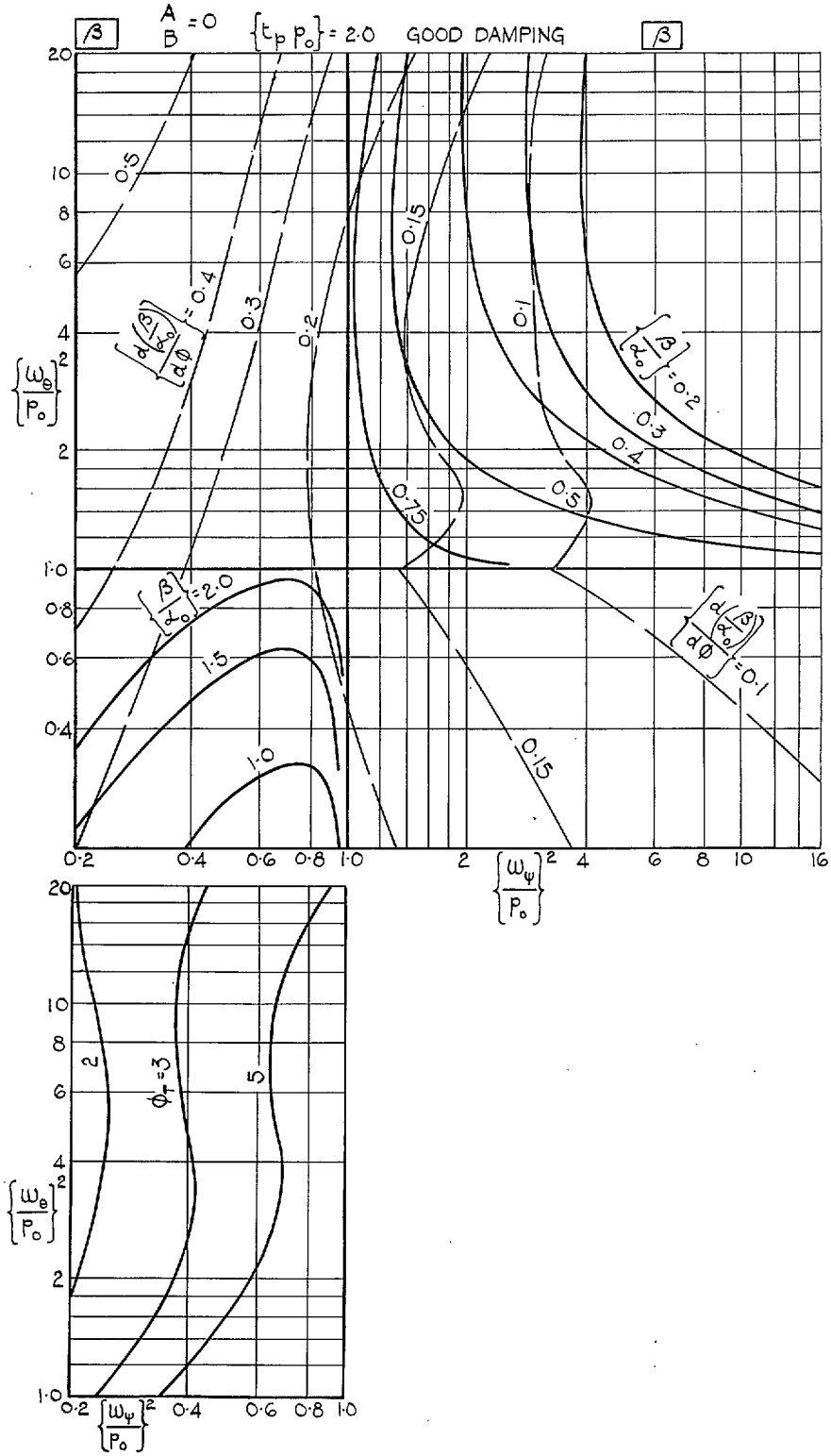

CHART 14. Ceiling values, and initial slopes of sideslip peak values, β_{MAX}, and critical bank angle of yaw divergence, ϕ_T. $A/B = 0$, $\{t_p p_0\} = 2{\cdot}0$, $\delta_\theta = 2{\cdot}0$, $\delta_\psi = 0{\cdot}5$.

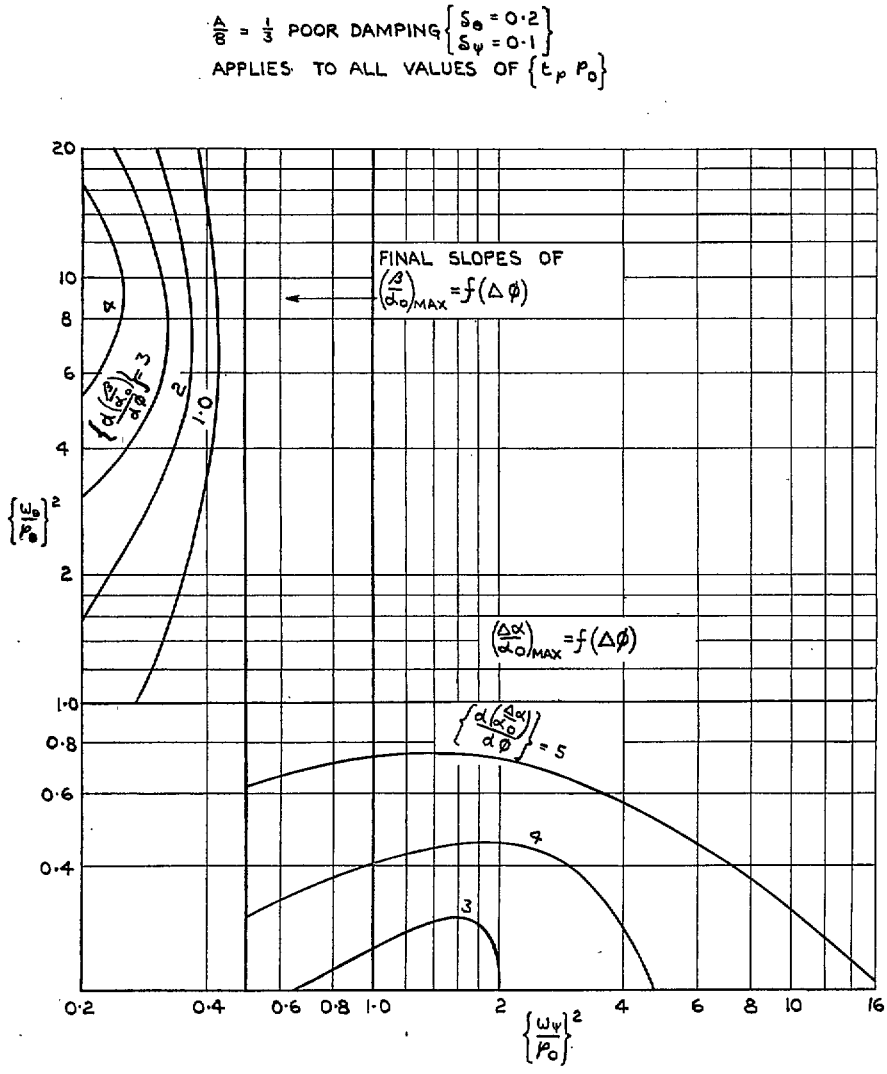

CHART 15. Final slopes of $\Delta\alpha_{MAX}$ and β_{MAX} with manoeuvre bank angle, $\Delta\phi$. $A/B = \frac{1}{3}$, poor damping.

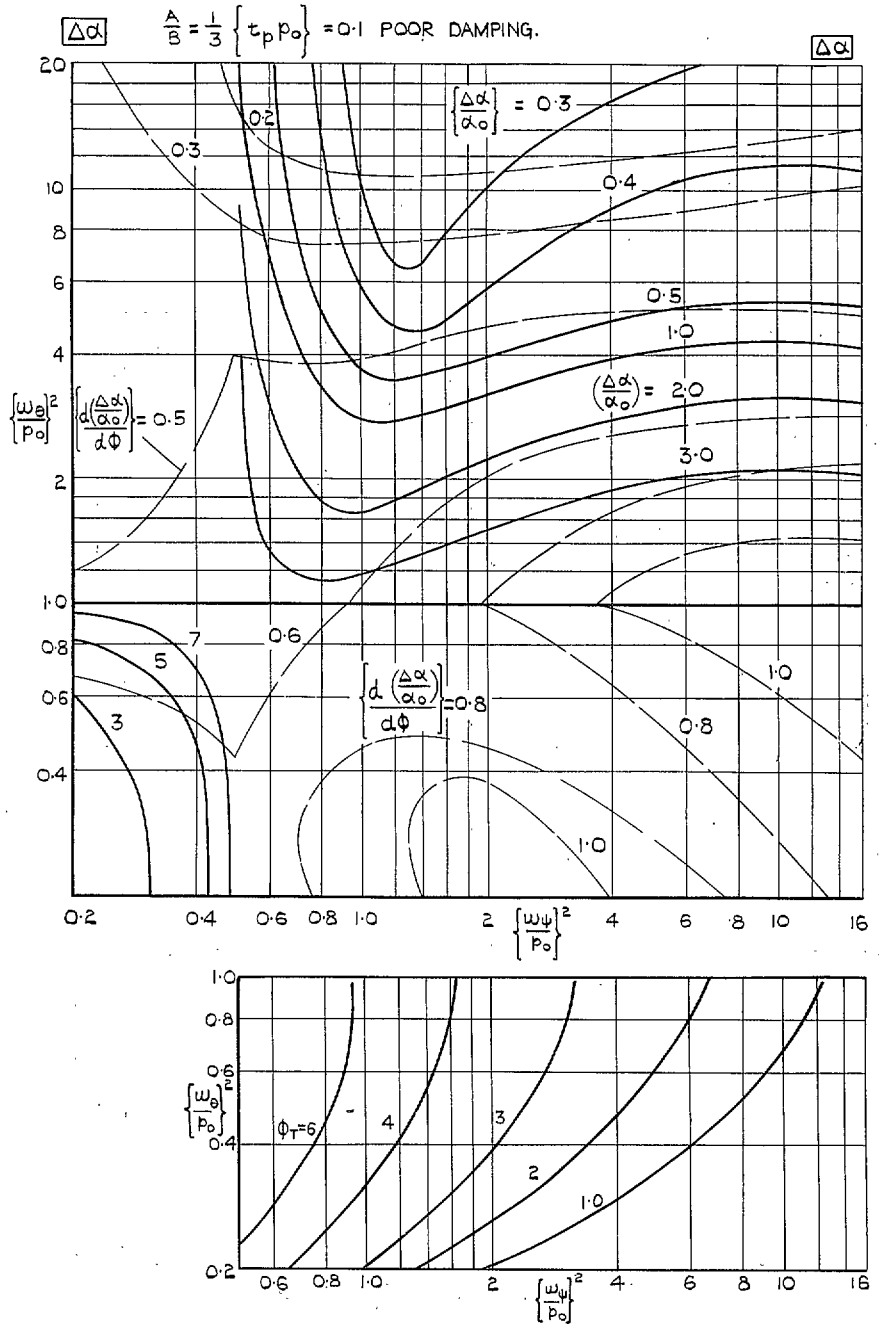

CHART 16. Ceiling values, and initial slopes with $\Delta\phi$, of incidence peak values, $\Delta\alpha_{MAX}$, and critical bank angle for pitch divergence, ϕ_T. $A/B = \frac{1}{3}$, $\{t_p p_0\} = 0{\cdot}1$, $\delta_\theta = 0{\cdot}2$, $\delta_\psi = 0{\cdot}1$.

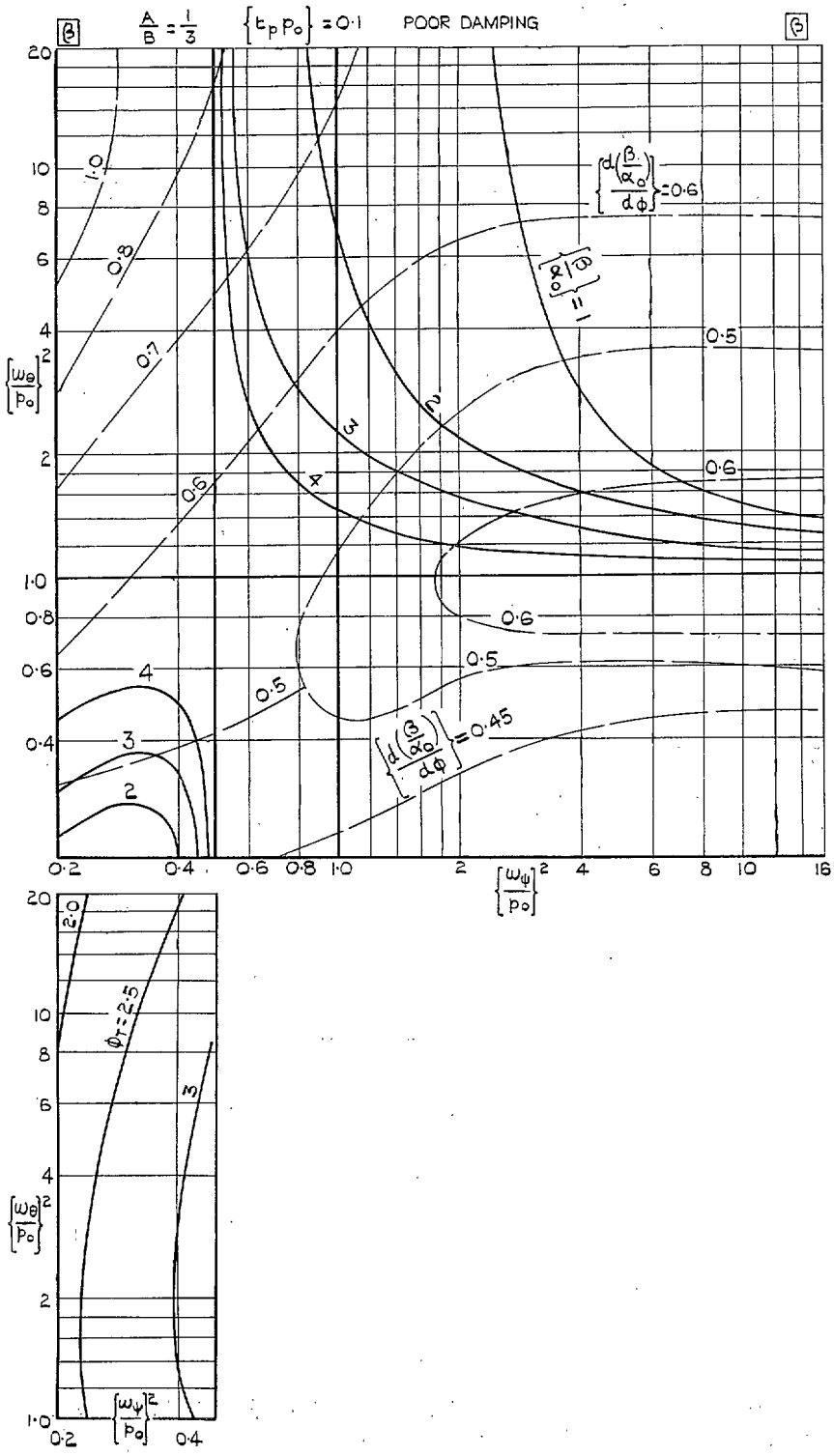

CHART 17. Ceiling values, and initial slopes with $\Delta\phi$, of sideslip peak values, β_{MAX}, and critical bank angle of yaw divergence, ϕ_T. $A/B = \frac{1}{3}$, $\{t_p p_0\} = 0{\cdot}1$, $\delta_\theta = 0{\cdot}2$, $\delta_\psi = 0{\cdot}1$.

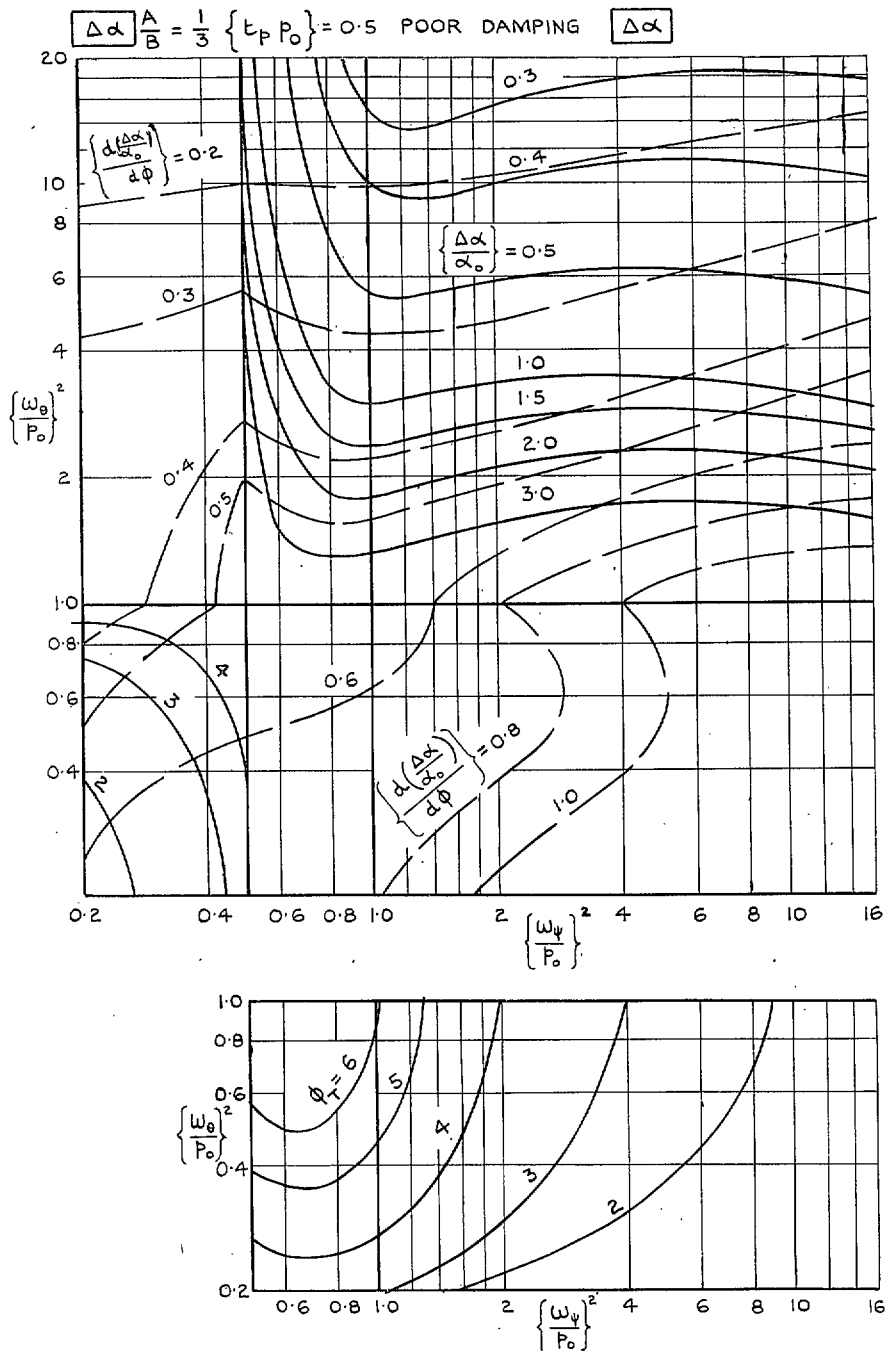

CHART 18. Ceiling values, and initial slopes with $\Delta\phi$, of incidence peak values, $\Delta\alpha_{MAX}$, and critical bank angle for pitch divergence, ϕ_T. $A/B = \frac{1}{3}$, $\{t_p p_0\} = 0{\cdot}5$, $\delta_\theta = 0{\cdot}2$, $\delta_\psi = 0{\cdot}1$.

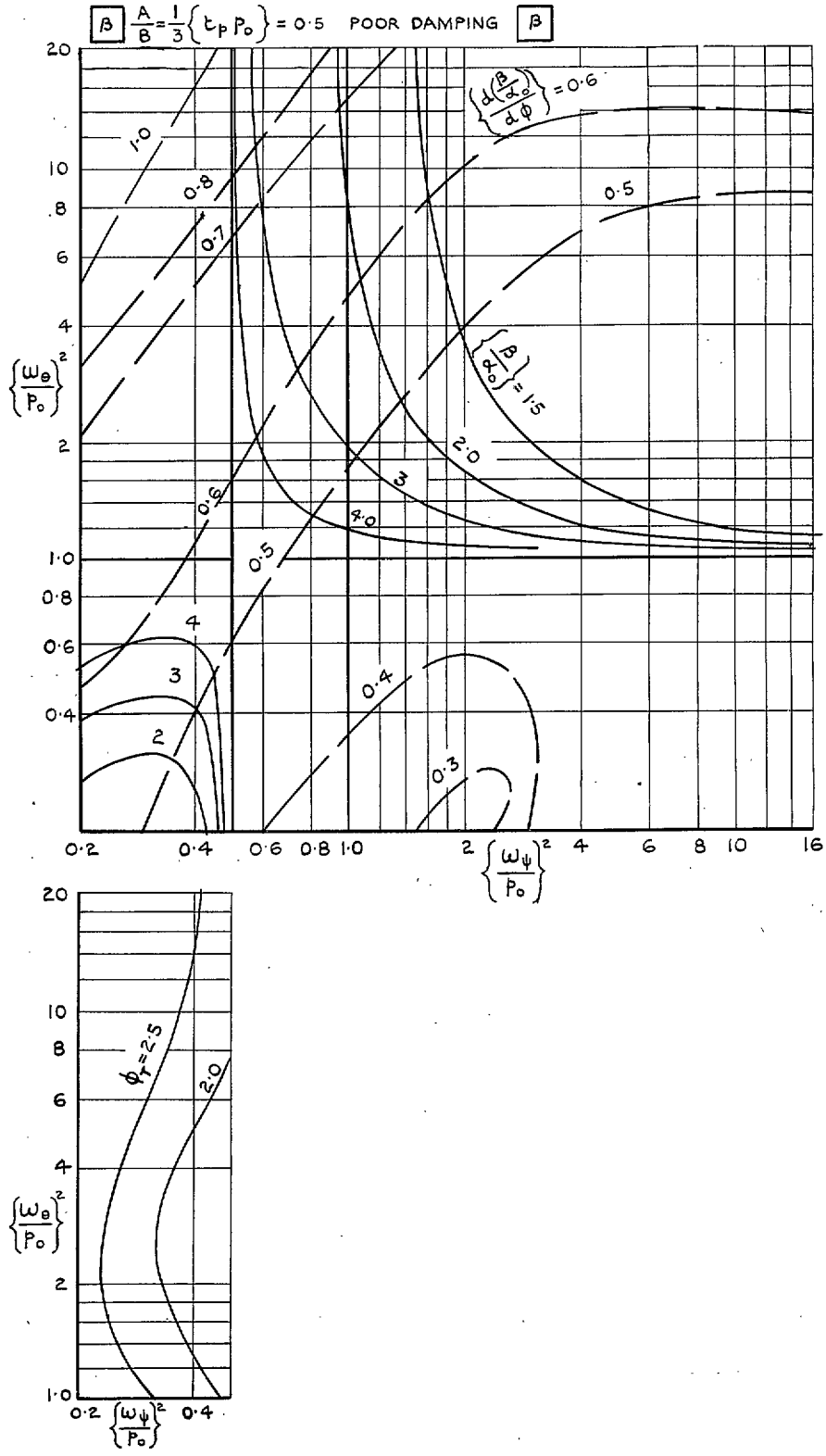

CHART 19. Ceiling values, and initial slopes of sideslip peak values, β_{MAX}, and critical bank angles for yaw divergence, ϕ_T. $A/B = \frac{1}{3}$, $\{t_p p_0\} = 0{\cdot}5$, $\delta_\theta = 0{\cdot}2$, $\delta_\psi = 0{\cdot}1$.

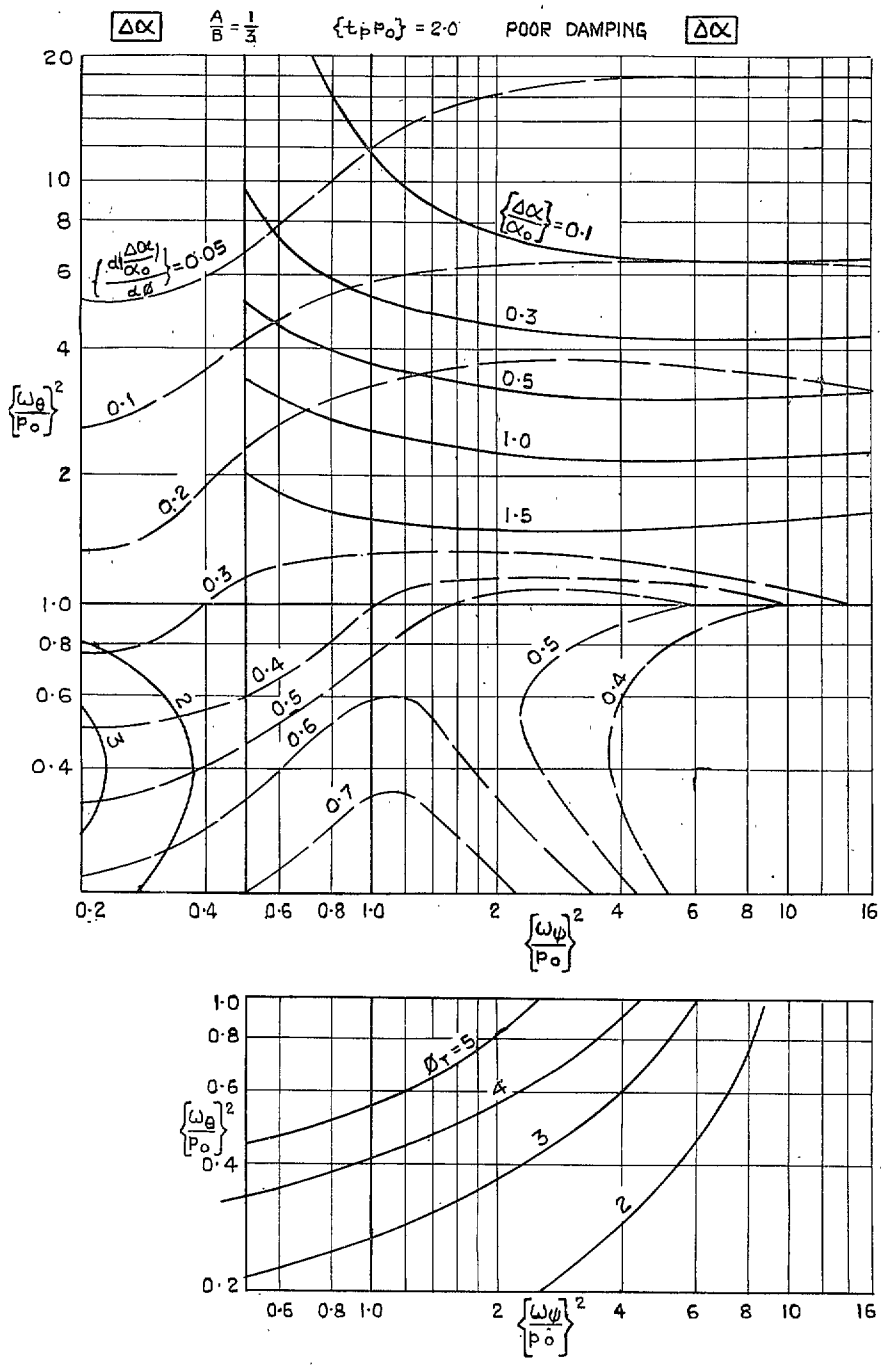

CHART 20. Ceiling values, and initial slopes of incidence peak values, $\Delta\alpha_{MAX}$, and critical bank angle for pitch divergence, ϕ_T. $A/B = \frac{1}{3}$, $\{t_p p_0\} = 2{\cdot}0$, $\delta_\theta = 0{\cdot}2$, $\delta_\psi = 0{\cdot}1$.

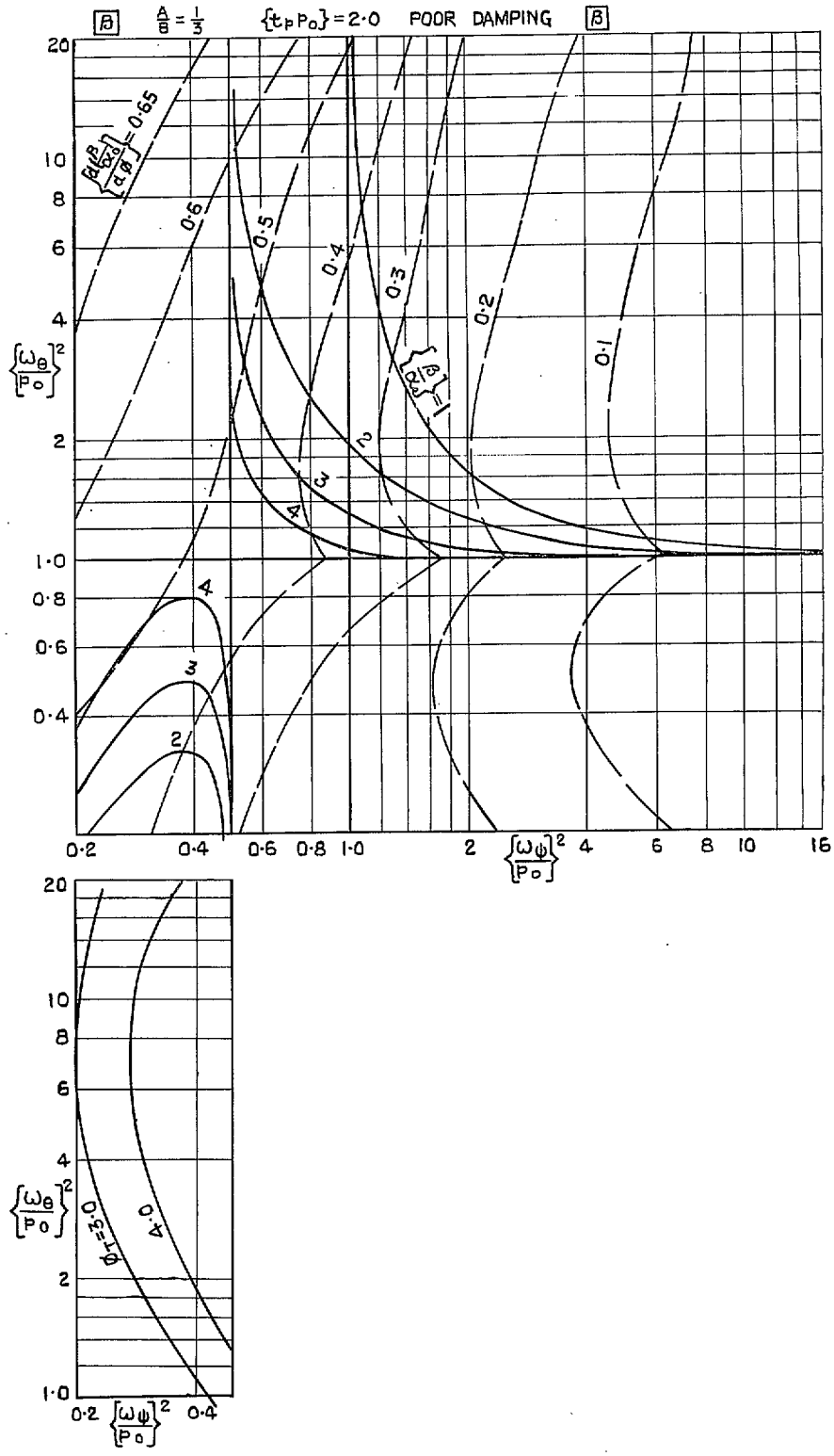

CHART 21. Ceiling values, and initial slopes of sideslip peak values, β_{MAX}, and critical bank angle for yaw divergence, ϕ_T. $A/B = \frac{1}{3}$, $\{t_p p_0\} = 2{\cdot}0$, $\delta_\theta = 0{\cdot}2$, $\delta_\psi = 0{\cdot}1$.

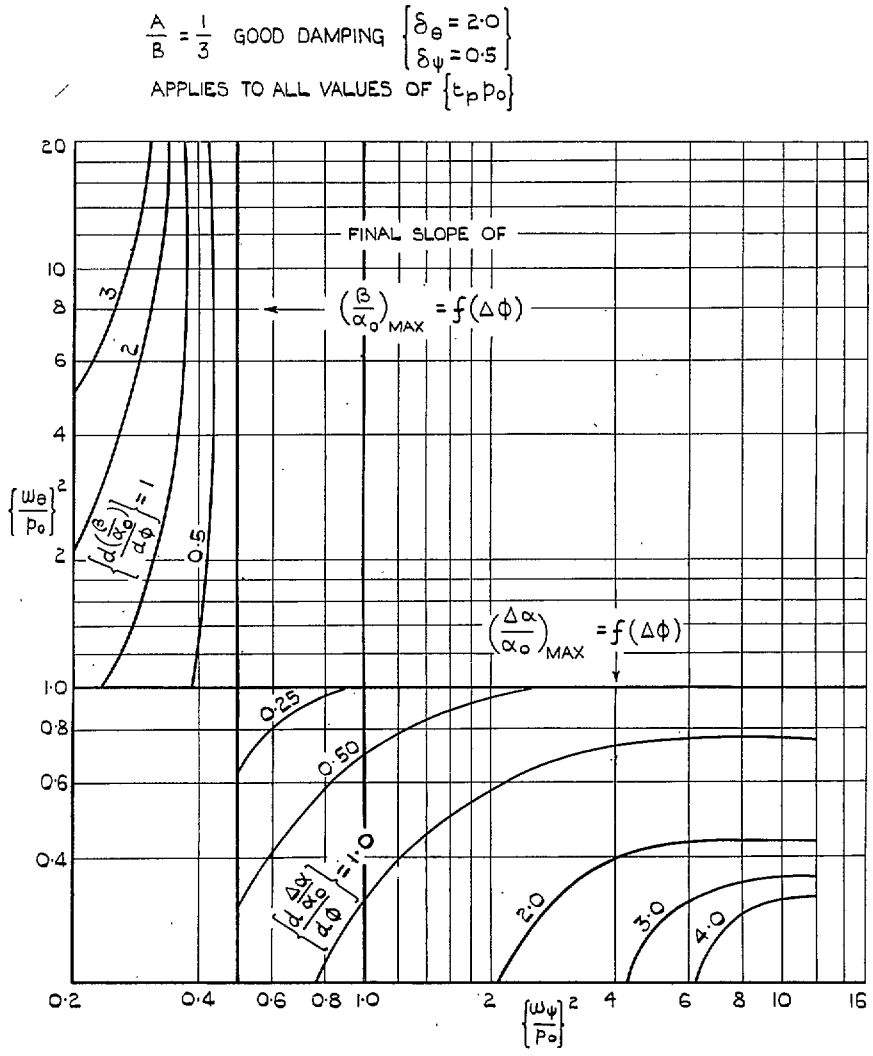

CHART 22. Final slopes of $\Delta\alpha_{MAX}$ and β_{MAX} with manoeuvre bank angle, $\Delta\phi$. $A/B = \frac{1}{3}$, good damping.

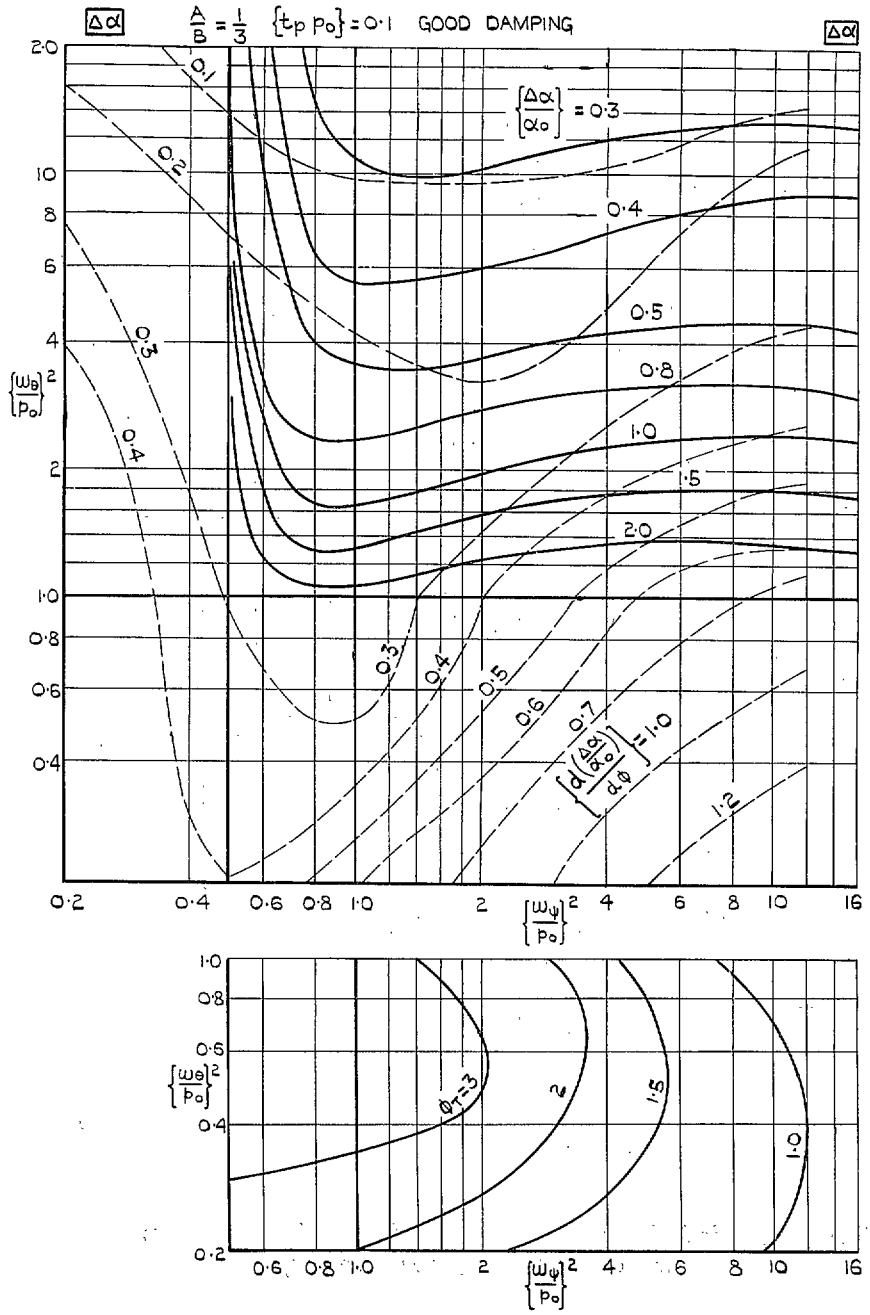

CHART 23. Ceiling values, and initial slopes with $\Delta\phi$, of incidence peak values, $\Delta\alpha_{MAX}$, and critical bank angle for pitch divergence, ϕ_T. $A/B = \frac{1}{3}$, $\{t_p p_0\} = 0{\cdot}1$, $\delta_\theta = 2{\cdot}0$, $\delta_\psi = 0{\cdot}5$.

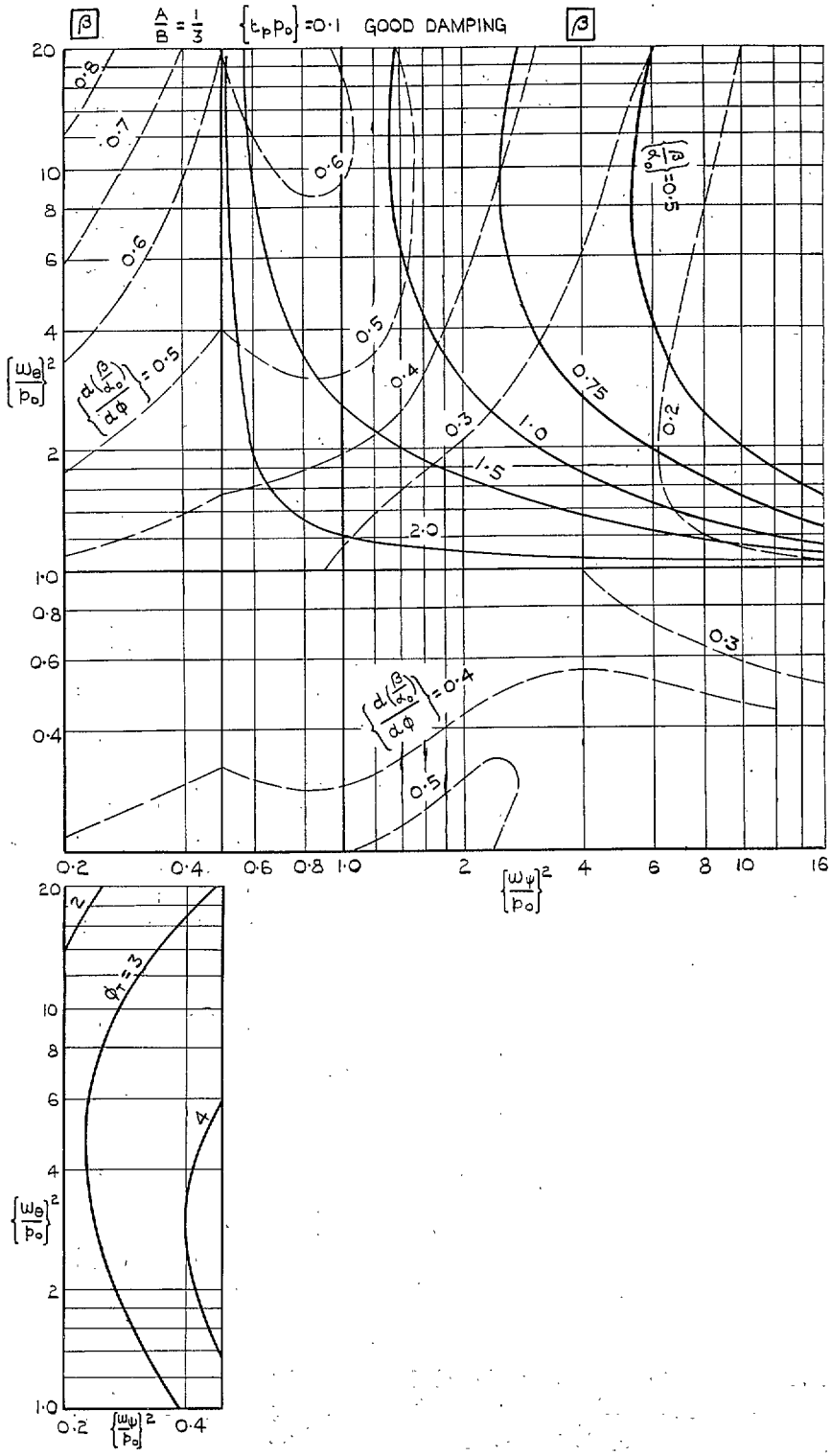

CHART 24. Ceiling values, and initial slopes with $\Delta\phi$, of sideslip peak values, β_{MAX}, and critical bank angle for divergence, ϕ_T. $A/B = \frac{1}{3}$, $\{t_p p_0\} = 0{\cdot}1$, $\delta_\theta = 2{\cdot}0$, $\delta_\psi = 0{\cdot}1$.

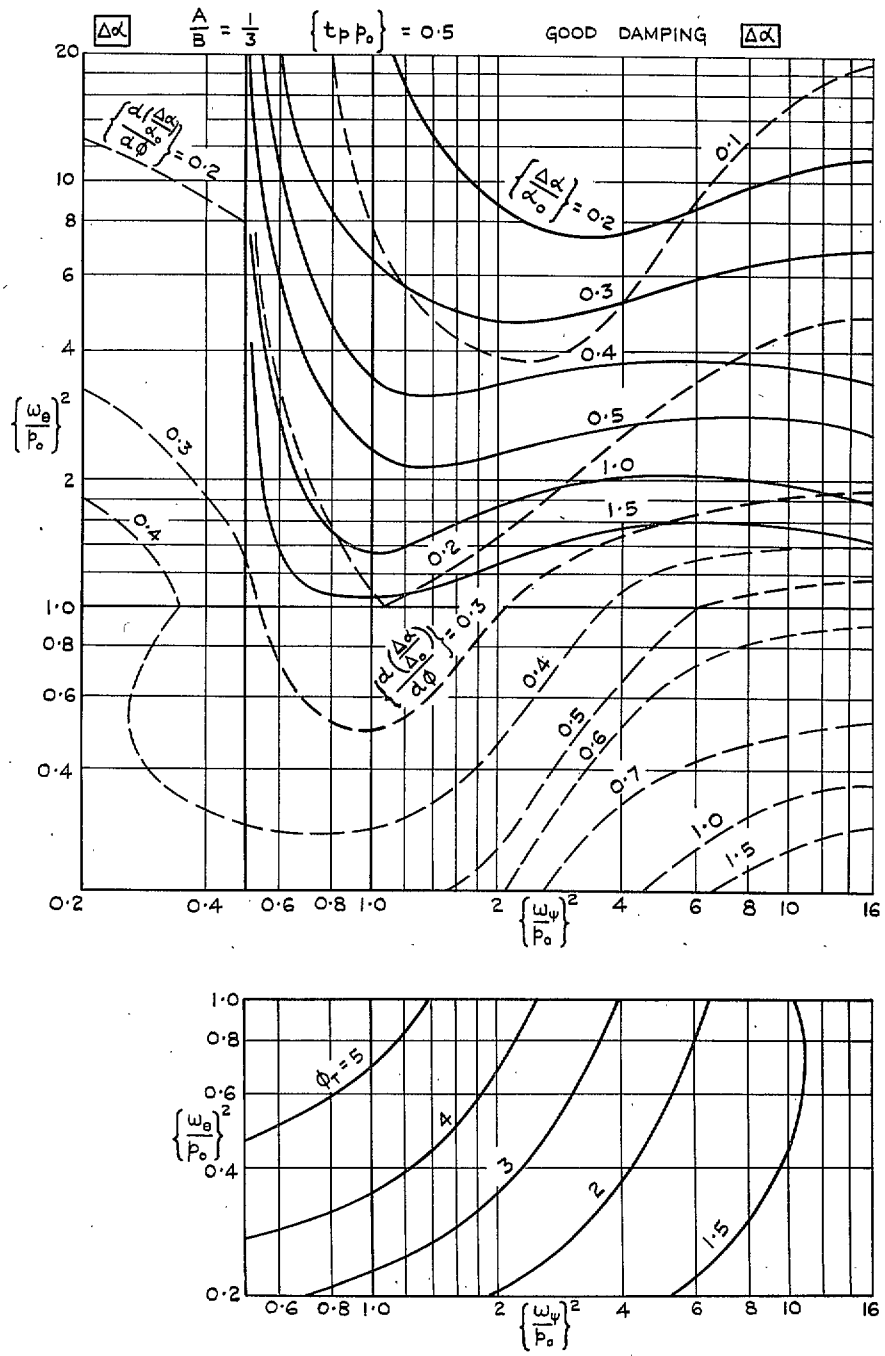

CHART 25. Ceiling values, and initial slopes with $\Delta\phi$, of incidence peak values, $\Delta\alpha_{MAX}$, and critical bank angle for pitch divergence, ϕ_T. $A/B = \frac{1}{3}$, $\{t_p p_0\} = 0{\cdot}5$, $\delta_\theta = 2{\cdot}0$, $\delta_\psi = 0{\cdot}5$.

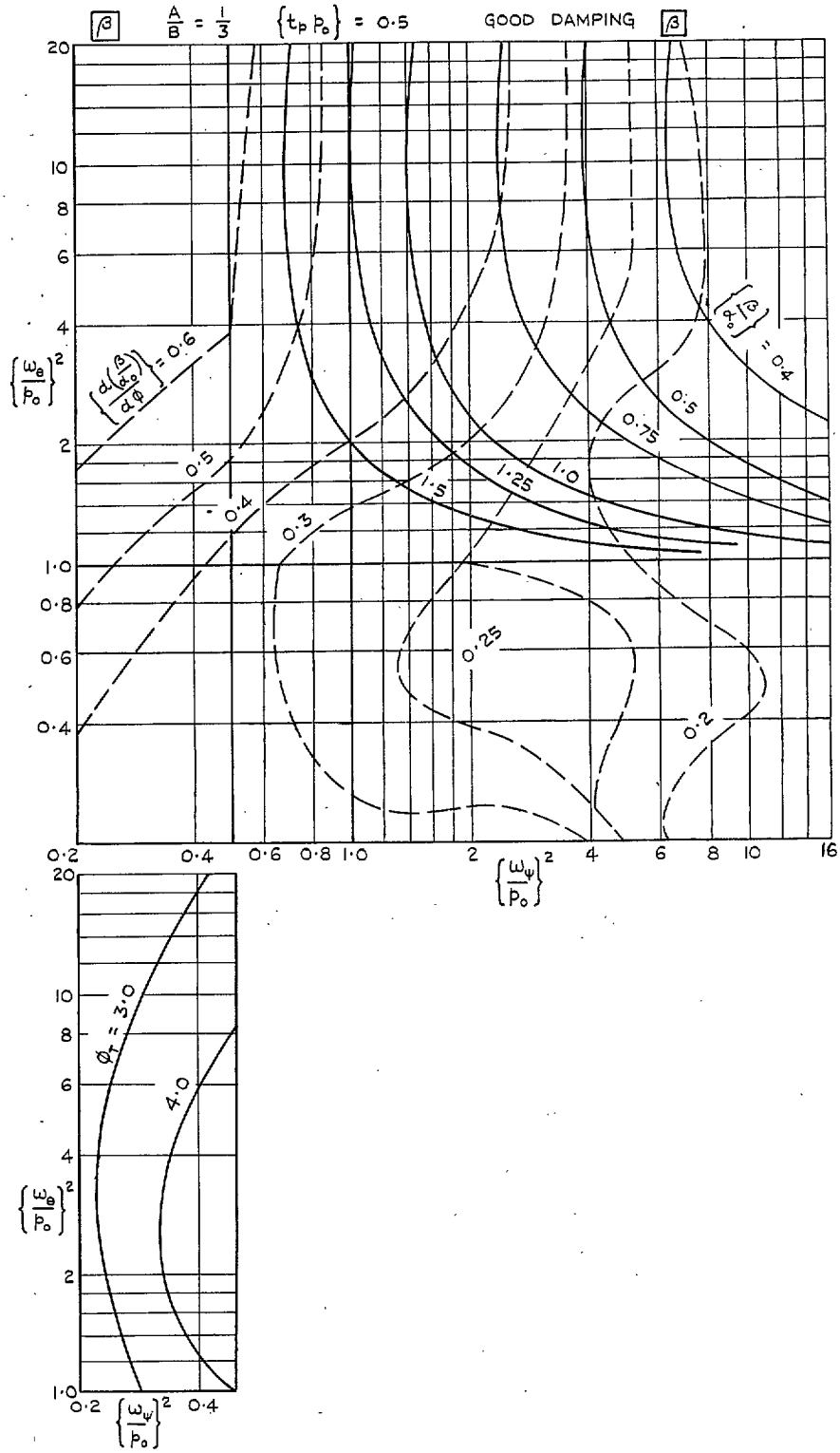

CHART 26. Ceiling values, and initial slopes with $\Delta\phi$, of sideslip peak values, β_{MAX}, and critical bank angle for yaw divergence, ϕ_T. $A/B = \frac{1}{3}$, $\{t_p p_0\} = 0{\cdot}5$, $\delta_\theta = 2{\cdot}0$, $\delta_\psi = 0{\cdot}5$.

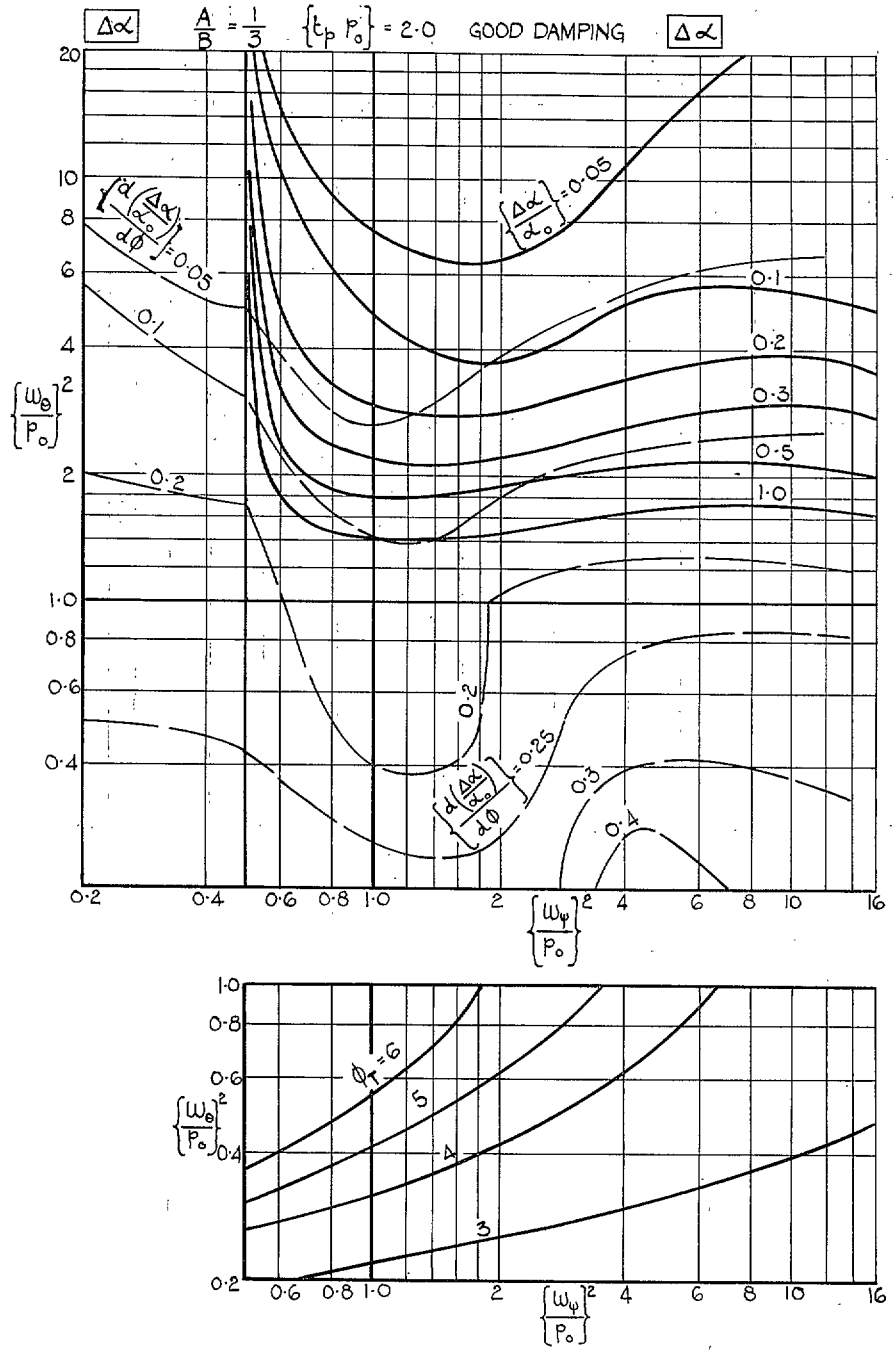

CHART 27. Ceiling values, and initial slopes with $\Delta\phi$, of incidence peak values, $\Delta\alpha_{MAX}$, and critical bank angle for pitch divergence, ϕ_T. $A/B = \frac{1}{3}$, $\{t_p p_0\} = 2{\cdot}0$, $\delta_\theta = 2{\cdot}0$, $\delta_\psi = 0{\cdot}5$.

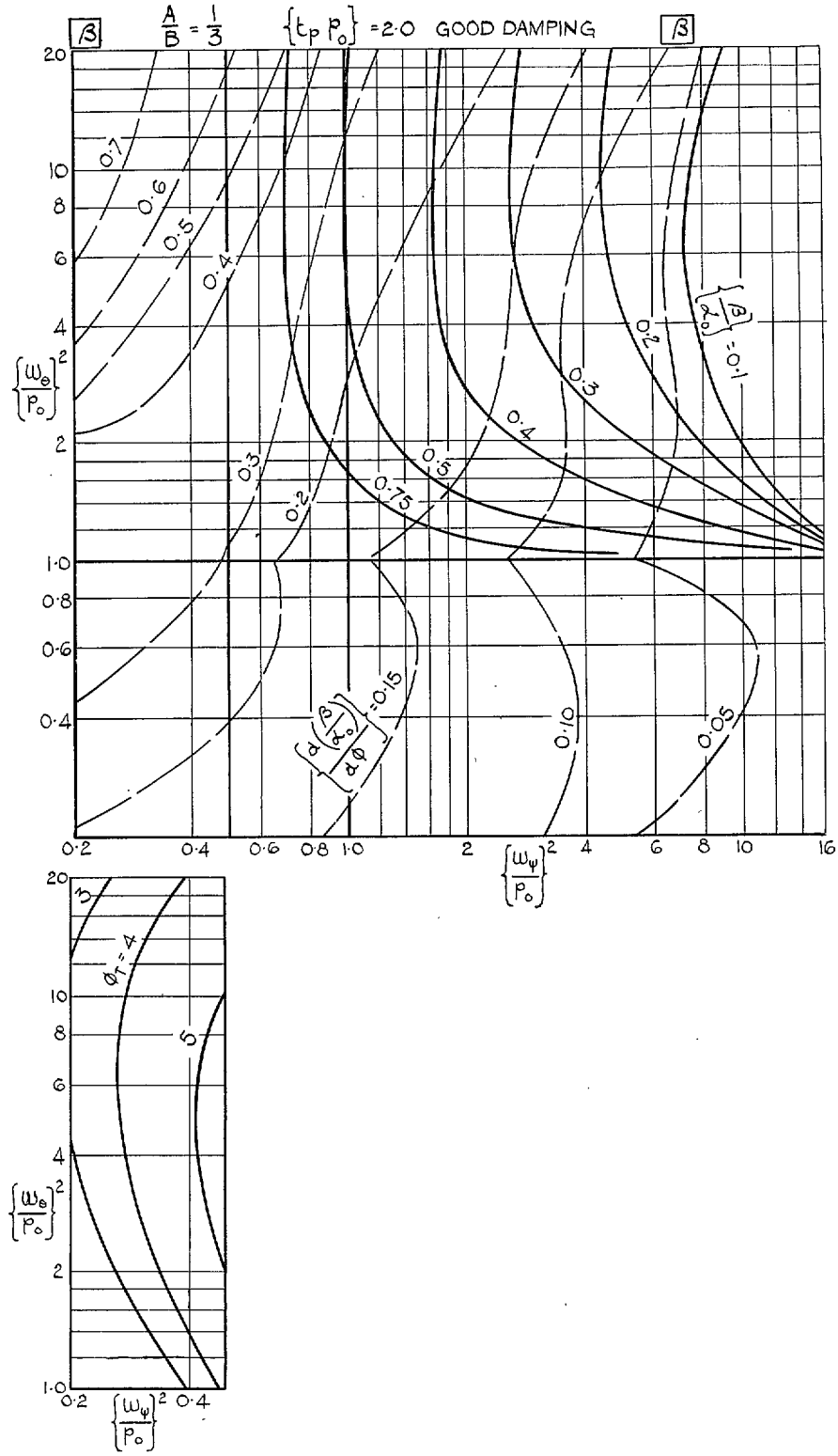

CHART 28. Ceiling values, and initial slopes with $\Delta\phi$, of sideslip peak values, β_{MAX}, and critical bank angle for yaw divergence, ϕ_T. $A/B = \frac{1}{3}$, $\{t_p p_0\} = 2{\cdot}0$, $\delta_\theta = 2{\cdot}0$, $\delta_\psi = 0{\cdot}5$.

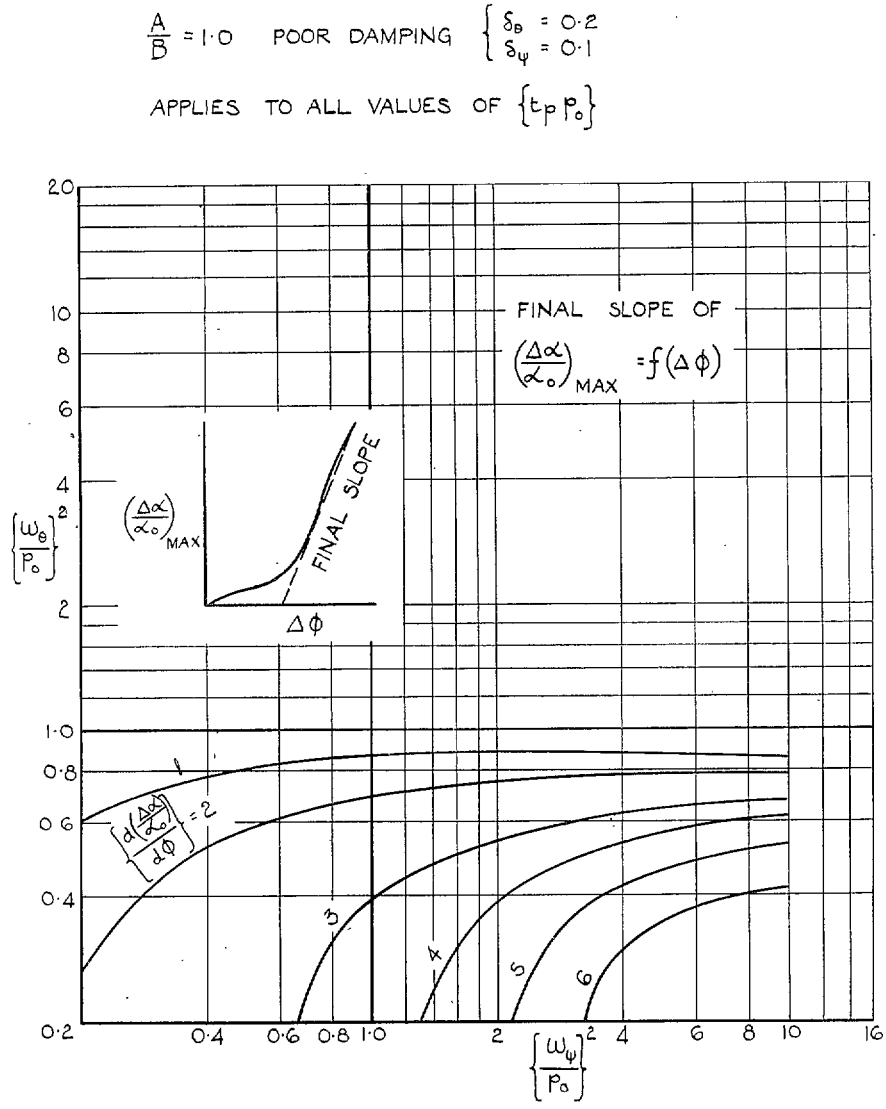

CHART 29. Final slopes of $\Delta\alpha_{MAX}$ with manoeuvre bank angle, $\{t_p p_0\}$.

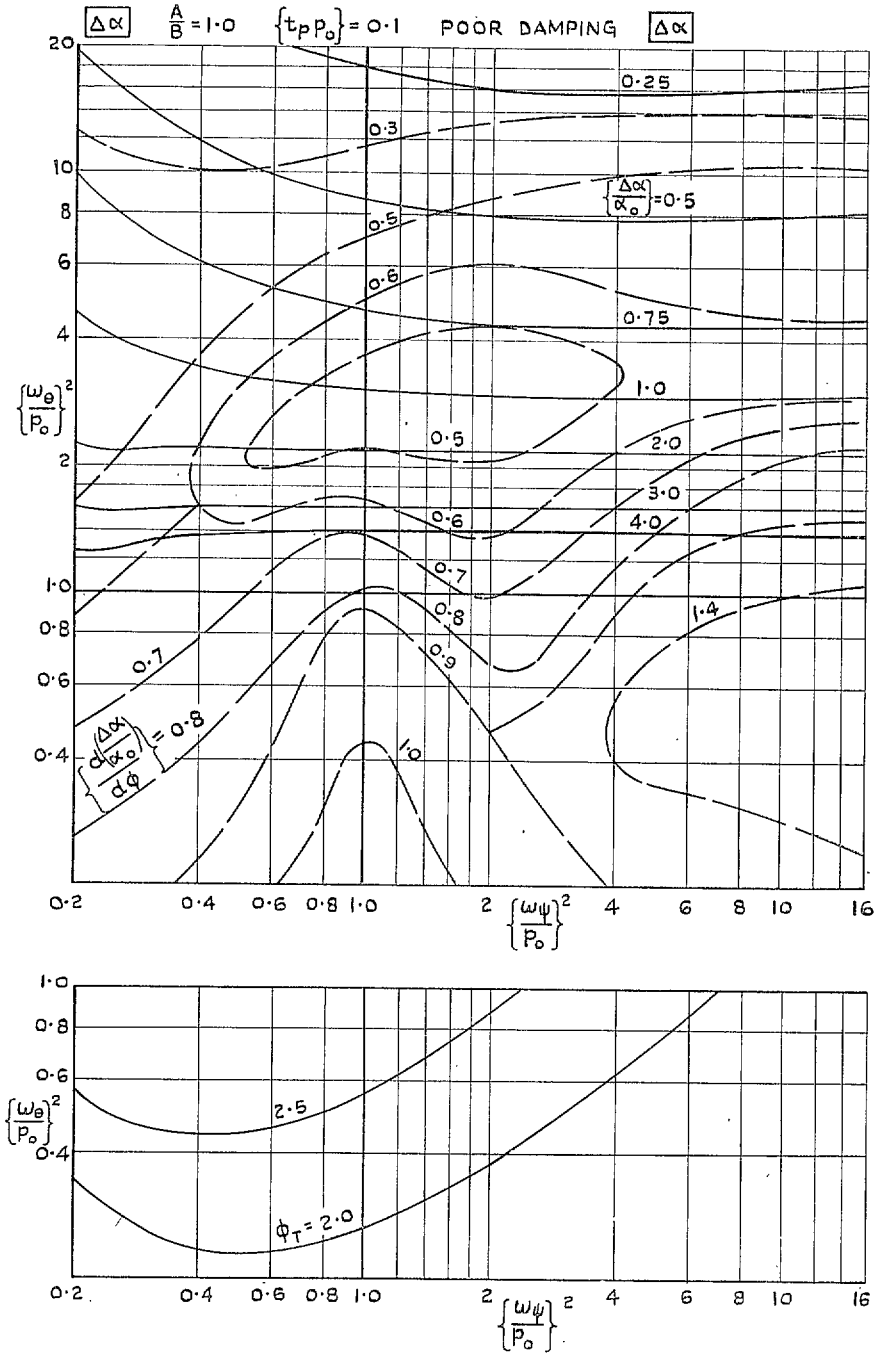

CHART 30. Ceiling values, and initial slopes with $\Delta\phi$, of incidence peak values, $\Delta\alpha_{MAX}$, and critical bank angle of pitch divergence, ϕ_T. $A/B = 1{\cdot}0$, $\{t_p p_0\} = 0{\cdot}1$, $\delta_\theta = 0{\cdot}2$, $\delta_\psi = 0{\cdot}1$.

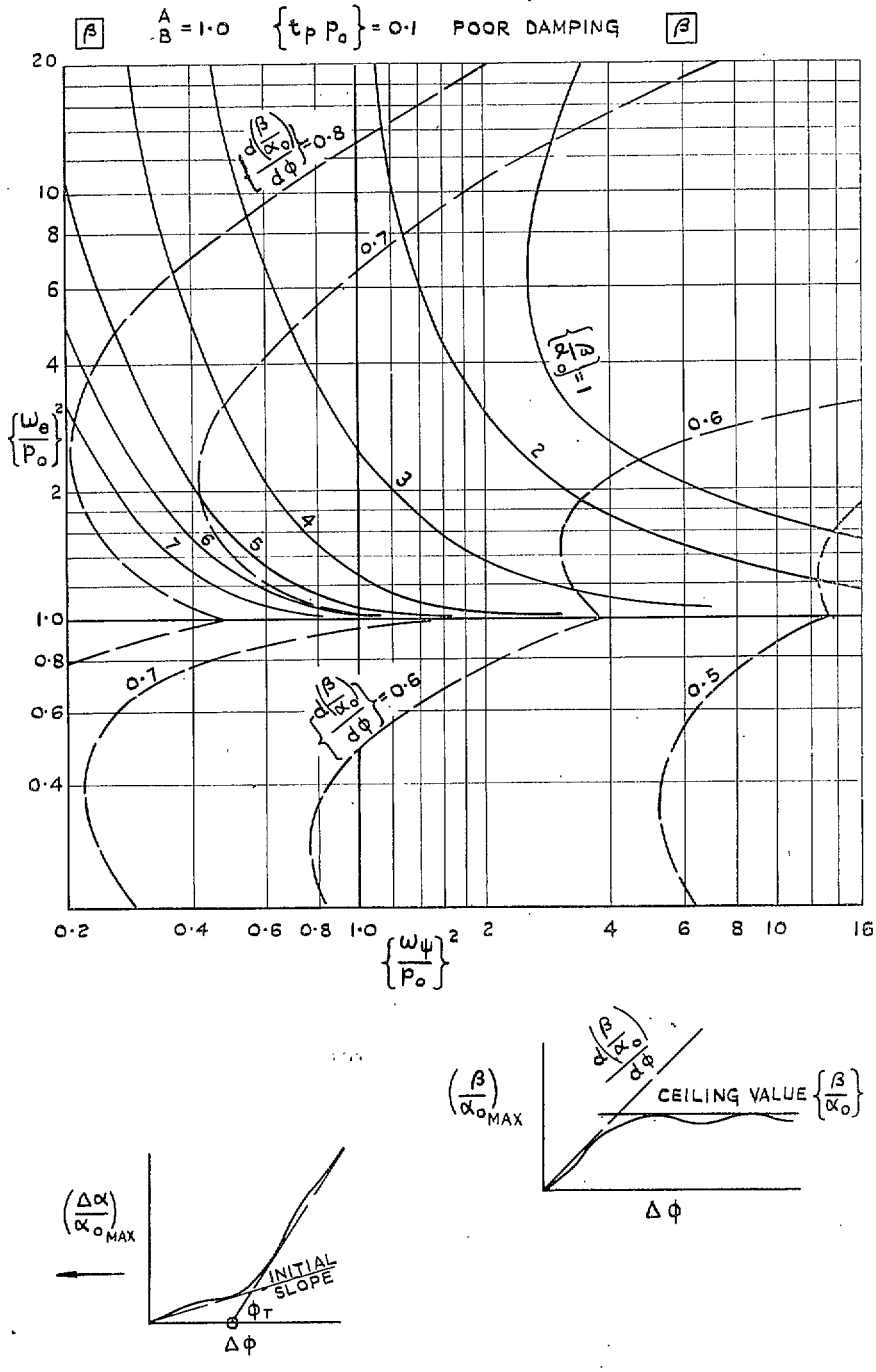

CHART 31. Ceiling values, and initial slopes with $\Delta\phi$, of sideslip peak values, β_{MAX}. $A/B = 1{\cdot}0$, $\{t_p p_0\} = 0{\cdot}1$, $\delta_\theta = 0{\cdot}2$, $\delta_\psi = 0{\cdot}1$.

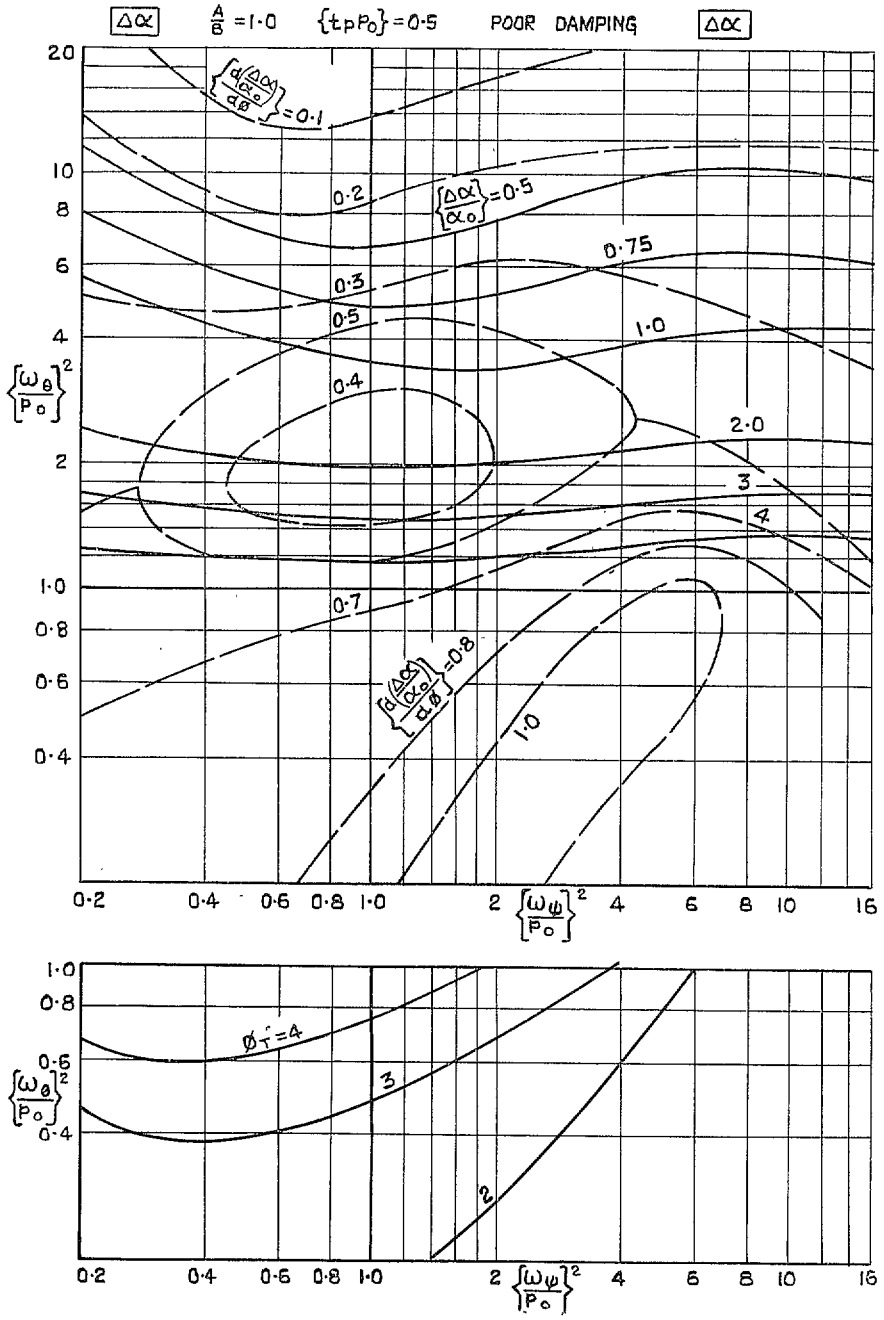

CHART 32. Ceiling values, and initial slopes with $\Delta\phi$, of incidence peak values, $\Delta\alpha_{MAX}$, and critical bank angles of pitch divergence. $A/B = 1{\cdot}0$, $\{t_p p_0\} = 0{\cdot}5$, $\delta_\theta = 0{\cdot}2$, $\delta_\psi = 0{\cdot}1$.

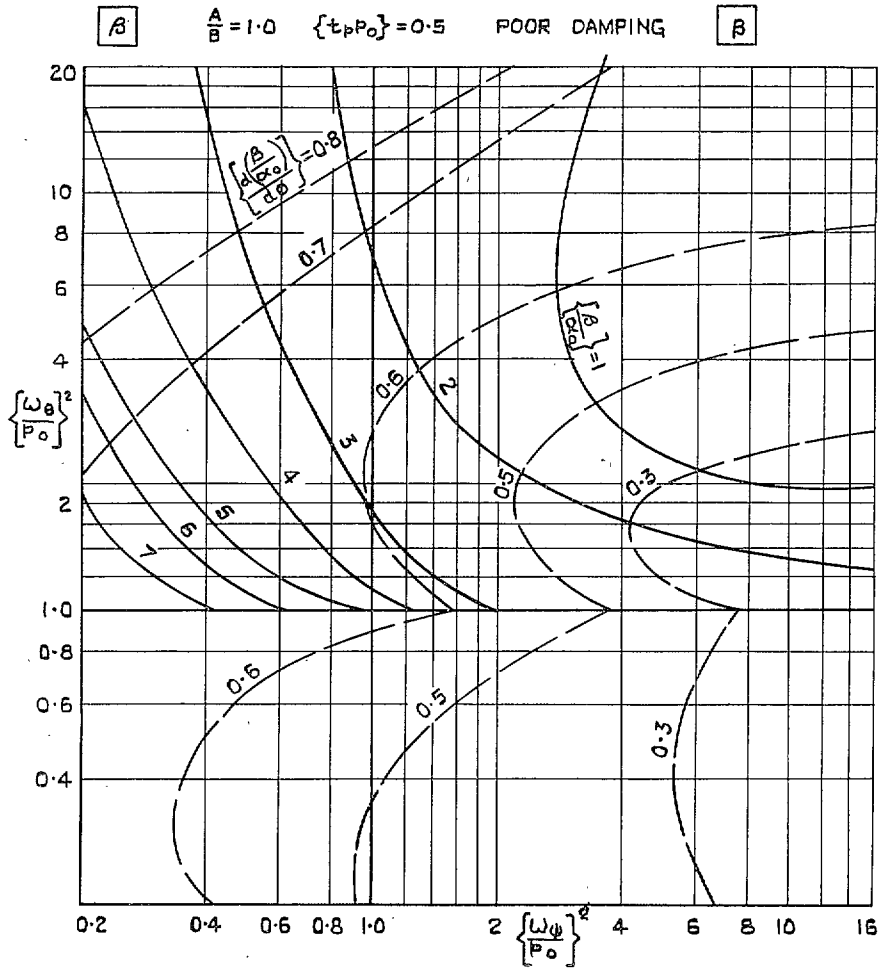

CHART 33. Ceiling values, and initial slopes with $\Delta\phi$, of sideslip peak values, β_{MAX}. $A/B = 1{\cdot}0$, $\{t_p p_0\} = 0{\cdot}5$, $\delta_\theta = 0{\cdot}2$, $\delta_\psi = 0{\cdot}1$.

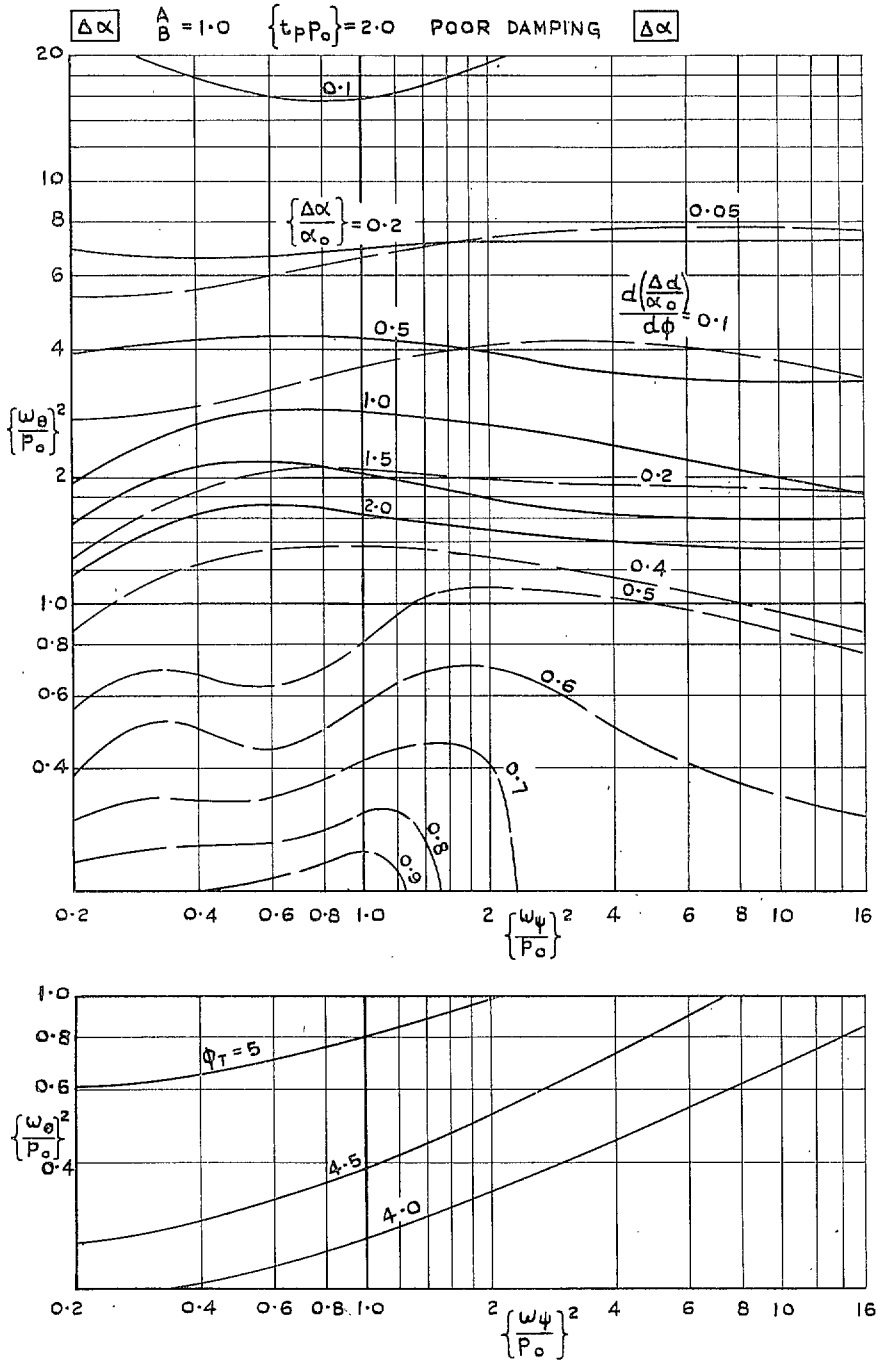

CHART 34. Ceiling values, and initial slopes with $\Delta\phi$, of incidence peak values, $\Delta\alpha_{MAX}$, and critical bank angle of pitch divergence, ϕ_T. $A/B = 1{\cdot}0$, $\{t_p p_0\} = 2{\cdot}0$, $\delta_0 = 0{\cdot}2$, $\delta_\psi = 0{\cdot}1$.

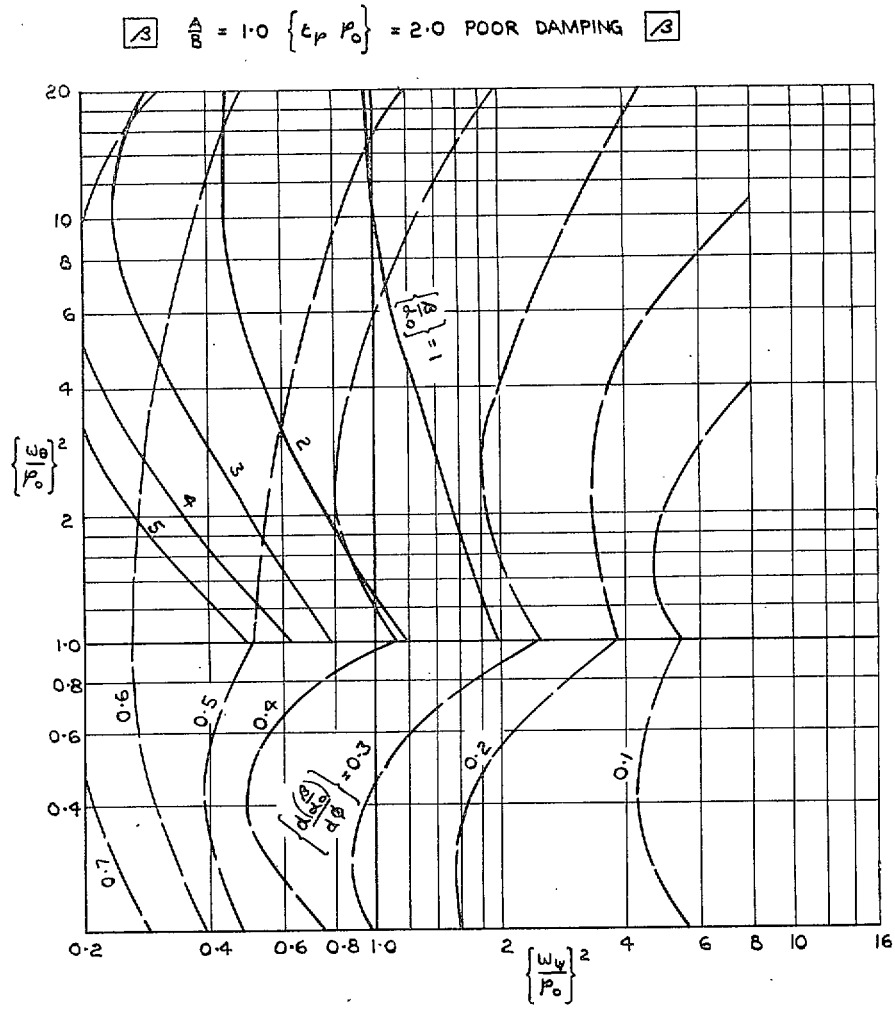

CHART 35. Ceiling values, and initial slopes with $\Delta\phi$, of sideslip peak values, β_{MAX}. $A/B = 1{\cdot}0$, $\{t_p p_0\} = 2{\cdot}0$, $\delta_\theta = 0{\cdot}2$, $\delta_\psi = 0{\cdot}1$.

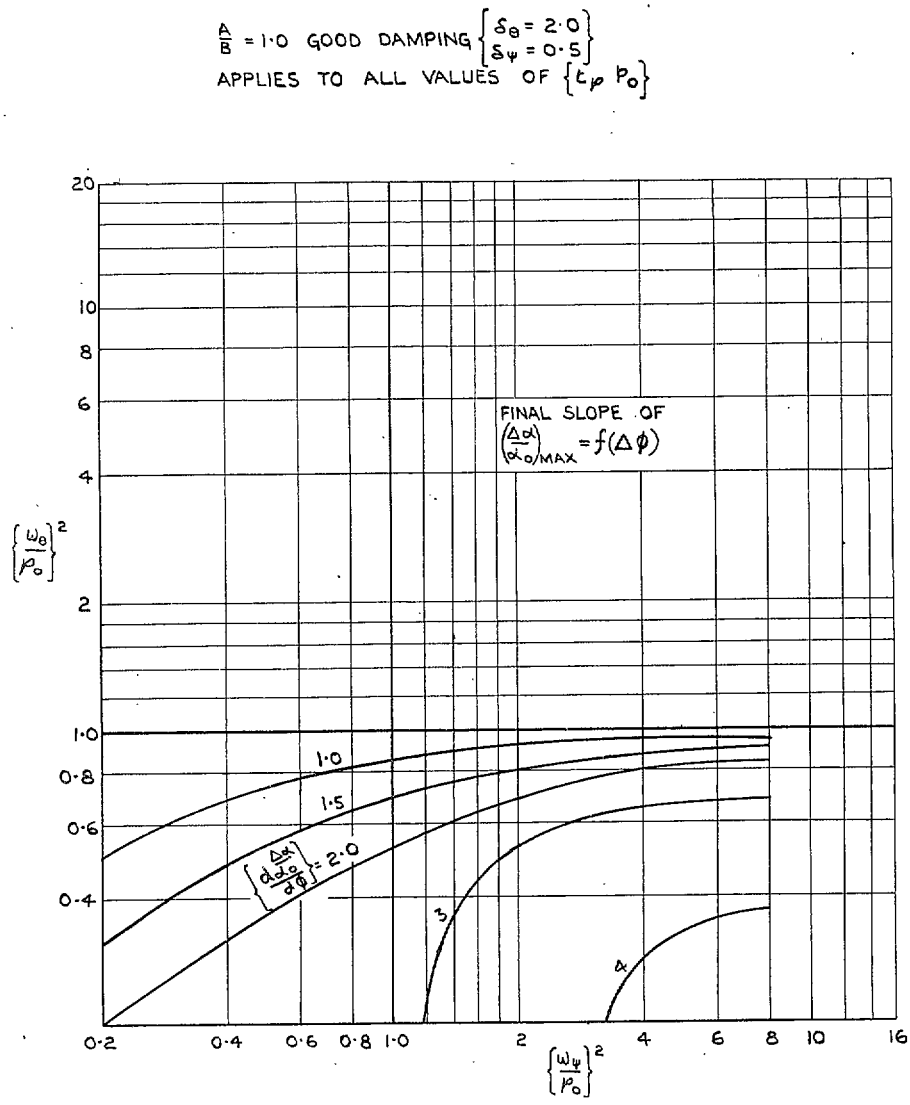

CHART 36. Final slopes of $\Delta\alpha_{MAX}$ with manoeuvre bank angle, $\Delta\phi$. $A/B = 1{\cdot}0$, good damping.

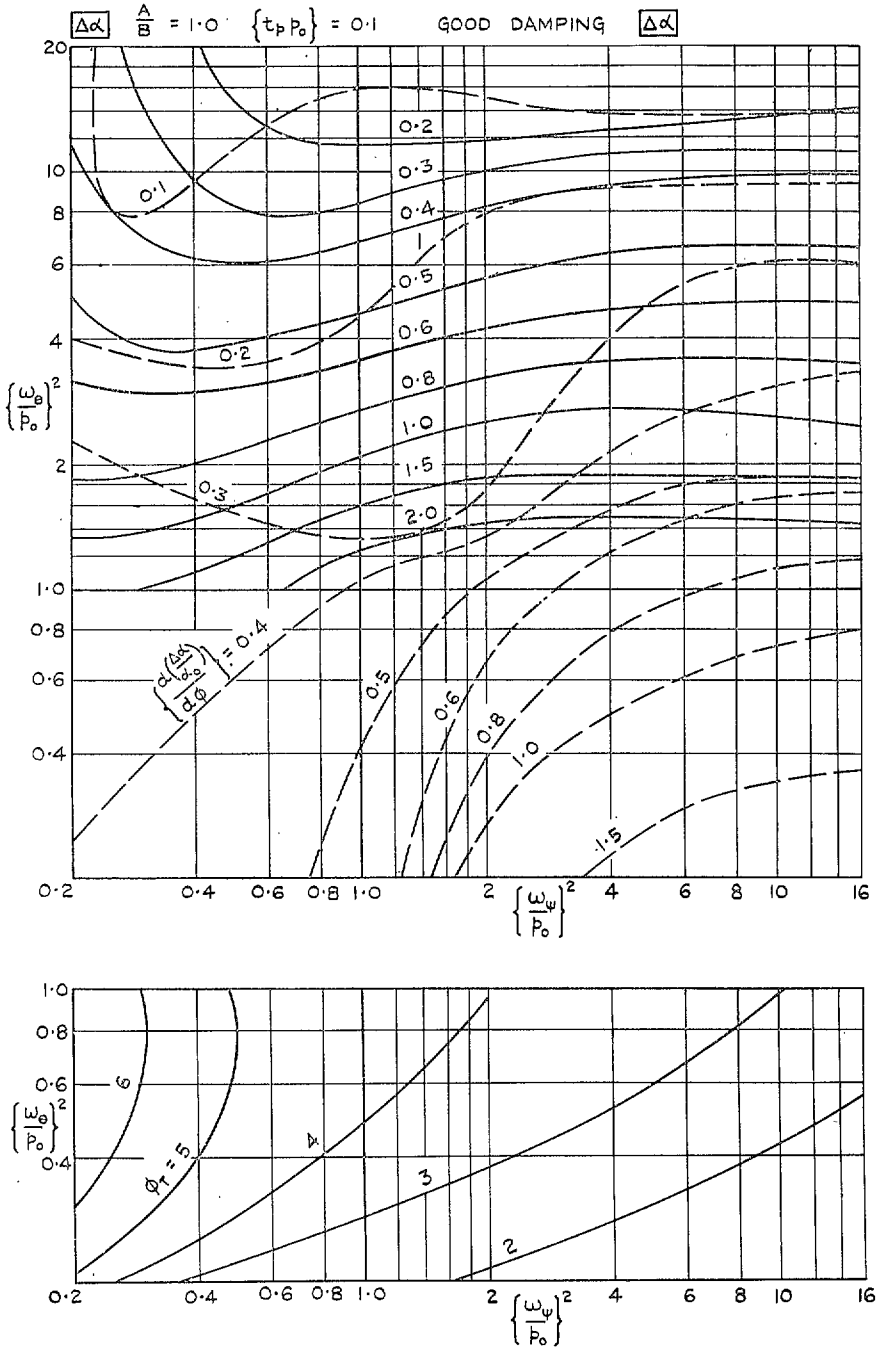

CHART 37. Ceiling values, and initial slopes with $\Delta\phi$, of incidence peak values, $\Delta\alpha_{MAX}$, and critical bank angle of pitch divergence, ϕ_T. $A/B = 1{\cdot}0$, $\{t_p p_0\} = 0{\cdot}1$, $\delta_\theta = 2{\cdot}0$, $\delta_\psi = 0{\cdot}5$.

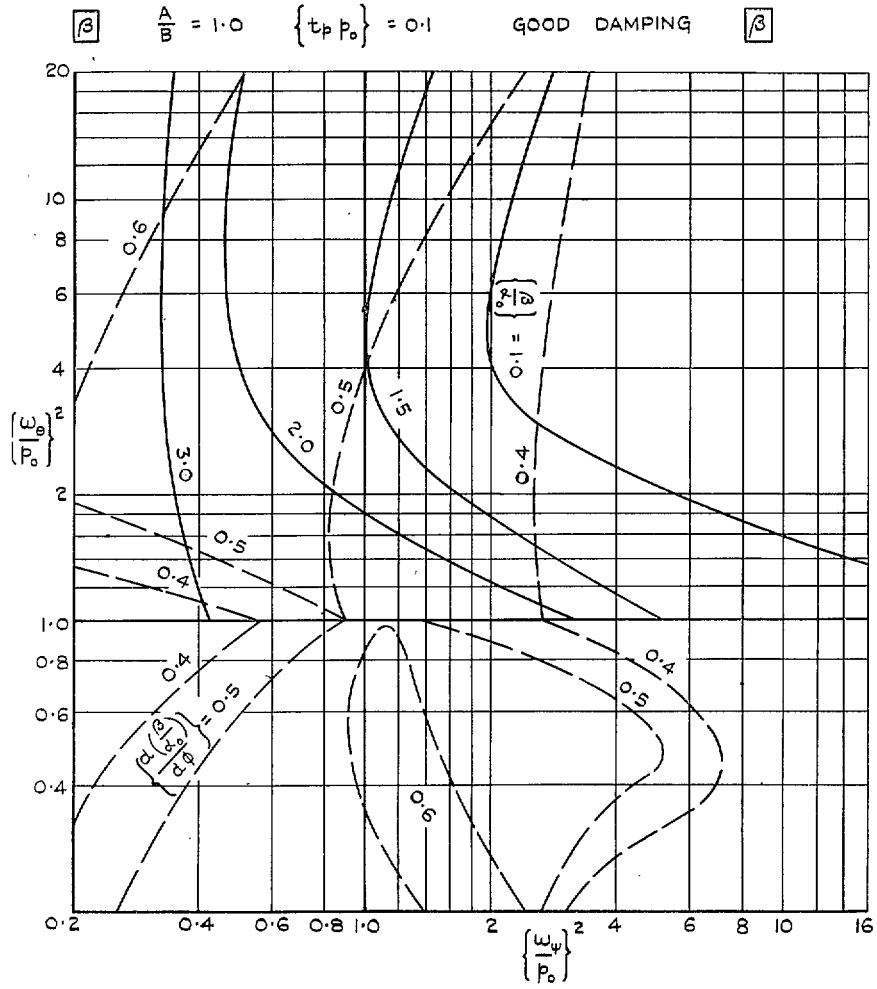

CHART 38. Ceiling values, and initial slopes with $\Delta\phi$, of sideslip peak values, β_{MAX}. $A/B = 1{\cdot}0$, $\{t_p p_0\} = 0{\cdot}1$, $\delta_\theta = 2{\cdot}0$, $\delta_\psi = 0{\cdot}5$.

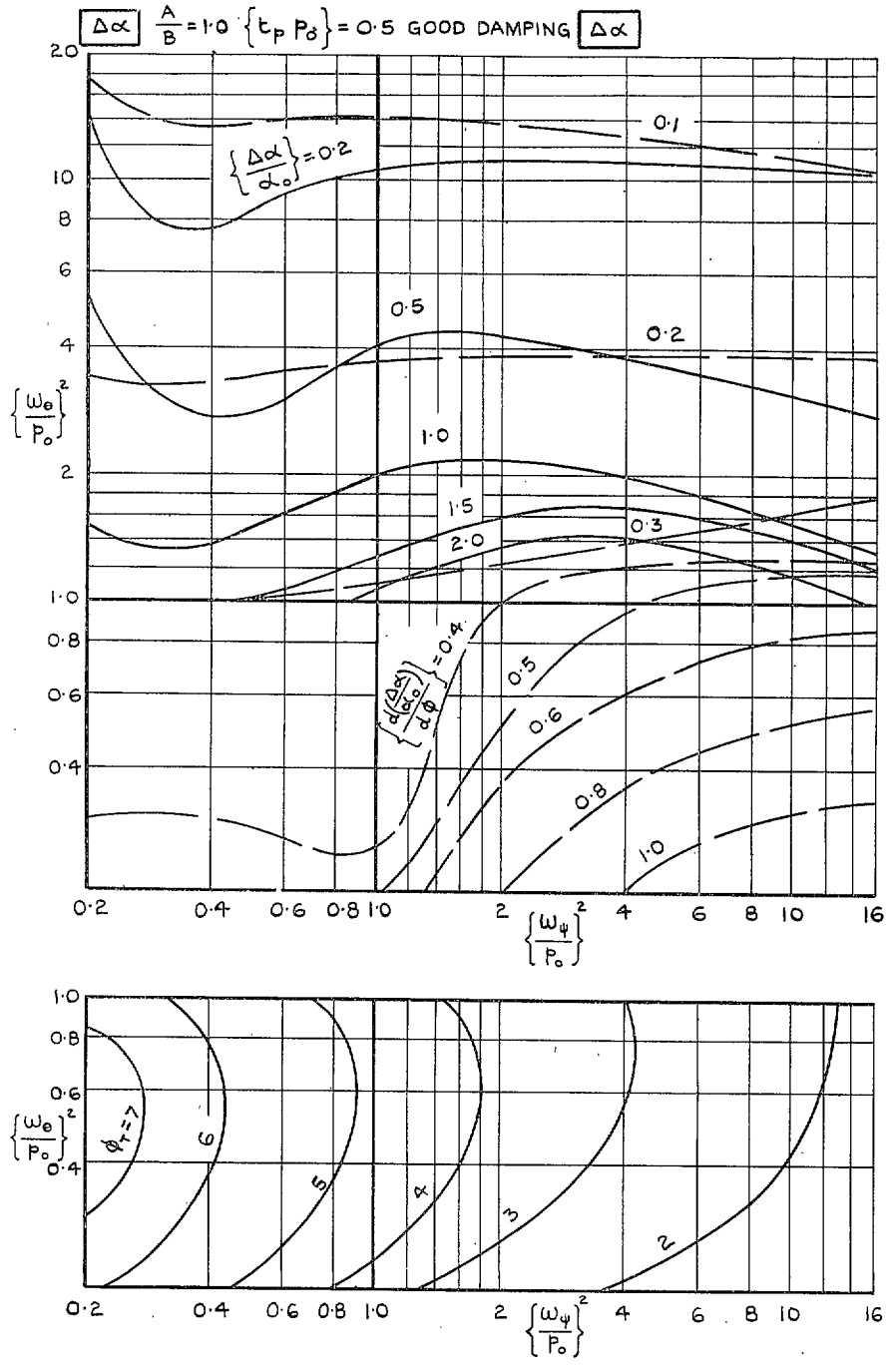

CHART 39. Ceiling values, and initial slopes with $\Delta\phi$, of incidence peak values, $\Delta\alpha_{MAX}$, and critical bank angles for pitch divergence, ϕ_T. $A/B = 1{\cdot}0$, $\{t_p p_0\} = 0{\cdot}5$, $\delta_\theta = 2{\cdot}0$, $\delta_\psi = 0{\cdot}5$.

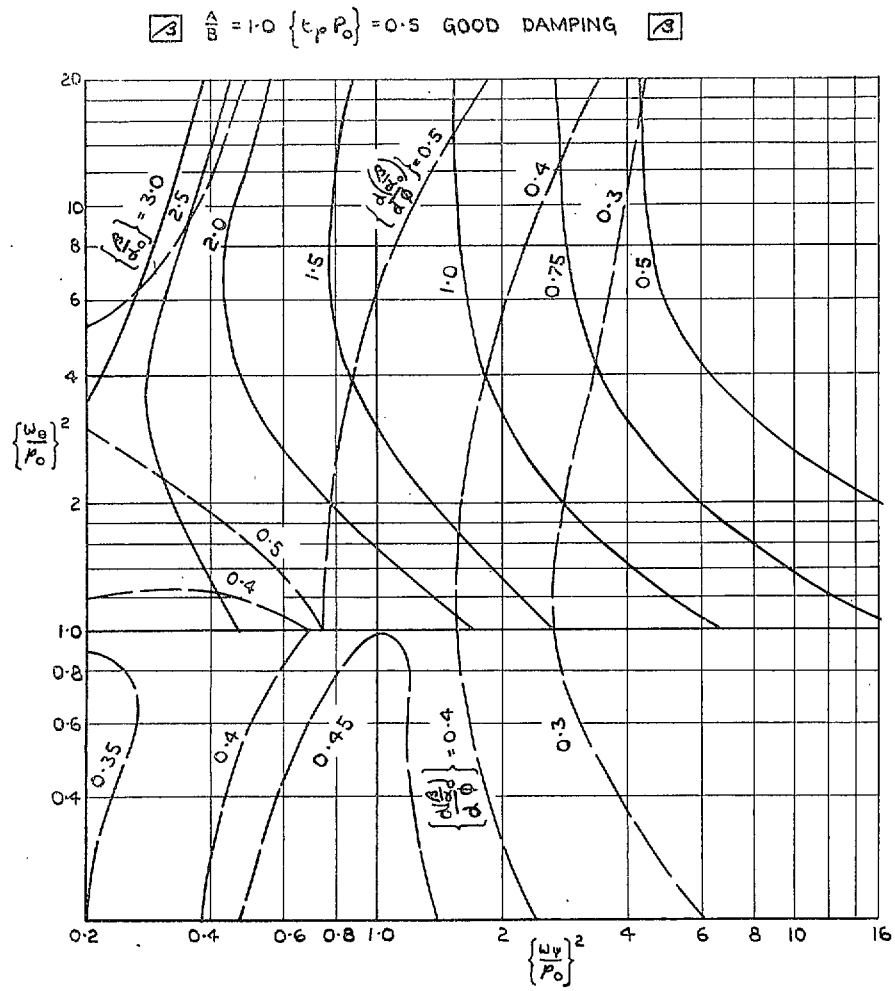

CHART 40. Ceiling values, and initial slopes with $\Delta\phi$, of sideslip peak values, β_{MAX}, $A/B = 1{\cdot}0$, $\{t_p p_0\} = 0{\cdot}5$, $\delta_\theta = 2{\cdot}0$, $\delta_\psi = 0{\cdot}5$.

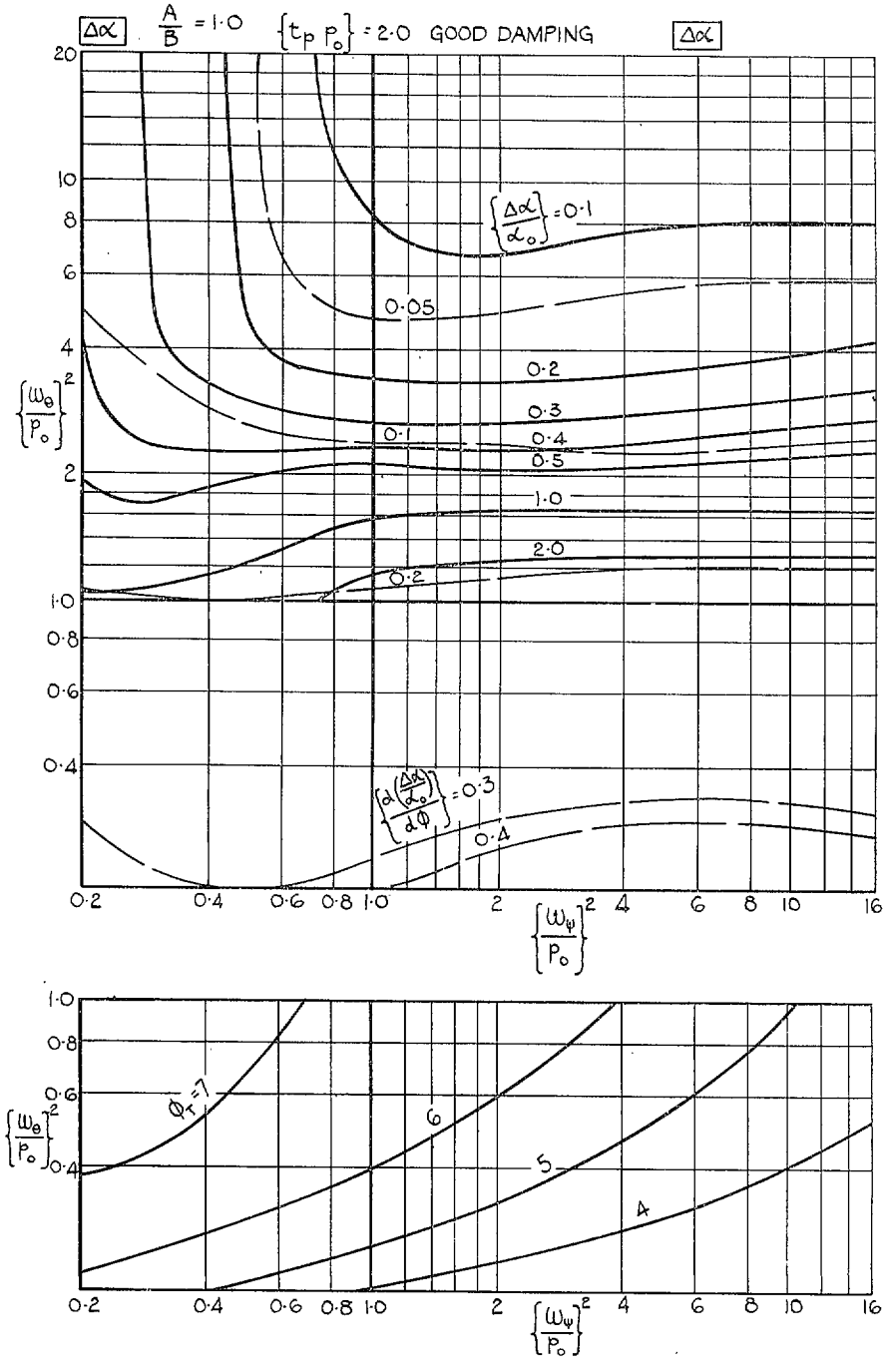

CHART 41. Ceiling values, and initial slopes with $\Delta\phi$, of incidence peak values, $\Delta\alpha_{MAX}$, and critical bank angle for pitch divergence, ϕ_T. $A/B = 1{\cdot}0$, $\{t_p p_0\} = 2{\cdot}0$, $\delta_\theta = 2{\cdot}0$, $\delta_\psi = 0{\cdot}5$.

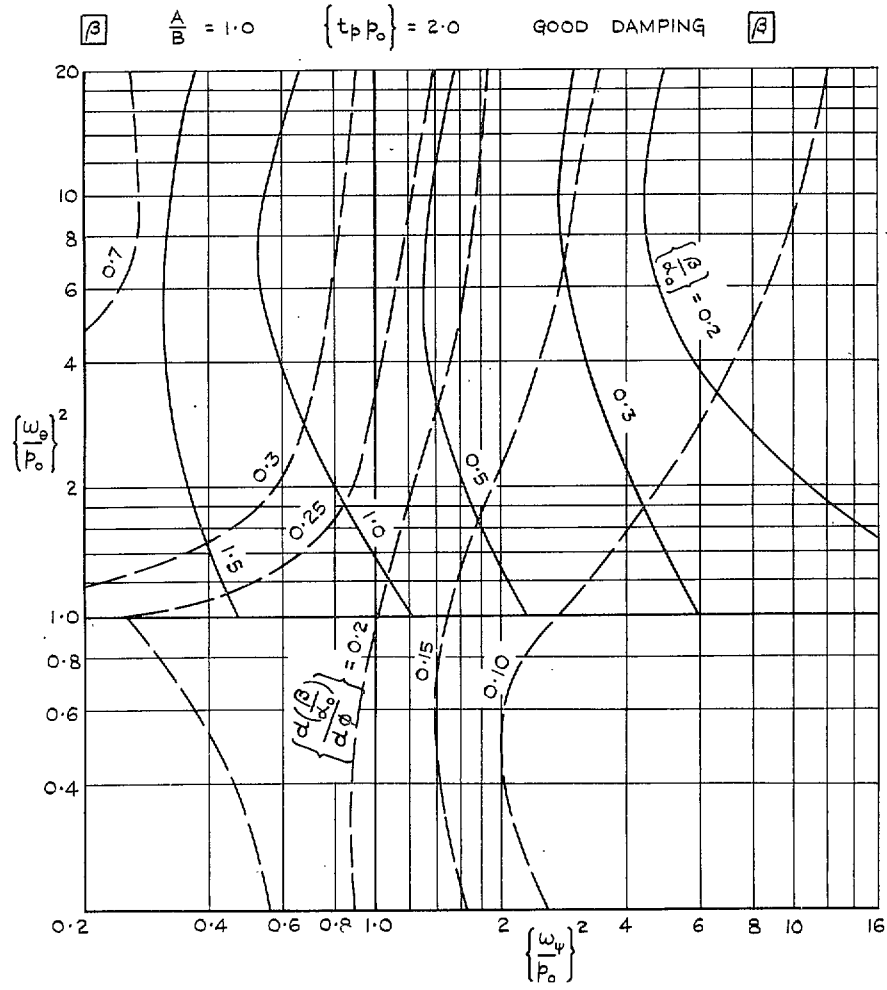

CHART 42. Ceiling values, and initial slopes with $\Delta\phi$, of sideslip peak values, β_{MAX}. $A/B = 1{\cdot}0$, $\{t_p p_0\} = 2{\cdot}0$, $\delta_\theta = 2{\cdot}0$, $\delta_\psi = 0{\cdot}5$.

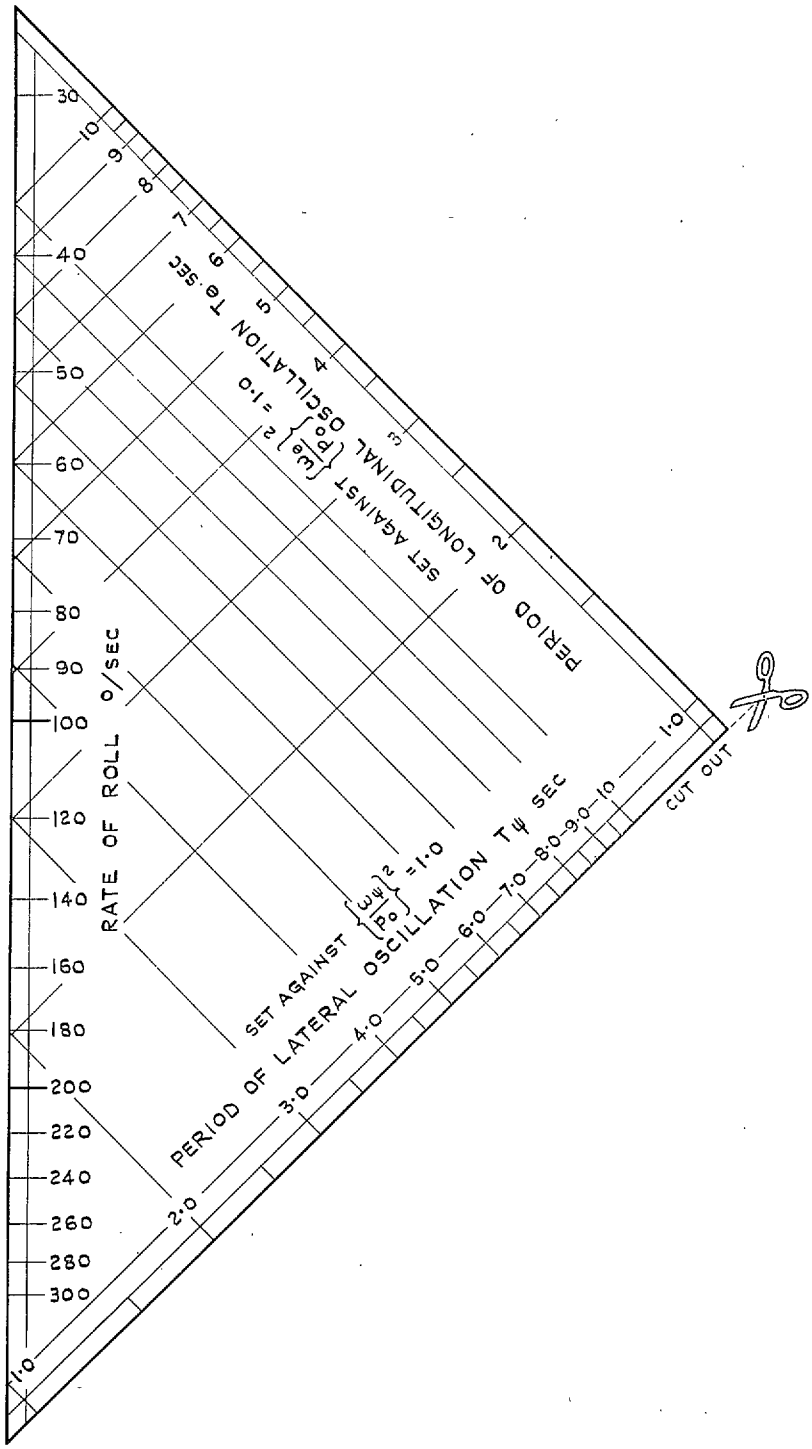

CHART 43. Nomogram to be used with peak-amplitude charts.

(85544) Wt. 64/1857 K5 11/62 Hw.

Publications of the Aeronautical Research Council

ANNUAL TECHNICAL REPORTS OF THE AERONAUTICAL RESEARCH COUNCIL (BOUND VOLUMES)

1942 Vol. I. Aero and Hydrodynamics, Aerofoils, Airscrews, Engines. 75*s.* (post 2*s.* 9*d.*)
Vol. II. Noise, Parachutes, Stability and Control, Structures, Vibration, Wind Tunnels. 47*s.* 6*d.* (post 2*s.* 3*d.*)

1943 Vol. I. Aerodynamics, Aerofoils, Airscrews. 80*s.* (post 2*s.* 6*d.*)
Vol. II. Engines, Flutter, Materials, Parachutes, Performance, Stability and Control, Structures. 90*s.* (post 2*s.* 9*d.*)

1944 Vol. I. Aero and Hydrodynamics, Aerofoils, Aircraft, Airscrews, Controls. 84*s.* (post 3*s.*)
Vol. II. Flutter and Vibration, Materials, Miscellaneous, Navigation, Parachutes, Performance, Plates and Panels, Stability, Structures, Test Equipment, Wind Tunnels. 84*s.* (post 3*s.*)

1945 Vol. I. Aero and Hydrodynamics, Aerofoils. 130*s.* (post 3*s.* 6*d.*)
Vol. II. Aircraft, Airscrews, Controls. 130*s.* (post 3*s.* 6*d.*)
Vol. III. Flutter and Vibration, Instruments, Miscellaneous, Parachutes, Plates and Panels, Propulsion. 130*s.* (post 3*s.* 3*d.*)
Vol. IV. Stability, Structures, Wind Tunnels, Wind Tunnel Technique. 130*s.* (post 3*s.* 3*d.*)

1946 Vol. I. Accidents, Aerodynamics, Aerofoils and Hydrofoils. 168*s.* (post 3*s.* 9*d.*)
Vol. II. Airscrews, Cabin Cooling, Chemical Hazards, Controls, Flames, Flutter, Helicopters, Instruments and Instrumentation, Interference, Jets, Miscellaneous, Parachutes. 168*s.* (post 3*s.* 3*d.*)
Vol. III. Performance, Propulsion, Seaplanes, Stability, Structures, Wind Tunnels. 168*s.* (post 3*s.* 6*d.*)

1947 Vol. I. Aerodynamics, Aerofoils, Aircraft. 168*s.* (post 3*s.* 9*d.*)
Vol. II. Airscrews and Rotors, Controls, Flutter, Materials, Miscellaneous, Parachutes, Propulsion, Seaplanes, Stability, Structures, Take-off and Landing. 168*s.* (post 3*s.* 9*d.*)

1948 Vol. I. Aerodynamics, Aerofoils, Aircraft, Airscrews, Controls, Flutter and Vibration, Helicopters, Instruments, Propulsion, Seaplane, Stability, Structures, Wind Tunnels. 130*s.* (post 3*s.* 3*d.*)
Vol. II. Aerodynamics, Aerofoils, Aircraft, Airscrews, Controls, Flutter and Vibration, Helicopters, Instruments, Propulsion, Seaplane, Stability, Structures, Wind Tunnels. 110*s.* (post 3*s.* 3*d.*)

Special Volumes

Vol. I. Aero and Hydrodynamics, Aerofoils, Controls, Flutter, Kites, Parachutes, Performance, Propulsion, Stability. 126*s.* (post 3*s.*)
Vol. II. Aero and Hydrodynamics, Aerofoils, Airscrews, Controls, Flutter, Materials, Miscellaneous, Parachutes, Propulsion, Stability, Structures. 147*s.* (post 3*s.*)
Vol. III. Aero and Hydrodynamics, Aerofoils, Airscrews, Controls, Flutter, Kites, Miscellaneous, Parachutes, Propulsion, Seaplanes, Stability, Structures, Test Equipment. 189*s.* (post 3*s.* 9*d.*)

Reviews of the Aeronautical Research Council

1939–48 3*s.* (post 6*d.*) 1949–54 5*s.* (post 5*d.*)

Index to all Reports and Memoranda published in the Annual Technical Reports

1909–1947 R. & M. 2600 (out of print)

Indexes to the Reports and Memoranda of the Aeronautical Research Council

Between Nos. 2351–2449	R. & M. No. 2450	2*s.* (post 3*d.*)
Between Nos. 2451–2549	R. & M. No. 2550	2*s.* 6*d.* (post 3*d.*)
Between Nos. 2551–2649	R. & M. No. 2650	2*s.* 6*d.* (post 3*d.*)
Between Nos. 2651–2749	R. & M. No. 2750	2*s.* 6*d.* (post 3*d.*)
Between Nos. 2751–2849	R. & M. No. 2850	2*s.* 6*d.* (post 3*d.*)
Between Nos. 2851–2949	R. & M. No. 2950	3*s.* (post 3*d.*)
Between Nos. 2951–3049	R. & M. No. 3050	3*s.* 6*d.* (post 3*d.*)
Between Nos. 3051–3149	R. & M. No. 3150	3*s.* 6*d.* (post 3*d.*)

HER MAJESTY'S STATIONERY OFFICE

from the addresses overleaf

Printed and published by
HER MAJESTY'S STATIONERY OFFICE

To be purchased from
York House, Kingsway, London W.C.2
423 Oxford Street, London W.1
13A Castle Street, Edinburgh 2
109 St. Mary Street, Cardiff
39 King Street, Manchester 2
50 Fairfax Street, Bristol 1
35 Smallbrook, Ringway, Birmingham 5
80 Chichester Street, Belfast 1
or through any bookseller

Printed in England

R. & M. No. 3293

S.O. Code No. 23-3293